

---

Electronic Thesis and Dissertation Repository

---

5-4-2011 12:00 AM

## Coupled heat and water transport in frozen soils

Ranjeet M. Nagare, *The University of Western Ontario*

Supervisor: Dr. Robert A. Schincariol, *The University of Western Ontario*

A thesis submitted in partial fulfillment of the requirements for the Doctor of Philosophy degree in Geology

© Ranjeet M. Nagare 2011

Follow this and additional works at: <https://ir.lib.uwo.ca/etd>



Part of the [Hydrology Commons](#), and the [Water Resource Management Commons](#)

---

### Recommended Citation

Nagare, Ranjeet M., "Coupled heat and water transport in frozen soils" (2011). *Electronic Thesis and Dissertation Repository*. 158.

<https://ir.lib.uwo.ca/etd/158>

This Dissertation/Thesis is brought to you for free and open access by Scholarship@Western. It has been accepted for inclusion in Electronic Thesis and Dissertation Repository by an authorized administrator of Scholarship@Western. For more information, please contact [wlsadmin@uwo.ca](mailto:wlsadmin@uwo.ca).

COUPLED HEAT AND WATER TRANSPORT IN FROZEN ORGANIC SOILS

(Spine title: Coupled heat and water transport in frozen soils)

(Thesis format: Integrated-Article)

by

Ranjeet M. Nagare

Graduate Program in Geology

A thesis submitted in partial fulfillment of the requirements for the degree of

Doctor of Philosophy

The School of Graduate and Postdoctoral Studies

The University of Western Ontario

London, Ontario, Canada

© Ranjeet M. Nagare 2011

THE UNIVERSITY OF WESTERN ONTARIO  
SCHOOL OF GRADUATE AND POSTDOCTORAL STUDIES

**CERTIFICATE OF EXAMINATION**

<u>Supervisor</u>	<u>Examiners</u>
_____ Dr. Robert A. Schincariol	_____ Dr. Sean Carey
<u>Supervisory Committee</u>	_____ Dr. Ernest Yanful
_____ Dr. William L. Quinton	_____ Dr. Kristy Tiampo
_____ Dr. Masaki Hayashi	_____ Dr. Brian Branfireun

The thesis by

**Ranjeet M. Nagare**

entitled:

**Coupled heat and water transport in frozen soils**

**is accepted in partial fulfillment of the**

**requirements for the degree of**

Doctor of Philosophy

Date \_\_\_\_\_

\_\_\_\_\_  
Chair of the Thesis Examination Board

## Abstract

The effect of freezing on soil temperature and water redistribution was examined in four Mesocosms maintained at different initial water content profiles. An innovative experimental setup involving use of a frozen base layer acting as a proxy to permafrost beneath an active layer made up of packed and undisturbed peat cores was used. The experimental setup was successfully validated for its ability to maintain one dimensional change in temperature and soil water content in frozen soil. There was a substantial amount of water redistribution towards the freezing front, enough to create an impermeable frozen, saturated zone within 15 cm of the soil surface. The water movement was likely due to the potential head gradients between colder and warmer regions created by temperature effects on matric potential of frozen soil. In addition, there is enough evidence that water migration in form of vapour contributed to moisture movement towards the freezing front. Initial moisture profiles appeared to have a significant effect on the freezing induced soil water redistribution likely through differences in moisture dependant hydraulic conductivity. Initial soil moisture profiles also affected the rate of freezing front movement. Frost propagation was controlled by latent heat for long periods, while soil thermal conductivity and heat capacity appeared to control the rate of frost migration once the majority of water was frozen. Using the observations of this study, a conceptual model was proposed to explain freezing of an active layer on a permafrost plateau assuming a variable moisture landscape at onset of winter.

Further, a one-dimensional model based on coupled cellular automata approach was developed. The model is based on first order conservation laws to simulate heat and water flow in variably-saturated soil. Inside the model, Buckingham-Darcy's -and Fourier's heat laws are used to define the local interactions for water and heat movement respectively. Phase change is brought about by the residual energy after sensible heat removal has dropped the temperature of the system below freezing point. Knowing the amount of water that can freeze, the change in soil temperature is then modeled by integrating along the soil freezing curve. This approach obviates the use of apparent heat capacity term. The 1D model is successfully tested by comparing with analytical and experimental solutions.

Keywords: vadose zone hydrology, soil water redistribution, freezing front migration, organic soils, permafrost, cellular automata.

## The Co-Authorship Statement

This thesis consists of a series of manuscripts for publication in peer-reviewed journals (Chapters 2 to 5), together with a general introduction (Chapter 1) and conclusion (Chapter 6). In accordance with the guidelines of University of Western Ontario's School of Graduate and Postdoctoral Studies, I declare that the research presented in these manuscripts is of my conception and execution with the input and assistance of the listed co-authors. The role of these co-authors is listed below:

Chapter 2 is a modified version of Nagare, R.M., Schincariol, R.A., Quinton, W.L., and Hayashi, M. 2011. *Laboratory calibration of time domain reflectometry to determine moisture content in undisturbed peat samples*, European Journal of Soil Science (in press). All three co-authors provided intellectual comments on the drafts of the manuscripts of this paper. Dr. Masaki Hayashi played a key role in strengthening the paper by providing ideas for vertical insertion of probe and experiments to determine the effect of container dimensions on the calibration results.

Chapter 3 is a modified version of Nagare R.M., Schincariol, R.A., Quinton, W.L., and Hayashi, M. *Moving the field into the lab: Simulation of heat and water transport in sub-Arctic peat* in review with Permafrost and Periglacial Processes Journal. All three co-authors provided intellectual comments on the drafts of the manuscripts of this paper. Dr. Schincariol was actively involved in selection of material for the experiments in the initial stages. This paper involves a proof of concept phase of Dr. Schincariol's idea of the two level walk-in environmental chamber for permafrost studies.

Chapter 4 is a modified version of Nagare, R.M., Schincariol, R.A., Quinton, W.L., and Hayashi, M. *Effects of freezing on soil temperature, frost propagation and moisture redistribution in peat: Laboratory investigations* in review with Hydrology and Earth System Sciences Journal. Dr. Schincariol, Dr. Quinton, and Dr. Hayashi have contributed in overall development of this paper through intellectual comments on the drafts of the manuscripts. In addition, Dr. Webb was actively involved in the isotopes part of the experiments, isotopes analysis and has contributed to the isotopes section of the chapter.

Chapter 5 is a modified version of Nagare, R.M., Bhattacharya, P., Khanna, J., and Schincariol, R.A. *A coupled cellular automata model for heat and water flow in variably wetted soils* to be submitted to a peer reviewed journal. Both Pathikrit Bhattacharya and Jaya Khanna were involved in the conceptual development of the model and computer coding part. Pathikrit Bhattacharya, Jaya Khanna and Dr. Schincariol also helped improve the manuscript with intellectual comments.

# Acknowledgment

First of all, I would like to thank my supervisor Dr. Robert Schincariol for providing me with the opportunity, freedom and support throughout this project. Rob thank you very much for being flexible and positive as well as discussing science and sharing your experience with me. I hope this partnership has been memorable for you as well.

I also want to thank my co-supervisors, Dr. William Quinton and Dr. Masaki Hayashi. Thank you Bill for all the meetings and the discussions. Your ability to put long stories in short conclusions has been inspirational. I hope this is something that comes with experience. Thank you very much for all the support, encouragement and most importantly helping me keep the things in perspective. Rob and Bill, thank you for bearing me in the field during the summer of 2007 as we cored the precious peat in no man's land near Fort Simpson. Thank you Masaki for being the perfect science player: starting with a blast in the first committee meeting, keeping me on my toes during the time domain reflectometry work, and providing detailed critique to all papers.

I want to thank Dr. Sean Carey, Dr. Ernest Yanful, Dr. Kristy Tiampo and Dr. Brian Branfireun for accepting to be reviewers of this thesis.

A big thank you to Dr. Elizabeth Webb, Dr. Gordon Southam, Dr. Bhabani Das and Dr. Charlie Woo for guiding me through different experiments. You people were the ones guiding me in areas of my weakest expertise. I also want to thank the entire non-teaching staff of the Earth Sciences Department, especially Mary Rice, Marie Schell and John Brunet for the support par excellence during my time at this department.

A special thanks to Dr. Lalu Mansinha. Sir, thank you very much for discussing everything and anything with me. Thank you very much for being the guidance away from home, sharing your life experiences and making me feel at home. I do not have words to express my gratitude towards you. Let that be reserved for many more sessions to come in the future.

I want to thank Frank van Sas and Brian Dalrymple for their untiring help in getting the Mesocosm experiments setup. You guys were fantastic. Frank, thank you very much for being kind to me. I always came to you with unusual demands. Thank you for getting the hard part done for me and also for being there whenever I called you for help. Your support is irreplaceable in context of this work. A big thank you also extends to Jon Jacobs for helping me in many of the machining jobs and during sample insertions. I also want to thank Steve Bartlett for making my work much easier after taking over as the facility manager at Biotron. Frank, Brian, Jon and Steve – THANK YOU VERY MUCH. Many thanks to Roger Peters and Bruce Kettner from Biochambers for providing perfect support. I also want to take this opportunity to thank Trevor Myers, Pete Whittington, Andrea Kenwood and Tyler Veness for their support in field sampling of the large peat cores and smaller samples.

Pathikrit Bhattacharya and Jaya Khanna were instrumental with their help in discussing my work from physics point of view. Their unconditional support during the conceptualization of the cellular automata work and all the coding and de-bugging thereafter is something that is unmatched. Well, I guess that is what great friends do. And guys thank you for doing this for me without any expectations. I forever remain grateful to you both.

Now on to my friends of past four years. Nelson, Ali, Ayumi, Caitlin, Javad, Matt, Lisa, Rashmi, Laxmikant, Prithwi, Ashok, Zhong Ying, Nevenka, Emad, Laura, Marie and all who have made my time at Western easier than it otherwise would have been. CHEERS for all the good and bad times we shared. Jeremy, thank you for being the friend I needed who would come on a single phone call to help me in any way I wanted. I believe the experiments would not be running the way they are if you would not have been helping me. Having said that, I have found a great friend in you.

And Jalpa (Jagmi), thank you for being my best friend. I cannot imagine being stress free for past 2 ½ years without you being around me. Thank you for doing all that you have done for me and playing roles of a best friend, cool housemate, awesome cook, fabulous navigator, superb defender and many more. Many thanks to you also for helping

me format my thesis. I am grateful to you for choosing me over so many in situations where you could have easily done otherwise. Your friendship is the best thing that has happened to me in many years. Thank you for being my family.

Finally, I want to express my deepest gratitude towards all those people who have played a part in my life so far: my family, all school teachers, and college and University professors. Your teachings and giving has always guided me. Professor. Voigt, you remain an inspiration and someone who I always look up to. To end with, thank you to the taxpayers of India, Germany and Canada for enabling me to educate myself. Nobody thanks you silent contributors and I am using this opportunity to thank you on behalf of all students.

# Table of Contents

Abstract.....	iii
The Co-Authorship Statement.....	v
Acknowledgment.....	vii
Table of Contents .....	x
List of Figures .....	xv
List of Tables.....	xxi
CHAPTER 1. GENERAL INTRODUCTION	
1.1. Introduction .....	1
1.2. Coupled heat and water flow in frozen soils .....	4
1.3. Laboratory column experiments with frozen soils .....	6
1.4. Numerical models with frozen schemes.....	10
1.5. Research objectives.....	11
1.6. Thesis organization .....	14
1.7. References .....	15
CHAPTER 2. LABORATORY CALIBRATION OF TIME DOMAIN REFLECTOMETRY TO DETERMINE MOISTURE CONTENT IN UNDISTRUBED PEAT SAMPLES	

2.1.	Introduction .....	21
2.1.1.	Basic Principles .....	23
2.1.2.	Empirical calibrations and dielectric mixing models.....	24
2.2.	Materials and methods .....	28
2.2.1.	Study site .....	28
2.2.2.	Calibration sample size .....	29
2.2.3.	Calibration method.....	30
2.2.4.	Temperature effects on water content and BEC measurements .....	32
2.3.	Results .....	33
2.3.1.	Peat characteristics.....	33
2.3.2.	TDR calibration .....	35
2.3.3.	Mixing model calibrations.....	41
2.3.4.	Calibration in travel time, BEC and effective frequency .....	43
2.4.	Discussions .....	45
2.5.	Conclusions .....	51
2.6.	References .....	52
CHAPTER 3. PHYSICAL SIMULATION OF WATER AND HEAT TRANSPORT IN SUB-ARCTIC PEAT		
3.1.	Introduction .....	59

3.2.	The climate chamber .....	62
3.3.	Field sampling of soil mesocosms .....	63
3.4.	Experiment setup .....	64
3.5.	Evaluation.....	66
3.6.	Implications .....	77
3.7.	References .....	79

## CHAPTER 4. EFFECTS OF FREEZING ON SOIL TEMPERATURE, FROST

### PROPAGATION AND MOISTURE REDISTRIBUTION IN PEAT

4.1.	Introduction .....	82
4.2.	Methodology.....	86
4.2.1.	Experimental setup.....	86
4.2.2.	Experimental conditions.....	91
4.2.3.	TDR calibration .....	92
4.2.4.	Final total water content.....	94
4.2.5.	Isotope profiling experiment .....	95
4.3.	Results and discussion.....	97
4.3.1.	Initial conditions .....	97
4.3.2.	Soil freezing characteristics.....	98
4.3.3.	Frost induced water redistribution within the active layer.....	103

4.3.3.1.	Variably wetted conditions with a water table at depth (Mesocosms 1 and 4)	103
4.3.3.2.	Dry conditions (Mesocosm 2)	106
4.3.3.3.	Saturated conditions (Mesocosm 3)	107
4.3.4.	Water movement from the transition zone	111
4.3.5.	Soil temperature and frost propagation	116
4.4.	Conclusions and implications	124
4.5.	References	126
CHAPTER 5. A COUPLED CELLULAR AUTOMATA MODEL FOR HEAT AND WATER FLOW IN VARIABLY WETTED SOILS		
5.1.	Introduction	132
5.2.	Cellular automata	135
5.2.1.	Mathematical description	137
5.2.2.	Physical description based on heat flow problem in a hypothetical soil column	139
5.3.	Coupled heat and water transport in unsaturated soils	141
5.4.	The coupled CA model	144
5.5.	Verification	149
5.5.1.	Comparison with analytical solutions	149
5.5.1.1.	Heat transfer by pure conduction	149

5.5.1.2.	Heat transfer by conduction and convection .....	151
5.5.1.3.	Heat transfer with phase change .....	155
5.5.2.	Comparison with experimental data .....	160
5.6.	Conclusions .....	166
5.7.	References .....	167
<b>CHAPTER 6. CONCLUSIONS AND FUTURE RESEARCH RECOMMENDATIONS</b>		
6.1.	General conclusions .....	172
6.2.	Future research recommendations .....	176
6.3.	References .....	178
<b>APPENDIX.....</b>		<b>180</b>
A1.	Description of peat corer .....	180
A2.	Description of experimental setup .....	184
Curriculum Vitae .....		188

## List of Figures

**Figure 2.1.** Soil moisture characteristic curves for peat from Scotty Creek watershed (Quinton and Hayashi, 2005). Numbers in legend indicate the depth of sample in cm below ground surface.....35

**Figure 2.2.** Regression curves fitted individually to M samples (peat plateau-bog periphery) and L samples (peat plateau), and a combined fit to data from M samples and L samples. ....36

**Figure 2.3.** Comparison of empirical calibration equations given in Table 2.1 with the combined experimental data from M samples (peat plateau-bog periphery) and L samples (peat plateau), and the combined empirical model (Table 2.4) of this study.....38

**Figure 2.4.** Effect of temperature on (a) apparent dielectric permittivity and (b) BEC measurements in peat. The gravimetric water content ( $\theta_g$ ) did not change over the duration of the test. ....40

**Figure 2.5.** Comparison of mixing models ( $\eta = 0.89$ ,  $\varepsilon_{fw} = 76.58$ ,  $\varepsilon_s = 3.25$ ,  $\theta_{bw} = 0.0094 \text{ m}^3 \text{ m}^{-3}$ ,  $\varepsilon_{bw} = 3.15$  and  $\alpha = 0.5$ ) with the combined experimental data from M samples (peat plateau-bog periphery) and L samples (peat plateau), and the combined empirical model (Table 2.4) of this study. ....42

**Figure 2.6.** Effect of porosity on the  $\varepsilon$ - $\theta$  relationship as simulated using the Maxwell-De Loor model ( $\theta_{bw} = 0 \text{ m}^3 \text{ m}^{-3}$ ). ....48

**Figure 2.7.** Comparison between empirical models proposed by Kellner and Lundin (2001) and the Maxwell-De Loor model ( $\varepsilon_{fw} = 79.4$ ,  $\varepsilon_s = 5$ ,  $\theta_{bw} = 0 \text{ m}^3 \text{ m}^{-3}$ ) for (a) pooled data from experimental samples, and samples with varying degrees of humification (on the von Post scale); (b) H3 and (c) H4. Also shown are calculated values of  $R^2$  and RMSE.....49

**Figure 2.8** Simulation of temperature effects on water content measurements of peat samples used in this study using the Maxwell-De Loor model. ....50

**Figure 3.1.** Initial water content in Mesocosms (a) 1, (b) 2, (c) 3, and (d) 4 for first freezing run. The depth to the groundwater table is shown by free water surface symbol in black.....68

<b>Figure 3.2.</b> Initial water content in Mesocosms (a) 1, (b) 2, (c) 3, and (d) 4 for second freezing run. The depth to the groundwater table is shown by free water surface symbol in black. Mesocosm # 2 was unsaturated throughout its depth before the second freezing run. ....	69
<b>Figure 3.3.</b> The temperature profile development for (a) Mesocosm 1 and (b) Mesocosm 3 during the first freezing run.....	71
<b>Figure 3.4.</b> Temperature profiles recorded at Scotty Creek field site during the winter seasons of (a) 2001-2002 and (b) 2007-2008. The day of recording for the first and last profiles is shown on both graphs. The intermediate profiles are separated by intervals of 30 days. The temperature at 100 cm depth is approximated from borehole temperature records of a nearby (20 km) station from the Norman Wells pipeline study (Smith <i>et al.</i> , 2004). ....	72
<b>Figure 3.5.</b> The temperature profile development for Mesocosm # 2 during the first freezing run. ....	73
<b>Figure 3.6.</b> Unfrozen water content time series for Mesocosms # 2 during the first freezing run. Labels show the time at which freezing commences at three different depths. ....	74
<b>Figure 3.7.</b> Comparison between temperature profiles for central location (grey circles) and near-edge sensors (white squares). The numbers on the right are the calculated absolute values of horizontal ( H ) and vertical ( V ) gradients in °C cm <sup>-1</sup> at 8 cm, 28 cm and 55 cm respectively. ....	76
<b>Figure 3.8.</b> Comparison between temperature time series of near-edge and central sensors located at (a) 8 cm, (b) 28 cm and (c) 55 cm below peat surface.....	77
<b>Figure 4.1.</b> Depth variation of (a) Bulk density (Hayashi <i>et al.</i> , 2007), (b) porosity (Hayashi <i>et al.</i> , 2007), (c) vertical hydraulic conductivity, and (d) soil water retention curves (Quinton and Hayashi, 2005) for peat from Scotty Creek watershed. The different symbols in (d) represent the samples taken at different depths as shown in legend. ....	89
<b>Figure 4.2.</b> Line diagram showing the experimental setup. <b>1U</b> : Upper level chamber of the BESM; <b>1L</b> : Lower level chamber of the BESM; <b>2</b> : 65-75 cm deep unfrozen layer; <b>3</b> : 45 cm bottom frozen layer (fully saturated before freezing); <b>4</b> : TDR probes connected to	

11 through low-loss coaxial cables; **5**: temperature probes connected to 11; **6**: heat flux plate; **7**: LDPE container lined with neoprene from inside and insulated from outside; **8**: stand pipe for water level measurements; **9**: weighing scale; **10**: custom made stand to support the entire experimental setup; **11**: multiplexers and datalogger connected to a personal computer.....90

**Figure 4.3.** (a) Effect of temperature on apparent dielectric permittivity measurements in peat. The gravimetric water content ( $\theta_g$ ) did not change over the duration of test. Effect of temperature on observed apparent dielectric permittivity of (b) water, and (c) air and oven dried peat as determined using TDR100. The relative permittivity of oven dried peat was derived from the bulk apparent dielectric permittivity using a 2-phase mixing formula. .93

**Figure 4.4.** Initial water content in Mesocosms (a) 1, (b) 2, (c) 3, and (d) 4 for second freezing run. The depth to the groundwater table is shown by free water surface symbol. Mesocosm # 2 was unsaturated throughout the depth for before the second freezing run. ....98

**Figure 4.5.** Soil freezing characteristics of all four Mesocosms obtained from observed unfrozen water and soil temperature data. .... 100

**Figure 4.6.** (a) Soil unfrozen water content and (b) temperature time series at selected depths in the four Mesocosms. The depths were selected such that initial water content was greater than  $0.5 \text{ m}^3 \text{ m}^{-3}$ ..... 101

**Figure 4.7.** Soil freezing curves in different Mesocosms (M1, M3 and M4). The effect of water redistribution on the shape of SFC is seen in form of deviation from an initial path the curves traverse (shown approximately by a thick gray line). The depth at which soil temperature-liquid water content relationship was observed is shown in parenthesis. ... 102

**Figure 4.8.** Soil freezing curves chosen from four different Mesocosms and initially at different water contents ( $\theta_i$ ). A best fit defined by van-Genuchten model (VG Model, van Genuchten, 1980) is also shown along with the VG Model parameters. The SFC's were chosen from each Mesocosm such that  $\theta_i \geq 0.5 \text{ m}^3 \text{ m}^{-3}$ . .... 103

**Figure 4.9.** Water movement towards freezing front: soil freezing characteristics of Mesocosm 4 shows change in slope of the curve at 25 cm depth exactly when the freezing front reaches 5 cm depth. .... 105

**Figure 4.10.** Comparison between the SFCs of Mesocosms 1 and 4 at 15 cm depth. This depth in both Mesocosms loses water before the soil temperature drops below freezing point, however M4 starts to lose water much earlier (1 hour) than M1 (43 hours). Both Mesocosms were exposed to air temperature of -7.5 °C at the surface at time = 0 hours. .... 106

**Figure 4.11.** Initial (liquid) and final (total) water content after 2000 hours of freezing in Mesocosms (a) 1, (b) 2, (c) 3, and (d) 4. Please note the different Y-axis limits in (c). . 109

**Figure 4.12.** Observed initial (liquid) and final water contents (liquid + ice) at Scotty Creek field site for winter of 2002-2003 (Quinton and Hayashi, 2008). The initial and unfrozen moisture content readings are from a soil pit being measured using a water content reflectometer. Two frozen cores were sampled at the end of winter season near the soil pit and total (liquid + ice) water content was determined gravimetrically. .... 110

**Figure 4.13.**  $\delta^{18}\text{O}$  vs  $\delta\text{D}$  plot of water samples collected in saturated zones of M1, M3 and M4 during first freezing run. The global meteoric water line is also shown for comparison. Note that the frozen layer was enriched only in Deuterium and the shift seen in Mesocosms 3 and 4 reflect enrichment in Deuterium with time. .... 113

**Figure 4.14.** Time series of  $\delta\text{D}$  signatures of water sampled within the saturated zones of M1, M3 and M4. Please note the different scales on y-axis. Data points after 70 days represent water sampled during thawing period. .... 116

**Figure 4.16.** (a) Observed ground heat flux in fully saturated M3 and dry M2 (at the start of freezing), and (b) Temperature time series for near surface sensors in Mesocosms M1 and M4. Note that the differences in time intervals. .... 120

**Figure 4.17.** Conceptual model describing freezing induced water redistribution and frost propagation inside an organic active layer on a peat plateau (a) onset of winter, (b) early winter, (c) early-mid winter, (d) mid winter, (e) and (f) mid-late winter, and (g) end of winter and spring runoff. Variable moisture landscape made up of regions with deeper unsaturated zones plus dry surface layer (zone of lower hydraulic conductivity) and shallow water table with wetter unsaturated zone (zone of higher hydraulic conductivity) result into variable amount of freezing induced moisture movement and different rates of freezing front movement. .... 123

**Figure 5.1.** One dimensional cellular automata grids based on von Neumann neighbourhood concept. How many neighbours (grey cells) interact with an active cell (black) is controlled by indicial radius ( $r$ ). ..... 139

**Figure 5.2.** Flow chart describing the algorithm driving the coupled CA code. Subscripts  $TC$ ,  $HC$  and  $FT$  refer to changes in physical quantities due to thermal conduction, hydraulic conduction and freeze-thaw processes respectively. Hydraulic conduction and thermal conduction are two different CA codes coupled though updating of volumetric heat capacity and the freeze-thaw module to simulate the simultaneous heat and water movement in soils. .... 145

**Figure 5.3.** Graphical description of the phase change approach used in this study. The curve is a soil freezing curve for a hypothetical soil. The change in water content ( $d\theta_w$ ) due to  $q_{resj}$  is used to determine  $T_{new}$  by integrating along the SFC (Equation 5.11). .... 147

**Figure 5.5.** Comparison between analytical (Stallman, 1965) and coupled CA model steady state solutions for conductive and convective heat transfer. The soil column in this example is infinitely long, initially at 20 °C, and upper surface is subjected to a sinusoidal temperature with amplitude of 5 °C and period of 24 hours..... 153

**Figure 5.6.** (a) Diagram showing the setting of Lunardini (1985) three zone problem. Equations 5.18, 5.19, and 5.20 are used to predict temperatures in completely frozen zone (no phase change and sensible heat only), mushy zone (phase change and latent heat + sensible heat), and unfrozen zone (sensible heat only) respectively. (b) Linear freezing function used to predict unfrozen water contents for two cases used in this study ( $T_m = -1^\circ\text{C}$  and  $T_m = -4^\circ\text{C}$ ). .... 155

**Figure 5.7.** Comparison between analytical solution of heat flow with phase change (Lunardini, 1985) and coupled CA model solutions for heat transfer with phase change. Lunardini (1985) solution is shown and compared with CA simulation for two cases (a)  $T_m = -1^\circ\text{C}$  and (b)  $T_m = -4^\circ\text{C}$  (Table 5.3, Figure 5.6)..... 158

**Figure 5.8.** Comparison of total water content (ice + water) between experimental (Mizoguchi, 1990 as cited by Hansson, 2004) and coupled CA model results: (a) 12 hours, (b) 24 hours, and (c) 50 hours. .... 163

<b>Figure 5.9.</b> Comparison between experimental (Jame and Norum, 1980) and coupled CA model. (a) Total water content (ice + liquid water) and (b) temperature. ....	165
<b>Figure A1.</b> The corer assembly (all dimensions in cm, not to scale). A: sample holder made out of fiber reinforced glass pipe material; B: bottom cap made out of same material as A; C: push-in plastic fasteners to secure bottom cap to the sample holder; D: alloyed carbon steel band saw blade; E: rotational head made of aluminum to facilitate rotation of the corer assembly; F & G: steel rods used as levers for rotating the corer assembly; H: quick release pins for quick mounting of rotational head on to the sample holder. ....	180
<b>Figure A2.</b> Pear core sampling. ....	181
<b>Figure A3.</b> Sample surface with live vegetation at the time of sampling. ....	183
<b>Figure A4.</b> The core bottom being detached from the permafrost at the time of sample uplifting once the core was fully sampled. ....	183
<b>Figure A5.</b> Experimental setup. 1: Symmetrically loaded undisturbed frozen sample being readied for insertion into EH; 2: Close-up of TDR probes inserted into the soil through rectangular holes with aluminum plates around probe heads; 3: Temperature probe inserted through male pipe adapter; 4: TDR probes, temperature probes and sampling ports shown on three different drums; 5: All the four LDPE containers placed in the upper chamber ready to be insulated from outside; 6: Completed and ready for experiments. ....	185
<b>Figure A6.</b> Line diagram showing the experimental setup. 1U: Upper level chamber of the BESM; 1L: Lower level chamber of the BESM; 2: 65-70 cm deep unfrozen layer; 3: 35-40 cm bottom frozen layer (fully saturated before freezing); 4: TDR probes connected to 11 through low-loss coaxial cables; 5: temperature probes connected to 11; 6: heat flux plate; 7: LDPE container lined with neoprene from inside and insulated from outside; 8: stand pipe for water level measurements; 9: weighing scale; 10: custom made stand to support the entire experimental setup; 11: multiplexers and datalogger connected to a personal computer.....	186
<b>Figure A7.</b> The external insulation housing and compressed air circulation around the peat samples. ....	187

## List of Tables

<b>Table 1.1.</b> Column experiments involving study of heat and water transport in frozen soils (not meant to be exhaustive or complete). .....	9
<b>Table 2.2</b> Details of wetting-drying cycles used during TDR calibration in individual peat M samples (peat plateau-bog periphery), and L samples (peat plateau). .....	33
<b>Table 2.3</b> Physical properties of individual peat M samples (peat plateau-bog periphery), and L samples (peat plateau) used in TDR calibration.....	34
<b>Table 2.4</b> Constants of polynomial fit (Equation 2.3) with 95% confidence bounds for combined data from M samples (peat plateau-bog periphery) and L samples (peat plateau), and individual peat samples from the two sampling sites obtained by regression analysis.....	37
<b>Table 2.6.</b> Model parameter values and fitting results (experimental vs predicted) for three phase $\alpha$ mixing model (Equation 2.6), four phase $\alpha$ mixing model (Equation 2.8), and MDL model (Equation 2.9). .....	42
<b>Table 2.7</b> Linear TDR calibration equations including travel time ( $t$ ), bulk electrical conductivity ( $BEC$ ), and effective frequency ( $f_{vi}$ ) terms for M samples (peat plateau-bog periphery) and L samples (peat plateau), and individual peat samples from the two sampling sites. ....	44
<b>Table 3.1.</b> Temperatures in the upper and lower chambers during first and second freezing runs.....	67
<b>Table 5.1.</b> Simulation parameters for heat conduction problem. Analytical solution for this example is given by Equation 5.13 as per Churchill (1972). .....	150
<b>Table 5.2.</b> Simulation parameters for predicting subsurface temperature profile in a semi-infinite porous medium in response to a sinusoidal surface temperature. The analytical solution to this one dimensional heat convection and conduction problem in response to a time varying Dirichlet boundary is given by Equations 5.14-5.17 as per Stallman (1965). .....	154
<b>Table 5.3.</b> Simulation parameters for predicting subsurface temperature profile with phase change in a three zone semi-infinite porous medium. The analytical solution to this	

one dimensional problem with sensible and latent heat zones is given by Equations 5.18-5.25 as per Lundardini (1985).....160

# CHAPTER 1. GENERAL INTRODUCTION

## 1.1. Introduction

Wetland-dominated terrain underlain by discontinuous permafrost covers extensive parts of northern North America and Eurasia. Wetlands cover 14 % of Canada's total land area (NWWG, 1988) and peatlands makeup 97 % of the total Canadian wetland area (Tarnocai, 2006). The wetlands underlain by discontinuous permafrost are mainly made up by peat plateaus, channel fens and ombrotrophic flat bogs (Robinson and Moore, 2000; Quinton *et al.*, 2003). Peat plateaus are underlain by permafrost, and their surfaces rise 1 to 2 m above the surrounding bogs and fens (Quinton and Hayashi, 2005). Mature plateaus support shrubs and trees (*Picea mariana*), with the ground cover composed of lichens and mosses overlying sylvic peat containing dark, woody material and the remains of lichen, rootlets and needles (Quinton and Hayashi, 2005). The hydrologic response of these areas is poorly understood, in large part due to the lack of study on the hydrologic functioning of the major wetland types, and the interaction among them (Quinton and Hayashi, 2008). The relatively high topographic position of the peat plateaus, with slopes leading into flat bogs and channel fens, plays an important role in runoff generation in these regions. In combination with the very low permeability of frozen, saturated peat underneath, the peat plateaus (1) act as 'permafrost dams' that obstruct and re-direct drainage in the surrounding wetlands (Quinton and Hayashi, 2005), (2) quicken the hydrological response of streams to rain and snowmelt (Woo, 1986), and (3) control flow pathways (Quinton *et al.*, 2003). Quinton *et al.* (2003)

found that in wetland dominated zones of discontinuous permafrost, drainage basins with greater percentage of peat plateaus had greater total annual runoff.

Peat layers play a critical role in the hydrology of these regions by providing significant water storage and in process attenuating stream-flow response to rainfall and snowmelt runoff. Peat deposits also play a key role in maintaining permafrost due to their strong insulating property. Presence of permafrost underneath the peat plateaus and the frost table topography play an important role in the runoff generation (Wright, 2009). Occurrence of overland flow is rare on slopes of peat plateaus underlain by permafrost and covered by highly permeable, moist peat (Wright *et al.*, 2009). The runoff generated by snowmelt and/or rain input is largely dominated by subsurface runoff through the active layer of the peat plateaus (Hayashi *et al.*, 2004). The position of the saturated layer largely depends on the depth and distribution of the frost table, which in turns is governed by the soil thaw depth (Woo, 1986).

For successful runoff modeling from the permafrost slopes, it is crucial to understand the factors that control frost table topography (Woo, 1986). There have been numerous field measurement and modeling studies describing the spatial and temporal variation in frost table depths (e.g., Smith, 1975; Hinkel and Nelson, 2003; Wright, 2009). Although field studies have helped advance the knowledge on dynamics of evolution of frost table topography, there is still need for isolating and assessing how different factors govern this evolution. Such understanding is crucial to increasing the precision of hydrological models. Further, with predicted effects of climate change on these regions, only fundamental understanding of the factors such as air temperature, rain

and snowmelt inputs, soil moisture, vegetation, and canopy and snow cover will enhance the predictive ability of models. There is a lack of knowledge on the small-scale spatial and temporal variability of frost table depths on permafrost slopes, including the factors controlling it, and more importantly, how these factor influence runoff generation (Wright *et al.*, 2009). Particularly, there is lack of understanding on how the winter freezing of the active layer affects the positioning of frost table and ice content of active layer. Soil moisture profiles at the onset of winter largely controls the soil water redistribution within the active layer. Along with the over-winter snowmelt, frost induced water redistribution within the active layer plays an important role in positioning of the frost table at the onset of spring melt season. However, it is not clear how the dynamics between these two processes control the frost table topography at the end of winter season (Quinton and Hayashi, 2008).

Field studies are often discontinued, or relegated to field sensors, in winters due to logistical constraints. In addition, it is difficult to understand the role of individual factors in freeze-up of active layer based on field studies alone. In this respect, laboratory Mesocosm studies, under controlled settings, can greatly supplement field observations. It is possible to isolate and assess the effects of individual factors under controlled laboratory settings. Such studies can be largely helpful, especially, in increasing the understanding of winter time processes when field studies are discontinued or relegated to sensors. Further, such studies can help in generating data that can be used in developing and testing mathematical theories that remain under continual development and modifications (e.g., Hansson *et al.*, 2004; Dall'Amico, 2010). In addition to

laboratory studies, numerical models also help greatly to increase the fundamental understanding of active layer freeze-thaw processes. However, such models must be rigorously tested and verified against laboratory and field data.

## **1.2. Coupled heat and water flow in frozen soils**

Water and heat flow in frozen soils are strongly coupled. Temperature gradients result in changes in the moisture-potential field and can induce substantial water movement, both in liquid and vapour form (Hillel, 2004). Moving water carries heat and changes the thermal properties of soils. Such coupled movement may not be important in fully saturated or nearly dry soils (as water may not move inside the saturated or nearly dry conditions), but is an important phenomenon for variably wetted soils (unsaturated or unsaturated above water table). In frozen soils, such coupled movement is much more significant as effects of freezing on soil moisture-potential field results in even greater water movement from warmer to colder regions.

In unsaturated soil, water moves by both vapour diffusion and by liquid flow in adsorbed water films (Smith and Burns, 1987). The most simplistic explanation of liquid water movement in unsaturated soils would be that of flow under potential gradients. Total soil water potential in unsaturated soils is a result of a number of forces acting on pore water. Attraction of water to the solid matrix (called matric potential or soil pressure potential) is a result of adhesion forces and surface tension. Osmotic potential is a result of solutes influencing the potential of pure water, whereas elevation differences change the potential due to gravity effects. Other forces are usually ignored and total potential can be assumed to be sum of matric potential, gravity potential and osmotic potential (if

known). Liquid water movement can occur because of differences in the total potential between any two points in the soil. Water movement in soils can also occur due to vapour transport as reported by Smith and Burn (1987), Woo (1982) and Kane *et al.* (2001) for frozen soils. Water vapour movement occurs through diffusion processes in the soil as vapour pressure gradients drive water vapour towards lower surface temperatures. Because of temperature differences, vapour pressure gradients exist in unsaturated frozen soils. Such gradients result in water vapour concentration gradients within the pore air and, as a consequence, vapour diffusion will occur through the pores from warm to cold regions. In this way, vapour transport directly augments conductive heat transfer since the latent heat associated with moisture vapour movement is transported in the direction of the temperature gradient (Kane *et al.*, 2001). Such movement is partially responsible for the development of depth hoar within arctic snow packs (Santeford, 1978). Although as argued by Smith and Burn (1987) that movement along connected liquid films is the main mechanism behind sustained (for entire winter) water movement in frozen soils, Santeford (1978) show that water vapour contribution can also be significant, especially in wet soils. Results of Santeford (1978) show that a large amount of water (> 2 cm depth equivalent) can be transported upwards due to vapour movement at wet sites, especially those covered with high porosity moss.

Heat in unsaturated soils is predominantly assumed to move by conductive transfer. However, in frozen soils non-conductive heat transfer by water (advection) and water vapour could be significant, and frequently are for specific periods the dominant modes of heat transfer near the ground surface (Kane *et al.*, 2001). Advective heat

transfer can be of greater importance, especially in peat, during infiltration at the start of thaw season. The migration of water in response to temperature effects on moisture-potential fields from unfrozen soil depths to the freezing front, and the redistribution of moisture within the frozen soil from warmer depths to colder depths, can also result in heat transfer.

### **1.3. Laboratory column experiments with frozen soils**

There have been very few soil column/Mesocosm studies on frozen soils under controlled laboratory settings in general and there have been none that examine the freeze-thaw hydrological functions of peat. Freeze-thaw studies on mineral soil columns under controlled laboratory settings, aimed at studying different aspects of frozen soils, have been reported in literature (Table 1.1). Experiments of Dirksen (1964), Hoekstra (1966), and Mizoguchi (1990) were aimed at understanding water redistribution towards the freezing front. Jame (1977) and Fukuda *et al.* (1980) performed a series of column experiments in order to understand how the processes of heat and water movement affect each other. Cary and Maryland (1972), Staehli and Stadler (1997) and Gergely (2007) conducted column experiments to understand water and solute movement in frozen mineral soils. All these experiments have established that soil temperatures below freezing induce significant water redistribution from unfrozen to frozen zones and increased the fundamental understanding of freeze-thaw processes in frozen mineral soils. For example, Dirksen (1964) reported that not only soil water movement took place from unsaturated unfrozen soil to the freezing front, but also the total water and ice content behind the freezing front continued to increase with time over an extended region.

Dirksen (1964) also suggested through his experiments that water migration in frozen soil took place mainly as liquid flow.

There have been no column experiments targeting the same processes in organic soils. Organic soils can hold far more amounts of water as compared to mineral soils because of their larger porosities, and therefore there can be far greater movement of water from unfrozen to frozen zones during freezing. Also, soil wetness may exhibit far greater influence in organic soils than in mineral soils given the fact that reduction of liquid water from pores due to water movement or freezing can have significant effects on hydraulic conductivity of unsaturated zones in peat. While Rezanezhad *et al.* (2009) show that increasing air content in unsaturated peat greatly affects unsaturated hydraulic conductivities, there is very little work being done on hydraulic conductivity of frozen organic soils. A recent attempt by Watanabe *et al.* (2011) to parameterize unsaturated hydraulic conductivity of frozen mineral soils is noteworthy. They used a combination of short column experiments and numerical simulation to parameterize unsaturated hydraulic conductivity of frozen soils. However, such attempts still use the generalized Clausius–Clapeyron equation (CCE) to correlate temperatures with soil matric potential. A very few studies (e.g., Williams 1967), have shown this correlation through experimental work and most have been for mineral soils. Andersland *et al.* (1995) measured hydraulic conductivity of frozen unsaturated gravelly sands (at different initial water content and frozen to  $-10^{\circ}\text{C}$ ) using antifreeze (decane) as a permeant in a falling head permeameter immersed in a constant temperature bath. Nixon (1991) reviewed the work of nine researchers done between 1982 and 1985 who determined hydraulic

conductivity for frozen fine grained soils under pressure gradients (e.g., Smith, 1985) or temperature gradients (Oliphant *et al.*, 1983). The experimental setup required for such tests is discussed by Andersland and Ladanyi (2004). More experimental verification, especially in frozen peat, is required to increase our understanding of how the matric potential is affected in frozen peat in order to further increase the precision of numerical models.

References	Soil type, $\rho_b$ , $\eta$	Column dimensions	Upper boundary <sup>1</sup>	Lower boundary <sup>1</sup>	Comments
Hoekstra (1966)	Silt, $1670 \text{ kgm}^{-3}$ , $0.36 \text{ m}^3\text{m}^{-3}$	11.43 cm x 15.24 cm	Hollow Brass plate with circulating fluid, [-10 °C]	Thermally insulated, [N.A]	Heat and water movement was investigated
Cary and Mayland (1972)	Silt Loam, $1200 - 1350 \text{ kgm}^{-3}$ , N.S Silty Clay, $1100 - 1250 \text{ kgm}^{-3}$ , N.S	3.7 cm x 24 cm	Not mentioned, [-6.5 °C]	Not mentioned, [-0.5 °C]	Water, heat and salt movement was investigated
Jame (1977)	Silica Flour, $1330 \text{ kgm}^{-3}$ , $0.49 \text{ m}^3\text{m}^{-3}$	10.7 cm x 30 cm	Hollow Brass plate with circulating fluid, [-10 °C, -5.9 °C, -5.3 °C]	Hollow Brass plate with circulating fluid, [20 °C, 4.2 °C, 5 °C]	Heat and water movement was investigated
Fukuda <i>et al.</i> (1980)	Silt, various, various	10 cm x 10 cm x 10 cm <sup>2</sup>	Hollow Brass plate with circulating fluid, [various]	Cooling chamber with circulating fluid, [various]	Heat and water movement was investigated. Multiple columns were used with different physical properties and end boundary temperatures
Mizoguchi (1990)	Sandy Loam, $1300 \text{ kgm}^{-3}$ , $0.535 \text{ m}^3\text{m}^{-3}$	8 cm x 20 cm	Hollow Brass plate with circulating fluid, [-6 °C]	Thermally insulated, [N.A]	Only water movement was investigated
Staehli and Stadler (1997)	Sand, $1090 \text{ kgm}^{-3}$ , N.S Loam, $390 \text{ kgm}^{-3}$ , N.S	12 cm x 20 cm	Exposed to air in a refrigerator, [-5 °C, 3 °C] <sup>3</sup>	Copper plate, [-5 °C, 3 °C]	Water, heat and solute movement was investigated
Gergely (2007)	Sand, N.S, $0.3-0.4 \text{ m}^3\text{m}^{-3}$	24 cm x 100 cm	Exposed to air in a cold room, [-15 °C, 15 °C] <sup>3</sup>	Cooling plate, [-3 °C]	Water, heat and solute movement was investigated

<sup>1</sup>Method of applying boundary condition, [end boundary temperature]; <sup>2</sup>Square columns were used; <sup>3</sup>Freezing and thawing cases were investigated;  $\rho_b$  – bulk density;  $\eta$  – total porosity; N.S – not specified; N.A. not applicable

**Table 1.1.** Column experiments involving study of heat and water transport in frozen soils (not meant to be exhaustive or complete).

#### 1.4. Numerical models with frozen schemes

Incorporating soil freeze-thaw processes in land-surface schemes is important for detailed simulations of hydrological processes. Models with fully formulated frozen soil simulation modules do a better job of simulating soil temperatures and soil water storage (e.g., Luo *et al.*, 2003; Wang *et al.*, 2010). Zhang *et al.* (2008) categorized the frozen soil models into three broad classes: empirical and semi empirical, analytical, and numerical physically-based. Empirical and semi empirical algorithms relate ground thawing-freezing depths (GTFD) to surface temperature by observation based coefficients (e.g., Quinton and Gray, 2001; Anisimov *et al.*, 2002). Analytical algorithms are specific solutions to heat conduction problems. These algorithms ignore volumetric heat removal and water redistribution towards the freezing front. Stefan's formula (Stefan, 1889 as cited by Aldrich and Paynter, 1966), modified Berggren equation (Aldrich and Paynter, 1966) and Hayashi's modified Stefan's algorithm (Hayashi *et al.*, 2007) are examples of analytical algorithms. Numerical physically-based algorithms simulate ground freezing by solving the Richard's and the complete energy equations using some numerical method. This class of models are the most accurate for both GTFD (Zhang *et al.*, 2008) and coupled heat and water movement as used in water balance studies (e.g., Wang *et al.*, 2010).

Coupled heat and water movement in soils, with or without phase change, is a highly non-linear mathematical problem. The non-linearity arises from dependency of hydraulic and thermal properties of soil and pressure head on soil water content, phase state and temperature of the soil. A number of models have been reported in literature

that solve the coupled Richard's and energy equations for unsaturated frozen/unfrozen soils using finite difference (e.g., Harlan, 1973; SHAW model by Flerchinger and Saxon, 1989; SOIL model by Jansson, 1998; HYDRUS by Simunek *et al.* 1998 and Hansson *et al.*, 2004), finite element (e.g., Guymon and Luthin, 1974; Guymon *et al.*, 1993) and finite volume (e.g., Engelmark and Svensson, 1993; Painter, 2010) methods.

Mathematical theory to simulate the freeze-thaw processes along with coupled heat and water transport in soils remain under continuing development and refinement (e.g., Hansson, 2004; Dall'Amico, 2010). The problem of coupled heat and water transport along with phase change is traditionally solved by Harlan's method (Harlan, 1973). In Harlan's approach it is assumed that there is analogy between heat and water movement in unfrozen- and frozen unsaturated soils. In other words, soil drying in unfrozen soils and soil freezing in frozen ground are assumed to be similar processes with exception of latent heat during phase change. The temperature induced potential gradient is assumed to be the major driving force behind mass movement and CCE is used to convert from temperature to soil matric potential assuming zero ice gauge pressure. Although the use of the CCE needs to be further verified studies (e.g., Williams, 1967) have experimentally shown that it predicts the temperature – soil matric potential relationship with fair degree of accuracy.

## **1.5. Research objectives**

The column experiments listed in Table 1.1 used a combination of cooling and heating plates, or a plate on one end with the other end exposed in refrigerator/cold room to simulate end boundary conditions. However, this is not sufficient for permafrost

studies as the influence of deeper frozen sections cannot be simulated. Using plates as boundary conditions does not create realistic replication of field permafrost conditions or the bidirectional freezing of the active layer, and hence, the influence of subsurface thermal properties on near surface energy balance is not the same. Study of coupled heat and water movement in frozen peat is important to increase our fundamental understanding of factors affecting the development of frost table topography, which strongly affects the runoff generation in wetland dominated, organic covered discontinuous permafrost regions of Canada. Of particular interest is to quantify the moisture dynamics at the active-layer and develop numerical models for estimating the position of frozen impermeable surface at the onset of spring. Such estimation is critically dependant on a fundamental understanding of role of different factors (e.g., soil moisture at onset of freezing) on development of this surface during freezing period. These dynamics need to be understood in order to estimate the volume and timing of runoff from wetland-dominated basins in discontinuous permafrost zones.

There are three main objectives of this study:

(1) *To build and validate a unique experimental setup involving a saturated, frozen layer of repacked peat at the base of undisturbed peat columns:* This study describes a new experimental setup that uses a base saturated, frozen layer to represent proxy permafrost in Mesocosm studies conducted on undisturbed peat samples. The two level biome (climate chamber) at the Biotron facility of the University of Western Ontario makes it possible to maintain a frozen section near column bottoms, and apply a wide range of boundary conditions to the column tops. This facility thus allows a close replication of an

active layer exposed to the atmosphere at the top and bounded by permafrost at the bottom.

Instrumentation plays a crucial role in success of monitoring key parameters in any field or laboratory experiments. Time domain reflectometry (TDR) was used to monitor liquid water content in unfrozen and frozen states of peat. Before applying TDR in determining moisture content, it was calibrated using undisturbed peat samples and effects of temperature and air content on calibration was studied in detail.

*(2) Use the unique setup to study effects of initial moisture profiles on freezing processes in peat:* The effects of freezing on soil temperature and water movement were monitored in four peat Mesocosms subjected to bidirectional freezing. Temperature gradients were applied by bringing the Mesocosm tops in contact with sub-zero air temperature while maintaining a continuously frozen layer at the bottom (proxy permafrost). Frost propagation and frost induced soil water redistribution was studied in four peat Mesocosms maintained at different initial soil moisture profiles. This experiment was conducted in order to understand the role of initial soil moisture in setting up the frost table and soil water redistribution. More specifically, the experiment was conducted to understand the key issue of frost table positioning at the end of winter season by correlating the results with field observations.

*(3) Develop a simple numerical model to simulate coupled heat and water movement in soils:* A one-dimensional model based on coupled cellular automata approach is presented in this study in which local laws based purely on empirical equations and with a clear physical meaning govern interactions among elementary cells. Buckingham-Darcy's law

and Fourier's heat law are used to define the local interactions for water and heat movement respectively. In addition to the novelty of using cellular automata for coupled heat and water transport in soils, phase change was handled based solely on soil freezing curves, and updating of heat capacity was done in a more natural way by avoiding use of apparent heat capacity as traditionally used in numerical models.

## **1.6. Thesis organization**

This thesis consists of a series of manuscripts for publication in peer-reviewed journals (Chapters 2 to 5), together with a general introduction (Chapter 1) and conclusion (Chapter 6). The manuscripts are reproduced here in a format consistent with thesis requirements. Chapter 2 describes the detailed laboratory calibration of time domain reflectometry to determine moisture content in undisturbed peat. Chapter 2 is a modification of an accepted original manuscript (European Journal of Soil Science) and is reproduced here with permission. Chapter 3 describes the experimental setup, and validation of the experimental setup. The validation exercise is first of its kind for laboratory experiments involving freeze-thaw processes. Chapter 4 describes the effects of initial soil moisture profiles on frost induced water redistribution, frost propagation, and thermal properties of frozen peat. Chapter 5 describes development of a one-dimensional model based on coupled cellular automata approach to simulate coupled heat and water movement in frozen soils. Chapters 3, 4 and 5 are modifications of manuscripts ready to be submitted for publication in peer-reviewed journals.

## 1.7. References

- Aldrich, H. P., and H. M. Paynter (1966). Depth of frost penetration in non-uniform soil, *CRREL Special Report 104*, US Army Cold Regions Research and Engineering Laboratory, Hannover, 148 pp.
- Andersland, O. B., S. H. Davies, and D. C. Wiggert (1995). Performance and formation of frozen containment barriers in dry soils, *Report to RUST Geotech, Inc.*, Grand Junction, Colorado.
- Andersland, O. B., and B. Ladanyi (2004). Frozen ground engineering, John Wiley and Sons, Inc., Hoboken, New Jersey.
- Anisimov, O. A., N. I. Shiklomanov, and F. E. Nelson (2002). Variability of seasonal thaw depth in permafrost regions: a stochastic modeling approach, *Ecol. Model.* **153**, 217-227.
- Cary, J. W., and H. F. Mayland (1972). Salt and water movement in unsaturated frozen soil, *Soil Science Society of America Proceedings* **36**, 549-555.
- Dall'Amico, M. (2010). Coupled water and heat transfer in permafrost modeling, Ph.D. Thesis, University of Trento, Italy.
- Dirksen, C. (1964). Water movement and frost heaving in unsaturated soil without an external source of water, Ph.D. Thesis, Cornell University, United States.
- Engelmark, H., and U. Svensson (1993). Numerical modeling of phase-change in freezing and thawing unsaturated soil, *Nordic Hydrol.* **24**, 95-110.
- Flerchinger, G. N., and K. E. Saxton (1989). Simultaneous heat and water model of a freezing snow-residue-soil System .1. Theory and Development, *Trans.ASAE* **32**, 565-571.

- Fukuda, M., A. Orhun, and J. N. Luthin (1980). Experimental studies of coupled heat and moisture transfer in soils during freezing, *Cold Reg.Sci.Technol.* **3**, 223-232.
- Gergely, M. (2007). Dynamics of a salty permafrost, M.Sc. Thesis, University of Heidelberg, Germany.
- Guymon, G. L., R. L. Berg, and T. V. Hromadka (1993). Mathematical model of frost heave and thaw settlement in pavements, *CRREL Special Report 93-2*, US Army Cold Regions Research and Engineering Laboratory, Hannover, 130 pp.
- Guymon, G. L., and J. N. Luthin (1974). Coupled heat and moisture transport model for Arctic soils, *Water Resour.Res.* **10**, 995-1001.
- Hansson, K., J. Simunek, M. Mizoguchi, L. C. Lundin, and M. T. van Genuchten (2004). Water flow and heat transport in frozen soil: Numerical solution and freeze-thaw applications, *Vadose Zone Journal* **3**, 693-704.
- Harlan, R. L. (1973). Analysis of coupled heat-fluid transport in partially frozen soil, *Water Resour.Res.* **9**, 1314-1323.
- Hayashi, M., W. L., Quinton, A., Pietroniro, and J. J., Gibson, J.J (2004). Hydrologic functions of wetlands in a discontinuous permafrost basin indicated by isotopic and chemical signatures. *J Hydrol*, 296:81-97.
- Hayashi, M., N. Goeller, W. L. Quinton, and N. Wright (2007). A simple heat-conduction method for simulating the frost-table depth in hydrological models, *Hydrol.Process.* **21**, 2610-2622.
- Hillel, D. (2004). Introduction to environmental soil physics, *Elsevier Academic Press*, San Diego, USA.

- Hinkel, K. M., and F. E. Nelson (2003). Spatial and temporal patterns of active layer thickness at Circumpolar Active Layer Monitoring (CALM) sites in northern Alaska, 1995-2000, *Journal of Geophysical Research-Atmospheres* **108**, 8168, 13pp.
- Hoekstra, P. (1966). Moisture movement in soils under temperature gradients with cold-side temperature below freezing, *Water Resour.Res.* **2**, 241-250.
- Jame, Y. (1977). Heat and mass transfer in freezing unsaturated soil, Ph.D. Thesis, The University of Saskatchewan, Canada.
- Jansson P-E. (1998). Simulating model for soil water and heat conditions: Description of SOIL model, Swedish University of Agricultural Sciences, Uppsala, 86pp.
- Kane, D.L., K. M. Hinkel, D. J. Goering, L. D. Hinzman, and S. I. Outcalt (2001). Non-conductive heat transfer associated with frozen soils, *Global and Planetary Change.* **29**, 275–292.
- Luo, L. F., A. Robock, K. Y. Vinnikov, C. A. Schlosser, A. G. Slater, A. Boone, H. Braden, P. Cox, P. de Rosnay, R. E. Dickinson, Y. J. Dai, Q. Y. Duan, P. Etchevers, A. Henderson-Sellers, N. Gedney, Y. M. Gusev, F. Habets, J. W. Kim, E. Kowalczyk, K. Mitchell, O. N. Nasonova, J. Noilhan, A. J. Pitman, J. Schaake, A. B. Shmakin, T. G. Smirnova, P. Wetzol, Y. K. Xue, Z. L. Yang, and Q. C. Zeng (2003). Effects of frozen soil on soil temperature, spring infiltration, and runoff: Results from the PILPS 2(d) experiment at Valdai, Russia, *J.Hydrometeorol.* **4**, 334-351.
- Mizoguchi, M. (1990). Water, heat and salt transport in freezing soil, Ph.D. Thesis, University of Tokyo, Tokyo.
- National Wetlands Working Group (NWWG). (1988). Wetlands of Canada: Ecological land classification series, **24**. Sustainable development branch, Environment Canada, Ottawa, and Polyscience Publications Inc., Montreal, 452 pp.

- Nixon, J. F. (1991). Discrete ice lens theory for frost heave in soils, *Can. Geotech. J.*, **28(6)**, 843-859.
- Oliphant, J. L., A.R. Tice, and Y. Nakano (1983). Water migration due to a temperature gradient in frozen soils, *Proc. 4<sup>th</sup> Int. Conference on Permafrost, Fairbanks, Alaska, National Academy Press, vol 1, pp. 951-956*, Washington, D.C.
- Painter, S. (2010). Three-phase numerical model of water migration in partially frozen geological media: model formulation, validation, and applications, *Computational Geosciences*, **15(1)**, 69-85.
- Quinton, W. L., and M. Hayashi (2008). Recent advances toward physically-based runoff modeling of the wetland-dominated central Mackenzie River Basin, in *Cold Region Atmospheric and Hydrologic Studies. The Mackenzie GEWEX Experience: Volume 2: Hydrologic Processes*, M. Woo (Editor), Vol. 2, Springer, Berlin. 257-279.
- Quinton, W. L., and M. Hayashi (2005). The flow and storage of water in the wetland-dominated central Mackenzie river basin: Recent advances and future directions, in *Prediction in ungauged basins: Approaches for Canada's cold regions*, C. Spence *et al.* (Editor), Canadian Water Resources Association, 45-66.
- Quinton, W. L., and D. M. Gray (2001). Estimating subsurface drainage from organic-covered hillslopes underlain by permafrost: toward a combined heat and mass flux model, *Soil-Vegetation-Atmosphere Transfer Schemes and Large-Scale Hydrological Models* 333-341.
- Quinton, W. L., M. Hayashi, and A. Pietroniro (2003). Connectivity and storage functions of channel fens and flat bogs in northern basins, *Hydrol.Process.* **17**, 3665-3684.
- Rezanezhad, F., W. L. Quinton, J. S. Price, D. Elrick, T. R. Elliot, and R. J. Heck (2009). Examining the effect of pore size distribution and shape on flow through unsaturated

- peat using computed tomography, *Hydrology and Earth System Sciences* **13**, 1993-2002.
- Robinson, S. D., and T. R. Moore (2000). The influence of permafrost and fire upon carbon accumulation in high boreal peatlands, Northwest Territories, Canada, *Arctic Antarctic and Alpine Research* **32**, 155-166.
- Santeford, H.S. (1978). Snow soil interactions in interior Alaska. In: Colbeck, S.C. and Ray, M. (eds.), *Modelling of Snow Cover Runoff. US Army Cold Regions Research and Engineering Laboratory*, Hanover, NH. pp. 311--318.
- Šimůnek, J., K. Huang, and M. Th. van Genuchten. (1998). The HYDRUS code for simulating the one-dimensional movement of water, heat, and multiple solutes in variably-saturated media. Version 6.0. 144, 1-164.
- Smith, M. W., and C. R. Burn (1987). Outward flux of vapour from frozen soils at Mayo, Yukon, Canada: Results and interpretation, *Cold Regions Sci. Technol.*, **13**: 143-152.
- Smith, M. W. (1985). Observations of soil freezing and frost heave at Inuvik, Northwest Territories, Canada, *Can. Geotech. J.*, **22(2)**, 283-290.
- Smith, M. W. (1975). Microclimatic influences on ground temperatures and permafrost distribution, Mackenzie Delta, Northwest Territories, *Canadian Journal of Earth Sciences* **12**, 1421-1438.
- Stahli, M., and D. Stadler (1997). Measurement of water and solute dynamics in freezing soil columns with time domain reflectometry, *Journal of Hydrology* **195**, 352-369.
- Stefan, J. (1889). On the theory of ice formation, particularly ice formation in the Arctic ocean, S-B Wien Academy **98**, 173 pp.

- Tarnocai, C. (2006). The effect of climate change on carbon in Canadian peatlands, *Global Planet.Change* **53**, 222-232.
- Wang, L., T. Koike, K. Yang, R. Jin, and H. Li (2010). Frozen soil parameterization in a distributed biosphere hydrological model, *Hydrology and Earth System Sciences* **14**, 557-571.
- Watanabe, K., T. Kito, T. Wake, and M. Sakai (2011). Freezing experiments on unsaturated sand, loam and silt loam, *Annals of Glaciology* **52**, 37-43.
- Williams, P. J. (1967). Properties and behavior of freezing soils, Norwegian Geotechnical Institute, Research paper # 359, 128pp.
- Woo, M. (1986). Permafrost hydrology in North America, *Atmosphere-Ocean* **24**, 201-203.
- Woo, M. K. (1982). Upward flux of vapour from frozen materials in the high arctic. *Cold Regions Sci. Technol.*, **5**(3): 269-274.
- Woo, M. K., and R. Heron (1981). Occurrence of ice layers at the base of high arctic snowpacks. *Arctic and Alpine Res.*, **13**(2): 225-230.
- Wright, N. (2009). Water and energy fluxes from a permafrost peat plateau: Examining the controls on runoff generation, Ph.D. Thesis, Simon Fraser University, Canada.
- Wright, N., M. Hayashi, and W. L. Quinton (2009). Spatial and temporal variations in active layer thawing and their implication on runoff generation in peat-covered permafrost terrain, *Water Resour.Res.* **45**, W05414, 13 pp.
- Zhang, Y., S. K. Carey, and W. L. Quinton (2008). Evaluation of the algorithms and parameterizations for ground thawing and freezing simulation in permafrost regions, *Journal of Geophysical Research-Atmospheres* **113**, D17116.

# **CHAPTER 2. LABORATORY CALIBRATION OF TIME DOMAIN REFLECTOMETRY TO DETERMINE MOISTURE CONTENT IN UNDISTURBED PEAT SAMPLES**

## **2.1. Introduction**

Accurate vadose zone soil water content measurement is a critical requirement in coupled heat and moisture transport studies. Volumetric soil water content ( $\theta$ ) largely controls the insulation effectiveness of the active layer in peat. Thermal conductivity of wet peat can be as much as 15 times greater than that of the same peat when dry and can vary significantly for a given total water content when ground temperature is below freezing and depending upon the fractions of ice and water. Time domain reflectometry (TDR) is widely used to measure soil water content and bulk electrical conductivity. Topp *et al.* (1980) reported the first application of TDR to soil water measurement. TDR has fast become a method of choice for many researchers because it offers reasonably improved accuracies (usually within 2% of volumetric water content once carefully calibrated), elimination of radiation hazards associated with neutron probe and gamma ray attenuation methods and ease of measurement because data loggers can be used. In addition, TDR can be used to monitor water level measurements (Moret *et al.*, 2004), the position of the advancing frost table in freezing soils (Overduin and Kane, 2006), and contaminated zones below the water table. TDR measurements can be converted to soil

water content by using empirical calibrations or multi-phase mixing models. Topp *et al.* (1980) gave a near universal calibration equation, chiefly applicable to mineral soils, with exception of large clay content and fine grained soils (Dirksen and Dasberg, 1993). In contrast, a universal calibration may not be applicable to organic soils because they are very porous and have large surface areas which bind substantial amounts of water.

While TDR calibrations have been performed in organic soils (Yoshikawa *et al.*, 2004; Kellner and Lundin, 2001; Pepin *et al.*, 1992; Roth *et al.*, 1992; Topp *et al.*, 1980), the calibrations are highly variable due to differences in origin of the organic matter and degree of decomposition (Oleszczuk *et al.*, 2007). Though there seems to be an agreement on the highly variable nature of these calibrations, there is no agreement on why there is deviation from calibrations in mineral soils. We used TDR to monitor unfrozen water content and bulk soil electrical conductivity (BEC) during freeze-thaw experiments on large-scale undisturbed peat Mesocosms. Given the large variability of TDR calibrations in peat, it was decided to perform the necessary calibration studies for the peat soils from our study site located near Fort Simpson, Northwest Territories, Canada. The objectives of this study were to assess the applicability of other published calibration equations and to recognize the most critical factors affecting the widely reported deviations of TDR calibrations in organic soils. Such clarification is critical to further applicability of mixing models, which in turn can save time and effort required to determine a complete TDR calibration curve. Because of wide range of temperature variations during the peat Mesocosm experiments, we also studied the effects of temperature on the measurements of  $\theta$  and BEC. Further, we tested the approach of Evett

*et al.* (2005) to determine the effect of BEC on TDR calibration as this has not yet been explored in organic soils.

### 2.1.1. Basic Principles

TDR exploits the high relative permittivity of free water ( $\epsilon_{fw}$  approximately 76.58 @ 30 °C) in a three-, four- and five-phase soil system to determine the quantity of soil water present. By comparison, the other phases, air ( $\epsilon_a$  approximately 1), soil solids ( $\epsilon_s$  approximately 2 – 11), bound water ( $\epsilon_{bw}$ = 3.15) and ice ( $\epsilon_i$  approximately 3.2), have remarkably different relative permittivities. A fast rising high frequency electromagnetic pulse (EM pulse) is generated and sent along a coaxial cable to a waveguide of known length ( $L$ ). When this short-lived EM pulse travels along a waveguide that is completely embedded in soil, an electrical field is formed around the rods. The time ( $t$ ) taken to travel the length of the waveguide and back ( $2L$ ) is recorded and used to calculate bulk (apparent) relative permittivity ( $\epsilon$ ) of the medium as:

$$\epsilon = \left(\frac{c}{v}\right)^2 = \left(\frac{ct}{2L}\right)^2 \quad (2.1)$$

where  $c$  is the speed of electromagnetic waves in a vacuum ( $3 \times 10^8 \text{ m s}^{-1}$ ) and  $v$  is the velocity of the pulse through soil medium along the waveguide.

Bulk electrical conductivity can be estimated by analysing the change in shape of TDR waveform as first shown by Giese and Tiemann (1975). Further equations based on the TDR waveform analysis to estimate BEC were proposed by Dalton *et al.* (1984), Topp *et al.* (1988), Zegelin *et al.* (1989) and others. All equations are of following form:

$$BEC = K_p \cdot G \quad (2.2)$$

where  $K_p$  is probe constant and  $G$  is the electrical conductance of the calibration medium. The probe constant was calibrated by using solutions of different electrical conductivities as proposed by Castiglione and Shouse (2003).

### 2.1.2. Empirical calibrations and dielectric mixing models

Both empirical equations and mixing models have been used widely to relate measured  $\varepsilon$  to  $\theta$ . Empirical equations simply fit a mathematical model of measured  $\varepsilon$  to gravimetrically determined  $\theta$ , while mixing models in their simplest form use dielectric permittivity and volumetric fraction of each soil phase (solids, air and water) to derive a relationship describing bulk soil dielectric permittivity (Jones *et al.*, 2002). Most empirical equations developed for soils have a third order polynomial form such that:

$$\theta = b_0 + b_1 \cdot \varepsilon + b_2 \cdot \varepsilon^2 + b_3 \cdot \varepsilon^3 \quad (2.3)$$

where the constants  $b_0$ ,  $b_1$ ,  $b_2$  and  $b_3$  are derived for various soils (Table 2.1). Empirical equations are the most accurate ways of correlating  $\varepsilon$  to  $\theta$  since calibration could depend upon unique physical characteristics of a soil.

Malicki, *et al.* (1996) presented empirical relationships that accounted for soil bulk density and porosity ( $\eta$ ) effects using a large dataset representing a broad range of soils:

$$\theta(\varepsilon, \rho_b) = \frac{\sqrt{\varepsilon - 0.819 - 0.618\rho_b - 0.519\rho_b^2}}{7.17 + 1.18\rho_b} \quad (2.4)$$

$$\theta(\varepsilon, \eta) = \frac{\sqrt{\varepsilon} - 3.47 - 6.22\eta - 3.82\eta^2}{7.01 + 6.89\eta - 7.83\eta^2} \quad (2.5)$$

Reference	Soil type <sup>a</sup>	$b_0$	$b_1$	$b_2$	$b_3$
Topp <i>et al.</i> (1980)	M	$-5.30 \times 10^{-2}$	$2.92 \times 10^{-2}$	$-5.50 \times 10^{-4}$	$4.30 \times 10^{-6}$
Roth <i>et al.</i> (1992)	M+O	$2.33 \times 10^{-2}$	$2.85 \times 10^{-2}$	$-4.31 \times 10^{-4}$	$3.04 \times 10^{-6}$
Pepin <i>et al.</i> (1992)	O	$8.50 \times 10^{-2}$	$1.92 \times 10^{-2}$	$-0.95 \times 10^{-4}$	0
Kellner and Lundin (2001)	O	$3.90 \times 10^{-2}$	$3.17 \times 10^{-2}$	$-4.50 \times 10^{-4}$	$2.6 \times 10^{-6}$
Yoshikawa <i>et al.</i> (2004) <sup>b</sup>	O <sup>c</sup>	-0.6286	0.4337	$-5.49 \times 10^{-2}$	$0.33 \times 10^{-2}$
Yoshikawa <i>et al.</i> (2004) <sup>b</sup>	O <sup>d</sup>	-0.1625	0.1108	$-0.21 \times 10^{-2}$	$4.33 \times 10^{-4}$

<sup>a</sup>M- Mineral soils, O- Organic soils, M+O- Mineral soils with 10 – 55 % organic content.

<sup>b</sup> $\theta = b_0 + b_1(\sqrt{\varepsilon}) + b_2(\sqrt{\varepsilon})^2 + b_3(\sqrt{\varepsilon})^3$ ; <sup>c</sup>Dead *Sphagnum* moss; <sup>d</sup>Live *Sphagnum* moss.

**Table 2.1** Constants of empirical models (Equation 2.3) relating apparent dielectric permittivity to volumetric soil moisture in different types of soils.

Dielectric mixing models fall in the class of empirical models to correlate  $\varepsilon$  to  $\theta$ . These can be divided into two categories: (a)  $\alpha$ -models that use a curve fitting parameter ( $\alpha$ ) and (b) the Maxwell-De Looor (MDL) model as stated by Dobson *et al.* (1985). Some researchers have assumed  $\alpha$  to be a parameter that characterizes the geometry of the

medium in relation to the axial direction of the wave guide such that  $-1 \leq \alpha \leq 1$  (Roth *et al.*, 1990). However, there is no experimental validation of this concept, and therefore  $\alpha$  can be defined alternatively as a curve fitting parameter. The three phase  $\alpha$ -mixing model (Roth *et al.*, 1990) can be stated as:

$$\theta = \frac{\epsilon^\alpha - (1-\eta)\epsilon_s^\alpha - \eta\epsilon_a^\alpha}{\epsilon_w^\alpha - \epsilon_a^\alpha} . \quad (2.6)$$

Birchak *et al.* (1974) found a value of  $\alpha = 0.5$  for an isotropic and homogenous medium calculated from the travel time of electromagnetic waves (Roth *et al.*, 1990). Dobson *et al.* (1985) proposed the four phase  $\alpha$ -mixing model that is inclusive of the bound water fraction and separates  $\theta$  into free ( $\theta_{fw}$ ) and bound ( $\theta_{bw}$ ) water. Bound water is a term used for sorbed water in films around soil solids which in general has less mobility as compared with free water. In peat, water sorbed by peat fibers can also be characterized as bound water. The amount of bound water depends upon the number of mono-layers sorbed around soil solids ( $l_n$ ), soil specific surface area ( $A_s$ ), the thickness of each monolayer ( $\delta$ ) and the bulk density of soil ( $\rho_b$ ); it and can be calculated as:

$$\theta_{bw} = l_n \delta A_s \rho_b . \quad (2.7)$$

In most cases,  $l_n$  is assumed to be 1 and  $\delta = 3 \text{ \AA}$  ( $3 \times 10^{-10} \text{ m}$ ), while the soil specific surface area can be measured by employing methods such as liquid-phase adsorption, gas-phase adsorption and retention of polar liquids (Pennell, 2002). When solved for  $\theta$  this model yields

$$\theta = \frac{\varepsilon^\alpha - \theta_{bw}(\varepsilon_{bw}^\alpha - \varepsilon_{fw}^\alpha) - (1-\eta)\varepsilon_s^\alpha - \eta\varepsilon_a^\alpha}{\varepsilon_{fw}^\alpha - \varepsilon_a^\alpha} \quad (2.8)$$

Dobson *et al.* (1985) found that  $\alpha = 0.65$  after introducing bound water as a fourth phase. However, many researchers have used  $\alpha$  simply as a curve fitting parameter and have obtained values between 0.26 and 0.65 (Kellner and Lundin, 2001; Roth *et al.*, 1990; Dobson *et al.*, 1985).

The Maxwell-De Looer (MDL) model is a four phase mixing model that solely includes physical parameters of the multi-phase soil system. The key assumption in MDL model is that soil solid phase is the primary medium with water and air as inclusions and there is no interaction between adjacent soil particles. This model can be solved to obtain  $\theta$ :

$$\theta = \frac{3(\varepsilon_s - \varepsilon) + \theta_{bw} \left( 2(\varepsilon_{bw} - \varepsilon_{fw}) - \varepsilon \varepsilon_s \left( \frac{1}{\varepsilon_{bw}} - \frac{1}{\varepsilon_{fw}} \right) \right) + \eta \left( 2(\varepsilon_a - \varepsilon_s) - \varepsilon \varepsilon_s \left( \frac{1}{\varepsilon_a} - \frac{1}{\varepsilon_s} \right) \right)}{\varepsilon \varepsilon_s \left( \frac{1}{\varepsilon_{fw}} - \frac{1}{\varepsilon_a} \right) + 2(\varepsilon_a - \varepsilon_{fw})} \quad (2.9)$$

In addition to traditional empirical equations and mixing models, Evett *et al.* (2005) presented a different approach using travel time, BEC and effective frequency ( $f_{vi}$ ) as calibration parameters. Their comparison using three different soil types (silty clay loam, clay and clay loam) showed that much improved linear calibrations can be achieved such that

$$\theta = b_0 + b_1 \left( \frac{ct}{2L} \right) + b_2 \sqrt{BEC} \quad (2.10)$$

and

$$\theta = b_0 + b_1 \left( \frac{ct}{2L} \right) + b_2 \sqrt{\left( \frac{BEC}{2\pi f_{vi} \varepsilon_0} \right)}, \quad (2.11)$$

where  $\varepsilon_0$  is the permittivity of free space ( $8.854 \times 10^{-12}$  F m<sup>-1</sup>). This approach, however, needs to be validated for different types of soils.

## 2.2. Materials and methods

### 2.2.1. Study site

Six undisturbed peat samples were extracted on August 17<sup>th</sup> and 18<sup>th</sup> 2007 from a permafrost plateau at the Scotty Creek watershed, Northwest Territories, Canada (61°18'N; 121°18'W). This site is located in a wetland-dominated, discontinuous permafrost zone of the Canadian sub-Arctic. The stratigraphy in this region includes an organic layer of up to 8-m thick overlying a silt-sand layer, below which lies a thick clay to silt-clay deposit of poor permeability (Aylesworth and Kettles, 2000). To avoid compaction the peat was cut with a 70-cm deep access trench around the sampling location to obtain large undisturbed cubes. Circular sub-samples 30-cm deep were cut into these larger cubes, shaved and carefully inserted into buckets, 28 cm in diameter and 30-cm deep, preserving the undisturbed state. Peat samples were extracted to frost-table depth (about 70 cm) at two different locations, high on the peat plateau where Labrador tea (*Ledum* sp.) and lichen cover the surface (referred to as L samples hereafter), and low at the peat plateau-bog perimeter level where sphagnum moss is the dominant vegetation (referred to as M samples hereafter). The groundwater level at sampling

location for M samples was still below the perimeter ground-surface and the surface level was approximately at the perimeter ground level. The samples were stored at  $-4^{\circ}\text{C}$  to avoid any structural changes to the samples.

### **2.2.2. Calibration sample size**

The choice of the containers used for TDR calibration depends on the critical distance between the TDR rods and container walls such that the entire TDR pulse energy is restricted within the soil. Critical distance was determined by using a simple experiment in a 40-cm deep,  $65 \times 45$ -cm plastic container completely filled with water. A CS635 TDR probe (15 cm long and three pronged: Campbell Scientific, Inc., Logan, UT) was immersed vertically in the container such that the probe head was below water. The probe was held in this position and moved laterally from middle of the container towards the walls. Measurements of  $\epsilon$  and TDR waveform were made for each location. The test was repeated at least three times to confirm the results. It was observed that the TDR measured values of  $\epsilon$  did not change nor did the TDR waveform deform until the probe rods were within 1 cm from the container walls. Thus, 22-cm deep LDPE containers with a  $12 \times 7$ -cm cross section were chosen as sample holders for the calibration tests. This allowed at least a 3-cm gap between the container walls and outer rods of the TDR probe when the probe was inserted vertically in the soil. Another experiment to verify the critical distance was conducted after choosing the container dimensions. Milled peat was packed into one of the chosen containers and a CS635 TDR probe was inserted vertically into the soil. Measurements of  $\epsilon$  and TDR waveform were made for three different values of water contents in the milled peat with the container held in air and fully immersed in

water (without allowing the external water to flow into the container). There was no change in TDR waveform and measured  $\epsilon$  when holding the container in air or in water confirming that the entire EM pulse energy was contained within the soil.

### **2.2.3. Calibration method**

Peat subsamples, representing depths of 0 –15, 20 –35, 40 –55 and 55 –70 cm, were extracted from the frozen bucket samples. Four of the M samples, taken from depths of 0 –15 (M1), 20 –35 (M2), 40 –55 (M3) and 55 –70 cm (M4), and two of the L samples, taken from depths of 10 –25 (L1) and 50 –65 cm (L2), were used for calibration. The M1 sample contained live moss. The sectioning was done by cutting laterally into the frozen samples so that the extracted samples had dimensions of 22 × 12 × 7 cm after air-drying. Representative samples were taken from the same portion of the frozen bucket samples to determine porosity and bulk density of the sub-samples. The sub-samples were air-dried at room temperature and then inserted into the sample holders in an upright position and the CS635 TDR probe was inserted vertically in each sample. It was ensured that the probe head was in firm contact with the top of the soil without causing too much compression. Using air-dried samples of the same size as the container ensured that the probe rods were not exposed because of shrinkage during the experiment. The probes were connected to a SDMX50 multiplexer (Campbell Scientific, Inc., Logan, UT) through LMR-200 low-loss coaxial cables. To avoid sample disturbance from buoyancy effects, samples were slowly saturated by spray-misting using reverse-osmosis water ( $EC = 0.0004 \text{ Sm}^{-1}$  at 24 °C) in a process spanning two weeks. During this period, samples

were allowed to equilibrate for at least 48 hours after the addition of water, until water ponding stabilized and volumetric water content equalled porosity.

Water evaporating from one end of the sample results in water content gradients or layered wetting along the waveguide of the vertically inserted probes. As long as water content is constant in the transverse plane, moisture gradients along the waveguide have negligible effects on average  $\epsilon$  as shown by Topp *et al.* (1982). In preliminary tests, a peat sub-sample was saturated in the chosen containers and subjected to evaporation. At each substantive change in water content, as determined by change in sample mass, the container was covered with plastic to avoid change in water content and apparent dielectric permittivity was recorded at 0, 1, 6, 12 and 24 hours. For three different water contents these measurement showed no change in  $\epsilon$  values, indicating that water content gradient along the waveguide and redistribution of water had minimal effects on bulk apparent dielectric permittivity.

The six completely saturated samples used for actual calibration were then placed in a climate chamber (biome) at the University of Western Ontario's Biotron facility in order to dry the sample by evaporation. The biome was operated at 30 °C, 135 W m<sup>-2</sup>, 10% RH and wind speed of 20 km per hour as measured at the surface of the samples. These conditions were chosen in order to achieve a greater rate of evaporation from the samples and to reduce the calibration time as much as possible. Measurements of travel time, 251 point waveforms and BEC were made every four hours using PCTDR software (Campbell Scientific). Sample depth was also recorded by using a ruler to account for volume change caused by shrinkage. Sample mass was recorded continuously during the

calibration process (SG16001 scale, 0.05-g repeatability: Mettler Toledo, Painesville, OH) for gravimetric determination of volumetric water content. The procedure was repeated for three wetting-drying cycles on four samples (M1, M2, M3, and L1) by allowing the soil water content to reach different values (Table 2.2) each time before saturating in identical fashion as before and subjecting to evaporation again. The other two samples (M4 and L2) were subjected to only one drying cycle. Dry sample weight was determined by oven-drying the samples at 86°C until no further weight change was detected (O'Kelly, 2005). Soil temperature was monitored with a platinum resistance thermometer (model PT100,  $\pm 0.01$  °C reproducibility: Lakeshore Cryotronics, Inc., Westerville, OH) multiplexed to a temperature monitor (TM218S series Lakeshore Cryotronics, Inc., Westerville, OH).

#### **2.2.4. Temperature effects on water content and BEC measurements**

The temperature effects on  $\theta$  and BEC measurements were studied in a separate experiment on peat samples with  $\theta$  values between  $0.94 \text{ m}^3 \text{ m}^{-3}$  (saturated) and  $0.35 \text{ m}^3 \text{ m}^{-3}$ . Samples were maintained at the same water content, by covering the container tops to avoid evaporation, and subjecting them to varying air temperatures between 2 °C and 35 °C in the biome. The temperature was varied by 3 °C steps every four hours, and  $\varepsilon$ , BEC and soil temperature measurements were made every 15 minutes. The temperature experiment was performed only once to determine the effect of temperature on measurements of soil relative permittivity and bulk electrical conductivity. Because the error introduced by temperature (water content: between  $-0.0021 \text{ m}^3 \text{ m}^{-3}$  per °C for  $\theta \geq 0.79 \text{ m}^3 \text{ m}^{-3}$  and  $-0.0005 \text{ m}^3 \text{ m}^{-3}$  per °C for  $\theta = 0.35 \text{ m}^3 \text{ m}^{-3}$  and BEC close to that of soil

solution) was similar to that observed in many past studies, the experiment was not repeated.

Sample	Total cycles	Water content at the end of cycle ( $\text{m}^3\text{m}^{-3}$ )		
		Cycle 1	Cycle 2	Cycle 3
M1	3	0.68	0.48	0.06
M2	3	0.61	0.50	0.04
M3	3	0.80	0.21	0.07
M4	1	0.02	-	-
L1	3	0.58	0.71	0.02
L2	1	0.11	-	-

**Table 2.2** Details of wetting-drying cycles used during TDR calibration in individual peat M samples (peat plateau-bog periphery), and L samples (peat plateau).

## 2.3. Results

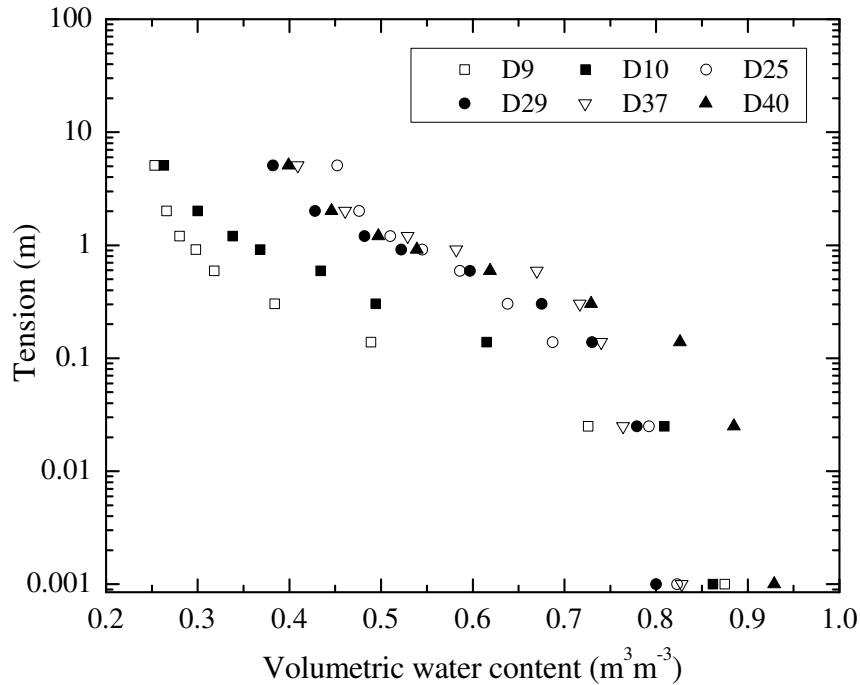
### 2.3.1. Peat characteristics

Table 2.3 gives the porosity and bulk density values for the peat samples used in this study. The organic content of the soil samples was greater than 98%. The peat samples extracted from the peat plateau (L samples) or close to bog (M samples) were markedly different in appearance. Both types were characterized by large pores in the upper 10 cm, but the peat in Samples L became finer, amorphous and darker in colour with depth while Samples M were fibrous (coarse to fine fibers) and light coloured even

at 50-cm depth. The structural differences in these two types could be because of the different physical and moisture conditions on the plateau and near the plateau-bog edge. Such differences are common and have been widely reported (Hobbs, 1986). Water-retention curves for peat from the same location have been reported by Quinton and Hayashi (2005) and are shown in Figure 2.1. In general, deeper samples hold more water at greater tension than shallower ones. When dried completely, the volume change in M samples was 22% and 18% in L samples when compared with the saturated state. For peat from the same site, Rezanezhad *et al.* (2009) found the degree of humification on the von Post scale (von Post, 1922 as cited by Hobbs, 1986) to change from H3 just below surface vegetation to H5 at about 65 cm. M samples were found to be more fibrous than L samples at the same depths.

Sample	Sampling Depth (cm)	Total Porosity (%)	Bulk Density (kg m <sup>-3</sup> )
M1	0-15	93.73	53.40
M2	20-35	87.99	88.13
M3	40-55	84.94	113.66
M4	55-70	77.98	127.27
L1	10-25	87.70	84.34
L2	50-65	73.06	183.10

**Table 2.3** Physical properties of individual peat M samples (peat plateau-bog periphery), and L samples (peat plateau) used in TDR calibration.



**Figure 2.1.** Soil moisture characteristic curves for peat from Scotty Creek watershed (Quinton and Hayashi, 2005). Numbers in legend indicate the depth of sample in cm below ground surface.

### 2.3.2. TDR calibration

At similar  $\theta$  values, L samples yielded larger values of  $\varepsilon$  compared with M samples. Deeper M samples progressively yielded slightly larger  $\varepsilon$  values for the same  $\theta$  than shallower depths. This effect could be attributed to increasing bulk density ( $\rho_b$ ) of the samples with depth and can be incorporated as a matrix effect as in the approach taken by Malicki *et al.* (1996).

Scatter plots and binned data tests for combined data were used to ascertain the type of fit. Both second and third order polynomial forms fitted our data well. However, a third-order polynomial was more robust in predicting  $\theta$  greater than  $0.9 \text{ m}^3 \text{ m}^{-3}$  (Figure 2.2, Table 2.4). Combining the data for all samples reduced the  $R^2$  value by only a small

amount: the much larger increase in root mean square error (RMSE) points to the need to separate out the regression analysis based on peat type. The statistical similarity between predicted  $\theta$  values (empirical models) and the experimental  $\theta$  values was tested using  $\chi^2$  test for a preselected significance level of 95%. The data was divided into 19 frequency bins and the calculated  $\chi^2$  score was used to obtain the critical value (28.87) for 18 degrees of freedom. The probability distributions of fits to data of individual samples were significant up to a preselected level of 95% ( $\chi^2$  scores  $< 28.87$ ). For simplicity we will limit the comparisons of empirical and mixing models to combined data.

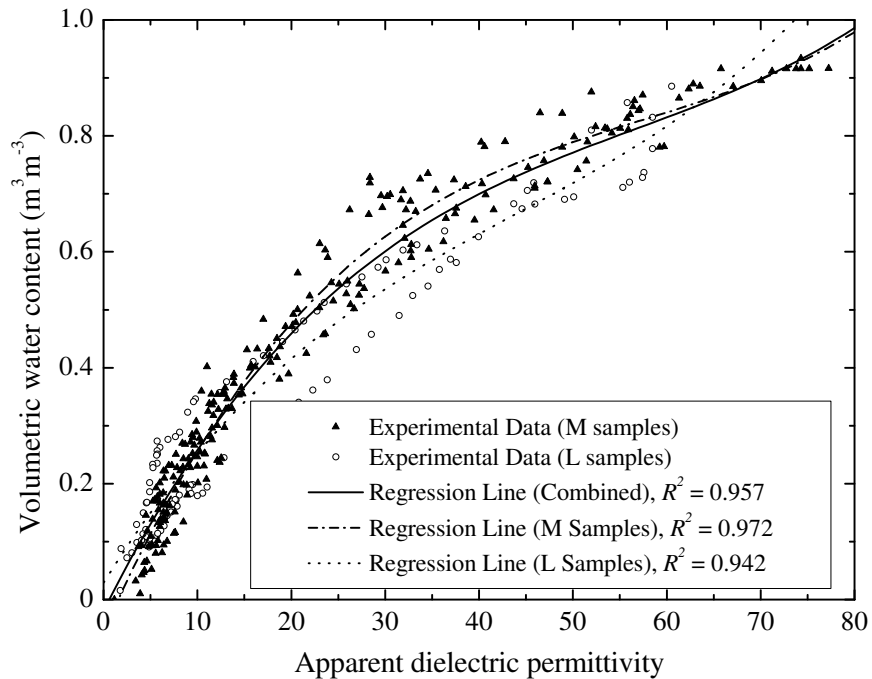


**Figure 2.2.** Regression curves fitted individually to M samples (peat plateau-bog periphery) and L samples (peat plateau), and a combined fit to data from M samples and L samples.

Parameter	Combined	M1	M2	M3	M4	L1	L2
$b_0$	$-1.89 (\pm 1.98) \times 10^{-2}$	$-4.89 (\pm 3.08) \times 10^{-2}$	$-9.25 (\pm 4.11) \times 10^{-2}$	$-9.5 (\pm 6.07) \times 10^{-2}$	$-4.3 (\pm 3.43) \times 10^{-2}$	$4.01 (\pm 0.79) \times 10^{-2}$	$6.41 (\pm 3.06) \times 10^{-2}$
$b_1$	$3.20 (\pm 0.28) \times 10^{-2}$	$3.66 (\pm 0.40) \times 10^{-2}$	$4.12 (\pm 0.65) \times 10^{-2}$	$3.64 (\pm 0.92) \times 10^{-2}$	$4.07 (\pm 0.55) \times 10^{-2}$	$1.52 (\pm 0.09) \times 10^{-2}$	$3.17 (\pm 0.54) \times 10^{-2}$
$b_2$	$-4.59 (\pm 0.93) \times 10^{-4}$	$-5.29 (\pm 1.24) \times 10^{-4}$	$-7.1 (\pm 2.52) \times 10^{-4}$	$-6.2 (\pm 3.55) \times 10^{-4}$	$-8.6 (\pm 2.12) \times 10^{-4}$	$-1.29 (\pm 1.71) \times 10^{-5}$	$-6.46 (\pm 2.23) \times 10^{-4}$
$b_3$	$2.70 (\pm 0.86) \times 10^{-6}$	$2.84 (\pm 1.06) \times 10^{-6}$	$4.76 (\pm 2.64) \times 10^{-6}$	$4.78 (\pm 3.82) \times 10^{-6}$	$6.93 (\pm 2.30) \times 10^{-6}$	0	$5.29 (\pm 2.46) \times 10^{-6}$
Number of observations	345	84	63	46	49	56	47
$R^2$	0.957	0.984	0.981	0.986	0.982	0.996	0.984
RMSE ( $\text{m}^3 \text{m}^{-3}$ )	0.053	0.037	0.036	0.033	0.029	0.014	0.026

**Table 2.4** Constants of polynomial fit (Equation 2.3) with 95% confidence bounds for combined data from M samples (peat plateau-bog periphery) and L samples (peat plateau), and individual peat samples from the two sampling sites obtained by regression analysis.

The probability distribution for the combined empirical model of this study was similar to the pooled experimental data to a significance level of 95% with a score of 21.15. The hypothesis for similarity between other models and the observed values was rejected with a score greater than 28.87. However, the dissimilar distributions result from contributions of larger differences in predicted and observed values at the peripheral frequency bins ( $\theta < 0.30 \text{ m}^3 \text{ m}^{-3}$  for all models, and  $\theta < 0.30 \text{ m}^3 \text{ m}^{-3}$  and  $\theta > 0.94 \text{ m}^3 \text{ m}^{-3}$  for Yoshikawa *et al.* (2004) and Malicki, *et al.* (1996)). This is not surprising for empirical models developed for different data sets and water content ranges. Therefore, we continue to compare the different models (Figure 2.3, Table 2.5) in order to identify the factors causing differences in TDR calibrations performed on mineral and peat soils.

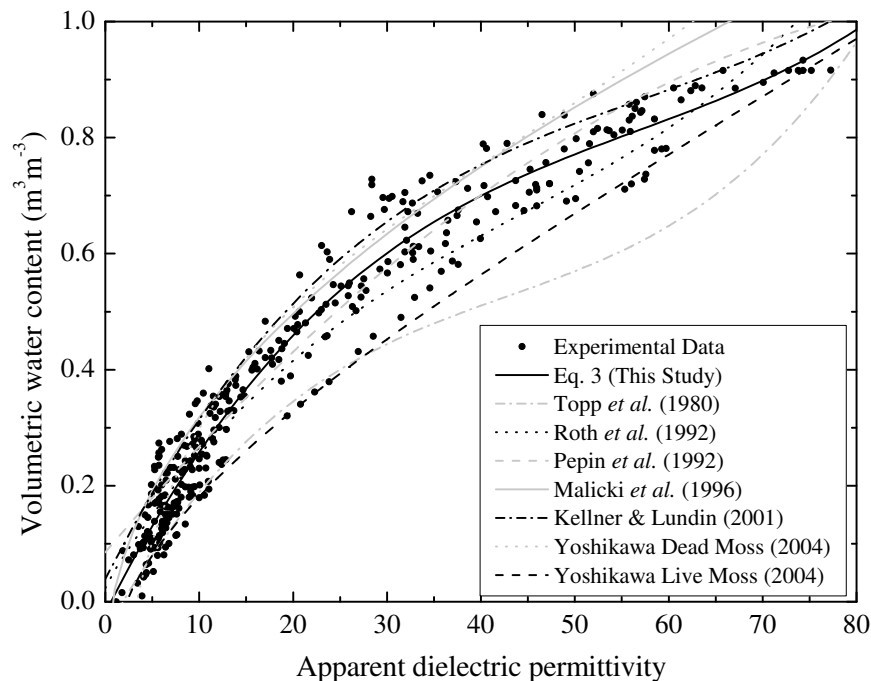


**Figure 2.3.** Comparison of empirical calibration equations given in Table 2.1 with the combined experimental data from M samples (peat plateau-bog periphery) and L samples (peat plateau), and the combined empirical model (Table 2.4) of this study.

Model	$R^2$	RMSE ( $\text{m}^3 \text{m}^{-3}$ )
This study	0.957	0.053
Topp <i>et al.</i> (1980)	0.778	0.125
Roth <i>et al.</i> (1992)	0.947	0.061
Pepin <i>et al.</i> (1992)	0.931	0.069
Malicki <i>et al.</i> (1996)	0.879	0.091
Kellner and Lundin (2001)	0.899	0.083
Yoshikawa <i>et al.</i> (2004) (dead material)	0.856	0.099
Yoshikawa <i>et al.</i> (2004) (live material)	0.837	0.106

**Table 2.5** Comparison with empirical models given in Table 2.1 relating the apparent dielectric permittivity to volumetric soil moisture for combined data from M samples (peat plateau-bog periphery) and L samples (peat plateau).

The impact of temperature variations on  $\varepsilon$  was explored to try to understand the role of bound water and determine any temperature induced errors. Data generated in independent experiments conducted on wet-peat samples, maintained at constant water contents and subjected to varying air temperature, were used for this analysis. At large  $\theta$  values ( $0.94 \text{ m}^3 \text{m}^{-3} \geq \theta \geq 0.79 \text{ m}^3 \text{m}^{-3}$ ),  $\varepsilon$  increased with decreasing temperature (Figure 2.4a). The regression slopes showed a  $0.0021 \text{ m}^3 \text{m}^{-3}$  variation in water content with a 30 °C change in temperature. Thus it appears that the bulk relative permittivity of the

medium is a function of  $\varepsilon_{fv}$  alone and there seems to be no release of bound water with increasing temperature as expected in soils with large surface areas (Wraith and Or, 1999). At smaller  $\theta$  values ( $\theta \leq 0.55 \text{ m}^3 \text{ m}^{-3}$ ) there was negligible variation in  $\varepsilon$  with change in temperature. However, in general,  $\varepsilon$  increased with decreasing temperature.

BEC increased with temperature and could be described by a linear function for all six samples. The slope decreased with decreasing water content and deeper samples had comparatively larger slopes than shallow ones (Figure 2.4b). This linear increase in soil BEC can be attributed to the temperature dependency of electrical conductivity of soil solution.

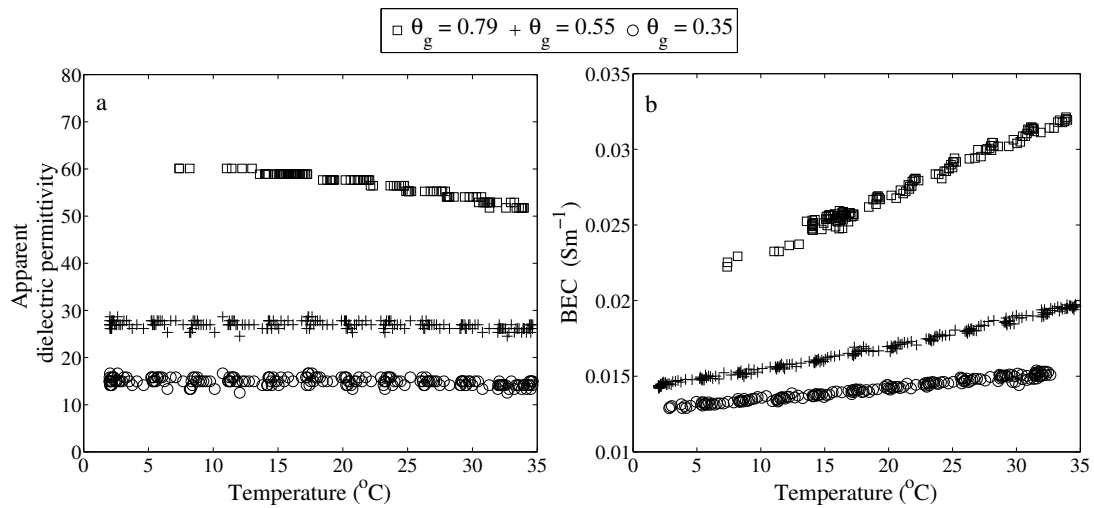


**Figure 2.4.** Effect of temperature on (a) apparent dielectric permittivity and (b) BEC measurements in peat. The gravimetric water content ( $\theta_g$ ) did not change over the duration of the test.

### 2.3.3. Mixing model calibrations

Most studies on soils with a large organic matter content have found that  $\alpha < 0.5$  produces a good calibration relationship using  $\alpha$ -models (Weitz *et al.*, 1997; Roth *et al.*, 1990). Comparing the mixing models described by Equations (2.6), (2.8) and (2.9) (Figure 2.5, Table 2.6), shows that Equations (2.6) and (2.8) fit our data best for  $\alpha = 0.495$  and  $0.52$ , respectively ( $\epsilon$  for water, soil and air phases was taken to be  $76.58$ ,  $3.25$  and  $1$ , respectively).  $\epsilon_s$  was computed by using  $\epsilon$  obtained for oven-dried samples and the two-phase mixing model (Equation (2.6),  $\alpha = 0.5$ ). A sensitivity analysis in which only  $\alpha$  was varied, showed that the models work only slightly better for  $\alpha = 0.495$  and  $0.52$  when compared with  $\alpha = 0.5$  (Table 2.6). The  $\chi^2$  test for a 95% significance level with 18 degrees of freedom shows that  $\theta$  values predicted by Maxwell-De Loo's model ( $\chi^2$  score =  $19.29$ ) were consistent with the observed  $\theta$  values. Because we did not determine the specific surface area ( $A_s$ ), the four phase models given by Equations (2.8) and (2.9) were solved using published data (Poots and McKay, 1979) for peat and assuming  $A_s = 250 \text{ m}^2 \text{ g}^{-1}$ . Given the range of bulk densities of the soils studied, the amount of bound water did not exceed  $0.00125$  by volume unless  $A_s$  is assumed to be significantly larger than that reported in literature for peat. Thus, the bound water fraction is very small and only the properties of free water are important.

Model	$\alpha$	$R^2$	RMSE ( $\text{m}^3\text{m}^{-3}$ )
Equation (2.6)	0.495	0.9506	0.0570
	0.50	0.9505	0.0571
Equation (2.8)	0.52	0.9497	0.0576
	0.50	0.9491	0.0580
Equation (2.9)	-	0.9541	0.0550

**Table 2.6.** Model parameter values and fitting results (experimental vs predicted) for three phase  $\alpha$  mixing model (Equation 2.6), four phase  $\alpha$  mixing model (Equation 2.8), and MDL model (Equation 2.9).

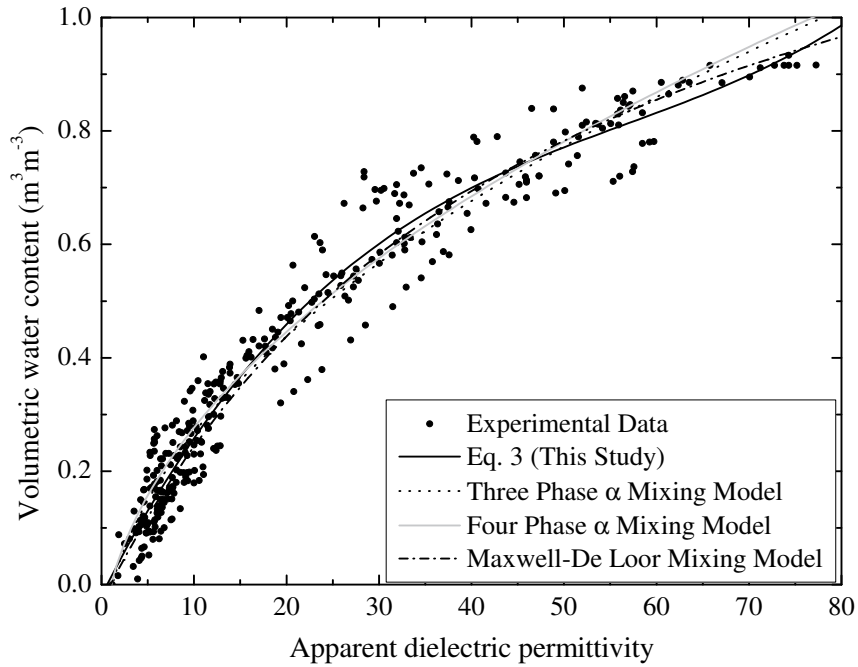


**Figure 2.5.** Comparison of mixing models ( $\eta = 0.89$ ,  $\varepsilon_{fw} = 76.58$ ,  $\varepsilon_s = 3.25$ ,  $\theta_{bw} = 0.0094$   $\text{m}^3\text{m}^{-3}$ ,  $\varepsilon_{bw} = 3.15$  and  $\alpha = 0.5$ ) with the combined experimental data from M samples

(peat plateau-bog periphery) and L samples (peat plateau), and the combined empirical model (Table 2.4) of this study.

#### **2.3.4. Calibration in travel time, BEC and effective frequency**

The effective frequencies were calculated as per Evett *et al.* (2005) from the TDR waveforms recorded during the actual calibration tests and were 1.08 GHz for dry soil and 0.4823 GHz for saturated soil (maximum and minimum of 345 calculated values). These values are larger, with a narrower range than Evett *et al.* (2005) found for clay soils. In general, the frequency content of measured TDR waveform extends from 20 kHz to approximately 1.5 GHz (Heimovaara, 1994). Calibration for M samples improved slightly when using Equation (2.11) instead of Equation (2.10), while there was minor improvement in calibration for lichen samples using Equation (2.11) (Table 2.7). As there is no other comparable study in peat soils, it is not possible to compare the linear coefficients obtained in this study with others. Moreover, we conducted the study at constant temperature and this could be a reason why there is no significant change in the slope of relative voltages as used for effective frequency calculations.

Soil Type	$b_0$	$b_1$	$b_2$	$R^2$	RMSE ( $\text{m}^3 \text{m}^{-3}$ )
$\theta = b_0 + b_1[ct/(2L)]$					
M samples	-0.1719	0.1370	-	0.9554	0.0564
L samples	-0.1397	0.1187	-	0.9719	0.0416
Combined	-0.1616	0.1316	-	0.9505	0.0587
$\theta = b_0 + b_1[ct/(2L)] + b_2[\text{BEC}]^{0.5}$ (Equation 2.10)					
M samples	-0.1155	0.1399	-0.1787	0.9556	0.0562
L samples	-0.1138	0.1202	-0.0853	0.9716	0.0416
Combined	-0.1313	0.1332	-0.0975	0.9504	0.0587
$\theta = b_0 + b_1[ct/(2L)] + b_2[\text{BEC}/(2\pi f_{vi}\epsilon_0)]^{0.5}$ (Equation 2.11)					
M samples	-0.1688	0.1383	-0.0214	0.9551	0.0565
L samples	-0.1292	0.1223	-0.0631	0.972	0.0413
Combined	-0.1575	0.1332	-0.0268	0.9505	0.0587

**Table 2.7** Linear TDR calibration equations including travel time ( $t$ ), bulk electrical conductivity ( $BEC$ ), and effective frequency ( $f_{vi}$ ) terms for M samples (peat plateau-bog periphery) and L samples (peat plateau), and individual peat samples from the two sampling sites.

## 2.4. Discussions

Six undisturbed peat samples were extracted at different depths for TDR ( $\varepsilon$ - $\theta$ ) calibrations in order to account for the structural resemblance with *in situ* peat soils. TDR calibration at various volumetric water contents was performed by measuring apparent relative permittivity of the soil and from gravimetric measurements. Calibrations made on mineral soils and repacked samples have been reported to have RMSE values of  $< 0.02 \text{ m}^3 \text{ m}^{-3}$  (Evelt *et al.*, 2005; Topp and Reynolds; 1998). In comparison, our result (RMSE =  $0.056 \text{ m}^3 \text{ m}^{-3}$ ) is an outcome of variation in measurements caused by structural differences, which is expected to be more for organic soils and undisturbed samples. Another explanation for the larger RMSE is that the calibrations were performed over a wide range of water contents. A comparison with empirical models from previous studies shows that not all of them perform satisfactorily with our data. The empirical models work satisfactorily within the range for which they were developed and when applied to soils with properties similar to those which they were originally derived for.

Mixing models include porosity for volumetric partitioning between soil components and this allows simulation of effects of soil properties on the  $\varepsilon$ - $\theta$  relationship. Though the  $\alpha$ -models fit our data well, we will limit the discussion to MDL model since there is no unique  $\alpha$  value for which the effects of physical soil properties on the  $\varepsilon$ - $\theta$  relationship can be modelled. The MDL mixing model clearly demonstrates the impact of soil properties on calibrations. For example, when  $\eta = 0.9$  for our experimental data, the MDL model is in close agreement with our calibration (Table 2.6) and when  $\eta = 0.45$  ( $\rho_b$

= 1450 kg m<sup>-3</sup> and  $A_s = 50 \text{ m}^2 \text{ g}^{-1}$ ) the model is in close agreement with Topp's equation (RMSE = 0.011 m<sup>3</sup> m<sup>-3</sup>). It is important to recall that Topp's model was developed for the  $\theta$  range between 0 m<sup>3</sup> m<sup>-3</sup> and 0.55 m<sup>3</sup> m<sup>-3</sup> and therefore is not suitable for more porous soils. The effect of porosity on  $\varepsilon$ - $\theta$  relationship is shown in Figure 2.6. Because of the large total porosity of peat, the bulk soil  $\varepsilon$  is much smaller in comparison with less porous soils at same soil water content. Using MDL model with the bound-water phase for bulk density values between 50 kg m<sup>-3</sup> and 350 kg m<sup>-3</sup> showed no major influence on the goodness of the fit. This is because the extremely small soil mass holds very small amounts of bound water despite large particle surface areas. Hence it appears that for low bulk density and porous soils, bound water can be completely ignored. For smaller water contents, multiple mono-layers of bound water, as assumed by Bohl and Roth (1994), and a constant  $\varepsilon_{bw} = 3.15$  results in a slightly inferior fit. However, this approach puts limitations on use of mixing models by creating additional uncertainty of use of Equation (2.7) to determine  $\theta_{bw}$ . In addition, as shown experimentally by Boyarskii *et al.* (2002), multiple layers of bound water cannot all be assumed to have a small and invariable relative permittivity ( $\varepsilon_{bw} = 3.15$ ), as rotational dipole responses to the imposed electrical field must vary with distance from the sorbing surface.

Published data on soils with small  $\rho_b$  and large porosities, such as soils with much organic matter (Weitz *et al.*, 1997; Roth *et al.*, 1992) and volcanic soils (Regalado *et al.*, 2003), reveal that apparent relative permittivity of soil at similar water contents is significantly smaller than in mineral soils with larger  $\rho_b$ . As there is no consensus on an equation to determine soil water content in peat soils using TDR, it is best to calibrate the

instrument. Further, it is necessary to examine the influence of soil characteristics on  $\varepsilon$ - $\theta$  relationship derived from such calibrations. Our observations are comparable to those reported by Dirksen and Dasberg (1993) for fine textured soils. In peat, Topp's model fails because of the lower bulk density and greater air volume at the same  $\theta$  values and bound water appears to be of lesser importance. Further, the deviations in different calibrations in peat appear to be because of varying porosity and structural variability of the undisturbed samples as well as the pore size variability in the fibrous M samples and the finer L samples. In our experiments, moss-covered peat had a smaller apparent relative permittivity than lichen-covered peat at the same  $\theta$  values. Kellner and Lundin (2001) reasoned that bound water was the cause of progressively smaller  $\varepsilon$  values at the same  $\theta$  for samples with increasing degree of decomposition. Their samples had  $\rho_b < 70 \text{ kg m}^{-3}$  and  $\eta > 0.95$ . We experimented with their pooled data, and data for H3 and H4 (von Post scale) samples. Kellner and Lundin (2001) performed the calibration at ambient indoor temperature (about 22°C). The MDL model fit with  $\varepsilon_{fw} = 79.4$ ,  $\varepsilon_s = 5.0$ ,  $\theta_{bw} = 0 \text{ m}^3 \text{ m}^{-3}$  resulted in an excellent fit with their empirical models (Figure 2.7). Therefore, it appears that bound water might not have been important even in their case.

Temperature effects on  $\varepsilon$  measurements introduced an error of  $-0.0021 \text{ m}^3 \text{ m}^{-3}$  per °C for  $\theta \geq 0.79 \text{ m}^3 \text{ m}^{-3}$  which reduces to  $-0.0005 \text{ m}^3 \text{ m}^{-3}$  per C for  $\theta = 0.35 \text{ m}^3 \text{ m}^{-3}$ . The error values for greater water content are similar to those reported by Persson and Berndtsson (1998) for sand, Pepin *et al.* (1995) and Evett *et al.* (2005) for clay and silty clay loam. Figure 2.8 shows the effect of temperature on water content measurements as simulated using the MDL model without the bound-water phase. The porosity for this test

was kept constant at 0.9 and simulations assuming constant soil temperatures of 2°C and 30°C are shown. The error introduced from temperature dependence is between 0.0018 m<sup>3</sup> m<sup>-3</sup> per °C at  $\theta = 0.9 \text{ m}^3 \text{ m}^{-3}$  and -0.0009 m<sup>3</sup> m<sup>-3</sup> per °C at  $\theta = 0.27 \text{ m}^3 \text{ m}^{-3}$  for the simulated values (Figure 2.8). These values are comparable to our experimental values and therefore the MDL model appears to simulate the effects of temperature on TDR measurements reasonably well.

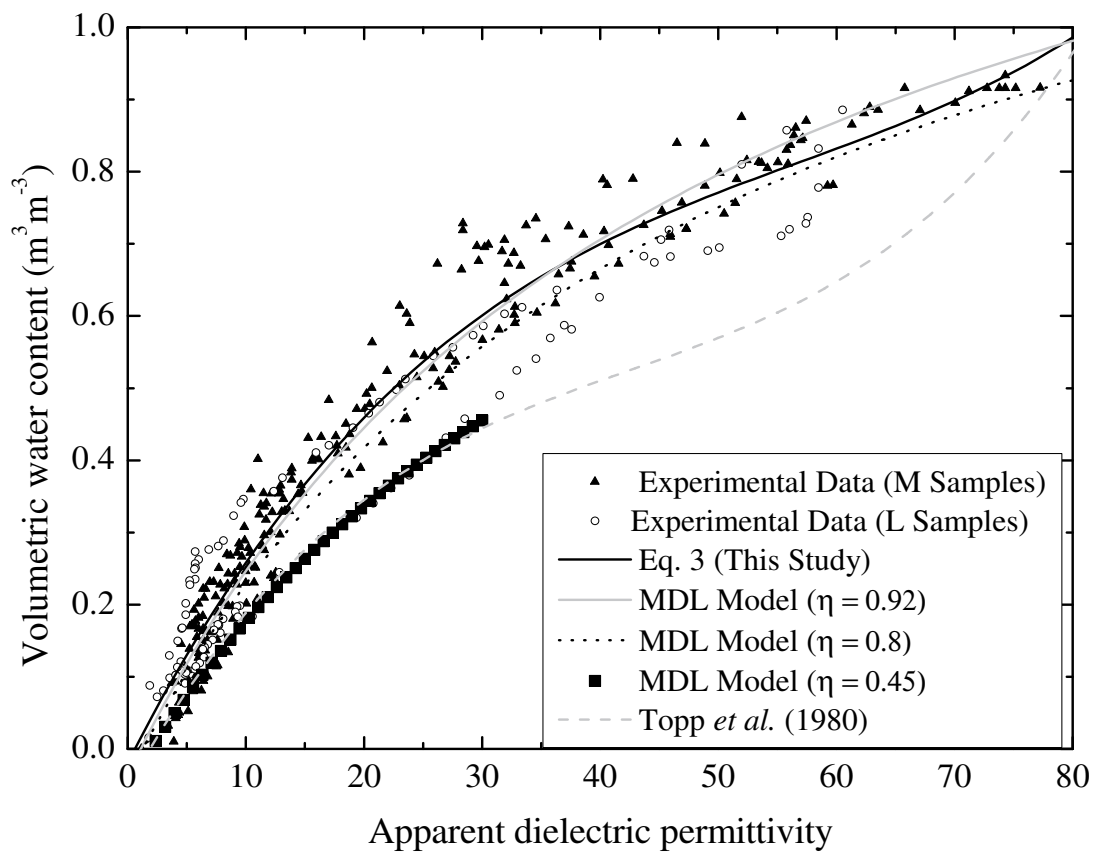


**Figure 2.6.** Effect of porosity on the  $\epsilon$ - $\theta$  relationship as simulated using the Maxwell-De Loor model ( $\theta_{bw} = 0 \text{ m}^3 \text{ m}^{-3}$ ).

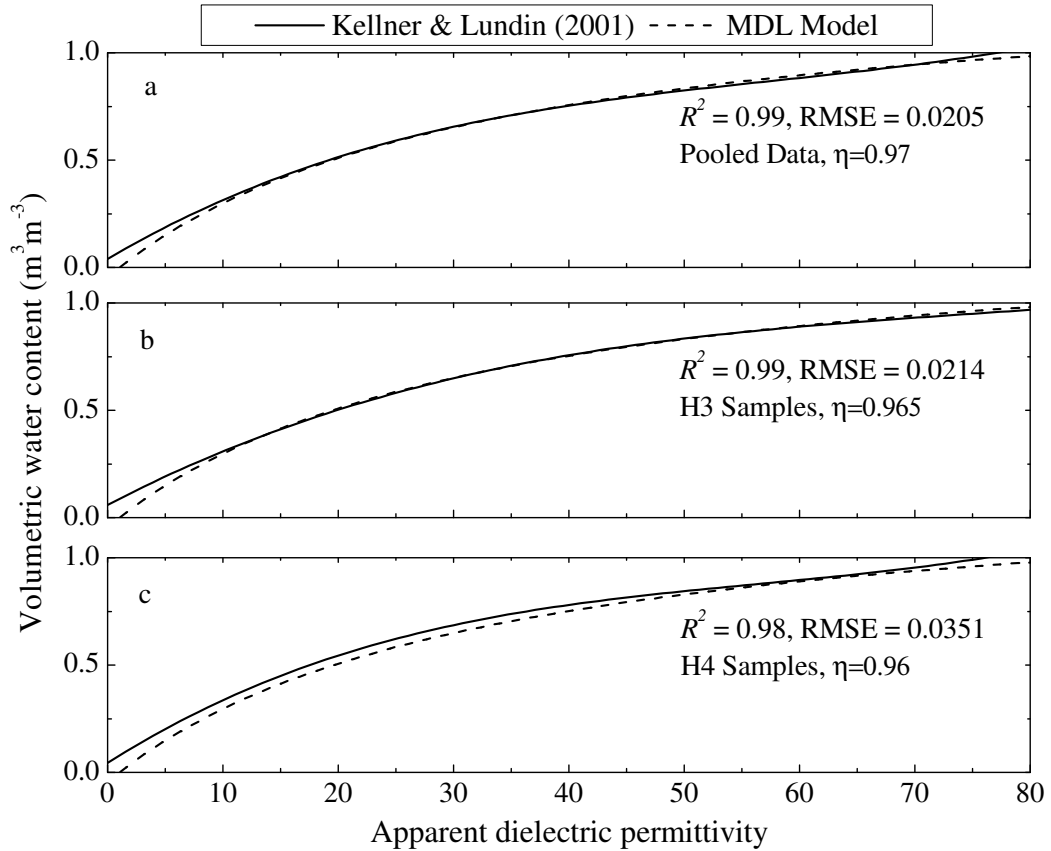


**Figure 2.7.** Comparison between empirical models proposed by Kellner and Lundin (2001) and the Maxwell-De Looor model ( $\epsilon_{fw} = 79.4$ ,  $\epsilon_s = 5$ ,  $\theta_{bw} = 0 \text{ m}^3 \text{ m}^{-3}$ ) for (a) pooled data from experimental samples, and samples with varying degrees of humification (on the von Post scale); (b) H3 and (c) H4. Also shown are calculated values of  $R^2$  and RMSE.

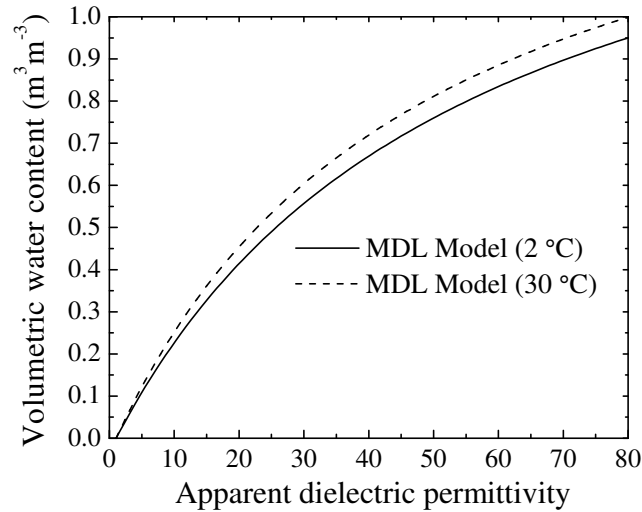


**Figure 2.8** Simulation of temperature effects on water content measurements of peat samples used in this study using the Maxwell-De Loor model.

The incorporation of BEC and effective frequency of the measured waveform as presented in Evett *et al.* (2005) was also tested by comparing the coefficients for Equations (2.10) and (2.11) for peat soils. The data used in this analysis came from the actual calibration experiments that were conducted at constant temperature (30°C). The objective was to determine if the resulting coefficients for Equations (2.10) and (2.11) for peat soils were comparable to those found by Evett *et al.* (2005). Our findings were similar to those of their study, linear calibration improved when the BEC term was introduced in linear calibration (Equation 2.10). The regression coefficient  $b_2$  in both equations was negative. This is an indication that an increase in BEC results in a corresponding increase in  $\epsilon$  not related to increase in water content. When the effective frequency term was introduced (Equation 2.11), the range of the slope (regression coefficient  $b_1$ ) of the travel time component was reduced. Given that our experiments were performed at constant temperature and that the BEC values were much smaller than

in Evett *et al.* (2005), we cannot conclude that the resulting coefficients for Equations (2.10) and (2.11) are universal for peat. The variation in temperature and a wider range of BEC needs to be tested to confirm the validity of coefficients that we present. However, it is evident that the calibrations can be improved if the effect of BEC and temperature is taken into consideration and we find the method proposed in Evett *et al.* (2005) is applicable to peat as well. It will be of value to conduct a study in peat soils using a similar approach at varying temperatures to compare the coefficients as obtained in their study.

It is noted that the pore structure of peat samples would reversibly or irreversibly change during the drying and wetting cycles implemented in the procedures employed in this study. However, such changes are inherent to the peat found in permafrost-affected sites where alternate freezing and thawing is a regular phenomenon. The developed TDR calibration curves in essence incorporate the effects of such pore structure changes and thus are more suited to our broader studies with peat.

## **2.5. Conclusions**

Variability in observed  $\epsilon$  values occurs because of structural differences between undisturbed peat samples. Differences in calibration between peat sampled on peat plateau (L samples) and near bog-peat plateau boundary (M samples) can be attributed to the different formation conditions that likely affected pore size and distribution. Porosity differences cause deviation of individual calibration curves, an effect efficiently simulated using the MDL model in this study. Bound water has a very small role to play

because of its negligible volumetric fraction owing to low bulk densities of peat. An increased volumetric fraction of air at greater porosities is the prime cause for the deviation from  $\varepsilon$ - $\theta$  relationships of mineral soils at similar water contents. The temperature correction factor for water content measurements appears to diminish with decreasing water content in peat. The correction factor of  $-0.0021 \text{ m}^3 \text{ m}^{-3} \text{ per } ^\circ\text{C}$  at greater water contents is close to that reported by Persson and Berndtsson (1998), Pepin *et al.* (1995) and Evett *et al.* (2005) for mineral soils. The results of our study are close to those of Roth *et al.* (1992) and Pepin *et al.* (1992) except for  $\theta < 0.3 \text{ m}^3 \text{ m}^{-3}$ , and it appears that the  $\varepsilon$ - $\theta$  relationship in peat can be narrowed to a band rather than a universal equation as in case of mineral soils. The MDL model can efficiently simulate the effects of temperature on water content measurements, and volumetric partitioning of all soil phases making it the most applicable of all mixing models. Depending on the desired accuracy, and knowing the type and physical characteristics of peat, TDR calibrations can be made more quickly by using fewer calibration points. The MDL model can be then used to fit a curve through these points with  $\varepsilon_s$  used as a fitting parameter to obtain a satisfactory calibration.

## 2.6. References

Aylesworth, J. M. and Kettles, I. M. 2000. Distribution of fen and bog in the Mackenzie Valley, 60°N-68°N. In: *The Physical Environment of the Mackenzie valley: A base line for the assessment of environmental change* (eds L.D. Dyke and G.R. Brooks), p. 208. GSC Bulletin # 547, Natural Resources Canada, Ottawa.

- Birchak, J. R., Gardner, C. G., Hipp, J. E. and Victor, J. M. 1974. High dielectric-constant microwave probes for sensing soil-moisture. *Proceedings of the IEEE*, **62**, 93-98.
- Bohl, H. and Roth, K. 1994. Evaluation of dielectric mixing models to describe the water content vs dielectric number relation. *Symposium on Time Domain Reflectometry in Environmental, Infrastructure, and Mining Applications*, Special Publication SP19-94, Bureau of Mines, US Department of Interior, NTIS PB95-105789, 309-319.
- Boyarskii, D. A., Tikhonov, V. V. and Komarova, N. Y. 2002. Model of dielectric constant of bound water in soil for applications of microwave remote sensing. *Progress in Electromagnetics Research*, **35**, 251-269.
- Castiglione, P. and Shouse, P. J. 2003. The effect of ohmic, cable losses on time-domain reflectometry measurements of electrical conductivity. *Soil Science Society of America Journal*, **67**, 414-424.
- Dalton, F. N., Herkelrath, W. N., Rawlins, D. S. and Rhoades, J. D. 1984. Time domain reflectometry - simultaneous measurement of soil-water content and electrical-conductivity with a single probe. *Science*, **224**, 989-990.
- Dirksen, C. and Dasberg, S. 1993. Improved calibration of time-domain reflectometry soil-water content measurements. *Soil Science Society of America Journal*, **57**, 660-667.

- Dobson, M. C., Ulaby, F. T., Hallikainen, M. T. and Elrayes, M. A. 1985. Microwave dielectric behavior of wet soil. 2: Dielectric Mixing Models. *IEEE Transactions on Geoscience and Remote Sensing*, **23**, 35-46.
- Evelt, S. R., Tolk, J. A. and Howell, T. A. 2005. Time domain reflectometry laboratory calibration in travel time, bulk electrical conductivity, and effective frequency. *Vadose Zone Journal*, **4**, 1020-1029.
- Giese, K. and Tiemann, R. 1975. Determination of complex permittivity from thin-sample time domain reflectometry improved analysis of step response waveform. *Advances in Molecular Relaxation Processes*, **7**, 45-59.
- Heimovaara, T. J. 1994. Frequency-domain analysis of time-domain reflectometry waveforms 1. Measurement of the complex dielectric permittivity of soils. *Water Resources Research*, **30**, 189-199.
- Hobbs, N. B. 1986. Mire morphology and the properties and behaviour of some British and Foreign Peats. *Quarterly Journal of Engineering Geology*, **19**, 7-80.
- Jones, S. B., Wraith, J. M. and Or, D. 2002. Time domain reflectometry measurement principles and applications. *Hydrological Processes*, **16**, 141-153.
- Kellner, E. and Lundin, L. C. 2001. Calibration of time domain reflectometry for water content in peat soil. *Nordic Hydrology*, **32**, 315-332.

- Malicki, M. A., Plagge, R. and Roth, C. H. 1996. Improving the calibration of dielectric TDR soil moisture determination taking into account the solid soil. *European Journal of Soil Science*, **47**, 357-366.
- Moret, D., Lopez, M. V. and Arrue, J. L. 2004. TDR application for automated water level measurement from Mariotte reservoirs in tension disc infiltrometers. *Journal of Hydrology*, **297**, 229-235.
- O'Kelly, B. C. 2005. New method to determine the true water content of organic soils. *Geotechnical Testing Journal*, **28**, 365-369.
- Oleszczuk, R., Gnatowski, T., Brandyk T., and Szatyłowicz, J. 2007. Calibration of TDR for moisture content monitoring in moorsh layers. In: *Wetlands: Monitoring, Modelling and Management*, (eds T. Okruszko, E. Maltby, J. Szatyłowicz, D. Swiatek and W. Kotowski), pp. 121-124.
- Overduin, P. P. and Kane, D. L. 2006. Frost boils and soil ice content: Field observations. *Permafrost and Periglacial Processes*, **17**, 291-307.
- Pennell, K. D. 2002. Specific surface area. In: *Methods of Soil Analysis Part IV: Physical Methods* (eds J.H. Dane and G.C. Topp), pp. 295-313. Soil Science Society of America, Inc., Madison, Wisconsin.

- Pepin, S., Plamondon, A. P. and Stein, J. 1992. Peat water-content measurement using time domain reflectometry. *Canadian Journal of Forest Research-Revue Canadienne De Recherche Forestiere*, **22**, 534-540.
- Pepin, S., Livingston, N. J., and Hook, W. R. 1995. Temperature-dependent errors in time domain reflectometry determinations of soil water. *Soil Science Society of America Journal*, **59**, 38-43.
- Persson, M. and Berndtsson, R. 1998. Texture and electrical conductivity effects on temperature dependency in time domain reflectometry. *Soil Science Society of America Journal*, **62**, 887-893.
- Poots, V. J. P. and McKay, G. 1979. Specific surfaces of peat and wood. *Journal of Applied Polymer Science*, **23**, 1117-1129.
- Quinton, W. L. and Hayashi, M. 2005. The flow and storage of water in the wetland-dominated central Mackenzie river basin: Recent advances and future directions. In: *Prediction In Ungauged Basins: Approaches for Canada's Cold Regions*, (eds C. Spence, J. W. Pomeroy and A. Pietroniro), pp. 45-66. Canadian Water Resources Association.
- Regalado, C. M., Carpena, R. M., Socorro, A. R. and Moreno, J. M. H. 2003. Time domain reflectometry models as a tool to understand the dielectric response of volcanic soils. *Geoderma*, **117**, 313-330.

- Rezanezhad, F., Quinton, W. L., Price, J. S., Elrick, D., Elliot, T. R. and Heck, R. J. 2009. Examining the effect of pore size distribution and shape on flow through unsaturated peat using computed tomography. *Hydrology and Earth System Sciences*, **13**, 1993-2002.
- Roth, C. H., Malicki, M. A. and Plagge, R. 1992. Empirical-evaluation of the relationship between soil dielectric-constant and volumetric water-content as the basis for calibrating soil-moisture measurements by TDR. *Journal of Soil Science*, **43**, 1-13.
- Roth, K., Schulin, R., Fluhler, H. and Attinger, W. 1990. Calibration of time domain reflectometry for water-content measurement using a composite dielectric approach. *Water Resources Research*, **26**, 2267-2273.
- Topp, G. C., Davis, J. L. and Annan, A. P. 1980. Electromagnetic determination of soil-water content - measurements in coaxial transmission-lines. *Water Resources Research*, **16**, 574-582.
- Topp, G. C., Davis, J. L. and Annan, A. P. 1982. Electromagnetic determination of soil water content using TDR: I. Applications of wetting fronts and steep gradients. *Soil Science Society of America Journal*, **46**, 672-678.
- Topp, G. C. and Reynolds, W. D. 1998. Time domain reflectometry: a seminal technique for measuring mass and energy in soil. *Soil and Tillage Research*, **47**, 125-132.

- Topp, G. C., Yanuka, M., Zebchuk, W. D. and Zegelin, S. 1988. Determination of electrical-conductivity using time domain reflectometry - Soil and Water Experiments in Coaxial Lines. *Water Resources Research*, **24**, 945-952.
- von Post, L. 1922. SGU peat inventory and some preliminary results (in Swedish). *Svenska Mosskulturforeningens Tidskrift*, **36**, 1-37.
- Weitz, A. M., Grauel, W. T., Keller, M. and Veldkamp, E. 1997. Calibration of time domain reflectometry technique using undisturbed soil samples from humid tropical soils of volcanic origin. *Water Resources Research*, **33**, 1241-1249.
- Wraith, J. M. and Or, D. 1999. Temperature effects on soil bulk dielectric permittivity measured by time domain reflectometry: Experimental evidence and hypothesis development. *Water Resources Research*, **35**, 361-369.
- Yoshikawa, K., Overduin, P. P. and Harden, J. W. 2004. Moisture content measurements of moss (*Sphagnum* spp.) using commercial sensors. *Permafrost and Periglacial Processes*, **15**, 309-318.
- Zegelin, S. J., White, I. and Jenkins, D. R. 1989. Improved field probes for soil-water content and electrical-conductivity measurement using time domain reflectometry. *Water Resources Research*, **25**, 2367-2376.

# CHAPTER 3. PHYSICAL SIMULATION OF WATER AND HEAT TRANSPORT IN SUB-ARCTIC PEAT

## 3.1. Introduction

Thick layered peat deposits in the vast organic covered permafrost terrains of the northern latitudes are subjected to repeated freeze and thaw cycles. Heat is conducted in soil under temperature gradients, while water moves in response to a combination of matric potential and temperature gradients. Moving water carries heat as well can significantly affect thermal properties of soils (Philip and de Vries, 1957; de Vries, 1963). Strong coupling in frozen soils moves a considerable amount of water from warmer to colder regions (Dirksen and Miller, 1966). In layered peat deposits of organic terrains upper soil horizons can have bulk densities as low as  $50 \text{ kg m}^{-3}$  and porosities exceeding 96% by volume. The high total soil water content strongly affects the thermal state of the permafrost and the rates of frost and thaw penetration within the active layer (the top layer of soil in permafrost regions that is subjected to seasonal freeze-thaw). Redistribution of water towards the freezing front plays a vital role in the spring hydrology of these regions. Freeze-thaw processes in mineral soils have been investigated over long periods, notably by the US Army Cold Regions Research and Engineering Laboratory (Aldrich and Paynter, 1966). The hydrological aspects have been studied in field, but studies are often discontinued, or relegated to field sensors, in winters due to logistical constraints. Correlating field-based soil freeze-thaw observations with the simultaneous forcing of climatological and hydrological parameters is fairly complex.

Separating the influence of each parameter is difficult; controlled experimental studies can greatly supplement the understanding gained from field observations. Theory extending the Fourier-Ohm and Darcy's laws to unsaturated soils has been proposed and developed, e.g., Buckingham (1907), Philip and de Vries (1957), and applied, e.g., (Harlan, 1973) to frozen soils, but the complex coupling usually limits analysis to one dimension.

General circulation models predict that the effects of climate change will be amplified in the northern high latitudes due to feedbacks in which variations in snow and sea ice extent, the stability of the lower troposphere and thawing of permafrost play key roles (Serreze *et al.*, 2000). Numerically modeled climate change scenarios predict on an average 7 °C increase in wintertime surface air temperatures and ~30 % increase in annual precipitation in North America by 2100 (IPCC, 2007). The largest warming is projected to occur in winter over northern parts of Alaska and Canada, reaching 10°C in the northernmost parts, due to the positive feedback from a reduced period of snow cover (IPCC, 2007). These scenarios result into widespread increases in thaw depth over much of the permafrost regions, while discontinuous permafrost regions could experience complete disappearance of permafrost (IPCC, 2007; Zhang *et al.*, 2008; Lawrence and Slater, 2005). Physical verification is necessary in order to increase confidence in such scenarios and also to clearly understand the feedback mechanisms. There have been very few soil column/Mesocosm studies on frozen soils under controlled laboratory settings in general and there have been none that examine hydrological functions of freezing and frozen peat. Freeze-thaw studies on mineral soil columns under controlled laboratory

settings have been reported by Dirksen (1964), Hoekstra *et al.* (1966), Fukuda *et al.* (1980), Mizoguchi (1990), Guymon *et al.* (1993), and Staehli and Stadler (1996). All these experiments used a combination of cooling and heating plates, or a plate on one end with the other end exposed in refrigerator/cold room to simulate end boundary conditions. This is not sufficient for permafrost studies as the effects of deeper frozen sections cannot be simulated. Permafrost contains a large amount of water/ice that modulates the thermal state of the subsurface and needs to be properly represented in order to clearly understand the feedback of frozen ground to climate change scenarios.

One-dimensional profiles need to be achieved for effective physical simulation of freeze-thaw in soils under controlled laboratory settings. For this lateral heat transfer needs to be minimized. Layered peat exhibits strong structural variability, laterally as well as with depth. A larger sample size is required to achieve a representative volume that accounts for such variability. This paper describes a unique two-level biome (climate chamber) that makes it possible to maintain a frozen section near column bottoms, and apply a wide range of boundary conditions to the column tops. This facility thus allows a close replication of an active layer exposed to the atmosphere at the top and bounded by permafrost at the bottom. An experimental setup with peat samples (56 cm diameter x 115 cm deep [the bottom ~45 cm of which is permanently frozen and the upper ~70 cm is the active layer]) is described and evaluated. There are studies that report the performance of heat and water movement experiments in soil columns, e.g., Zhou *et al.* (2006) for the unfrozen unsaturated case. There is no such reference to evaluation of a setup used in a freeze-thaw experiment. The ability to simulate the permafrost – active

layer interface in large field sampled peat monoliths is truly unique and offers new insights on the less understood aspects of heat and water storage and transfer during winter

### **3.2. The climate chamber**

The climate chamber can reproduce the Canadian subarctic solar and atmospheric environment and house soil monoliths up to 1.5 m in diameter and 4 m in height. The chamber was custom manufactured by BioChambers Inc. (Winnipeg, Manitoba) and delivered to Western in 2008 after over two years of engineering design and development (~ cost \$1.2 million Cdn.) During 2009-10 modifications to the experimental design were implemented during a 'proof of concept' phase. Several design features make the chamber unique and are key to replicating the Sub-Arctic surface and subsurface environment. The chamber's size allows one to work with soil monoliths of representative size to include all of the components of ecological interest (including vegetation) so that groundwater flow and biogeochemical processes do not require scaling. The chamber is a two level biome, with an adjustable insulated floor, enabling separate surface and subsurface environments. Dual compressors on each level allow for minimal temperature fluctuations and an air temperature control range of -40 °C to +40 °C ( $\pm 1$  °C). The wide range of temperatures allows physical simulations of environments ranging from desert to high Arctic. In addition to air temperature, it is possible to control the following solar and atmospheric parameters in the upper chamber: light intensity (mixture of metal halide and high pressure sodium lighting, dimmable, maximum 300 W

m<sup>-2</sup> at 1.5 m below the light bank); rain; relative humidity (10% to 90% at 25 °C); wind; and atmospheric CO<sub>2</sub> concentrations. Snow can be made using a custom made snow gun, e.g., Meyer *et al.* (2006) whenever required in the experiments. All environmental controls are fully programmable and can be remotely controlled. An automated backup generator ensures consistent power. Finally, four high precision platform scales (each 81 x 81 cm, KC600S, 10 g precision over 600 kg, Mettler Toledo Canada, Mississauga, ON) are installed in the base of the support structure. This allows continuous monitoring of soil mass for four independent monoliths or one large monolith (maximum 2400 ± 0.01 kg).

### **3.3. Field sampling of soil mesocosms**

Undisturbed peat cores, 60 cm in diameter, were extracted at the field site in the Scotty Creek watershed located in the wetland-dominated, discontinuous permafrost zone of Canadian Sub-Arctic. Details of the site location and characteristics can be found in (Quinton, 2008). Since the sampling site is in a remote area requiring float plane or helicopter access, a simple light weight peat corer was designed that allows coring and transport of the samples with minimum physical effort. Custom made fiber reinforced plastic (FRP) pipes (90 cm deep, 60 cm diameter) were fitted with a stainless steel blade on the bottom to cut through peat layers. The top was reinforced and machined to accept a rotating and lifting attachment. An aluminum tube and rod assembly fitted to the top of the pipe allowed for the pipe to be rotated into the ground powered by four persons. A side access trench is then dug and custom FRP bottom caps are attached securing the

sample for transport. The inexpensive corer allowed for the large diameter undisturbed sampling of peat to permafrost without the need for heavy equipment as in Millette and Demers (1984). The corer and sampling procedure is explained in detail in the appendix. The corer was used successfully and four samples with total depths of 42 cm, 52 cm, 55 cm and 60 cm intact with surface vegetation were extracted in one day. The variable depths of the undisturbed cores represent the actual depth of the permafrost table at the chosen sampling locations in August 2007. Depth to the permafrost table shows sharp spatial variations and depends on complex combinations of local factors such as canopy cover, surface albedo and soil moisture conditions during the thaw season. The cores were transported ~ 5500 km to the climate chamber by air and road transport. The samples were maintained at ~10 °C during transport and then maintained at -4 °C in order to (1) slow down biological degradation and avoid structural damage in peat, and (2) continue vernalization of plants to keep them active longer for participation in the Mesocosm experiments.

### **3.4. Experiment setup**

While the FRP pipes proved to be exceptionally strong and rigid sampling and transport containers, they might not accommodate continued sample expansion-contraction that would occur during freeze-thaw. In order to accommodate expansion, and add depth for the addition of a lower permafrost layer, 120 cm deep x 61 cm diameter LDPE containers were used to prepare peat Mesocosms in. The containers were lined from inside with 2.54 cm thick neoprene foam to provide additional insulation and to

provide for a tight seal between the container wall and peat during freeze-thaw. Neoprene has thermal conductivity comparable to that of dry peat under low hydrostatic pressures, e.g., Bardy *et al.* (2005). To represent the permafrost layer a ~45 cm thick layer of unprocessed catotelmic peat was first packed on the bottom to a bulk density of ~250 kg m<sup>-3</sup>. This layer was then completely saturated and allowed to freeze at -6 °C. Intermediate layers were then packed in each drum (bulk density varying from ~250 kg m<sup>-3</sup> to ~125 kg m<sup>-3</sup> to match field peat layering) to a thickness that allowed ~110 cm deep Mesocosms to be formed when the undisturbed field sampled cores were placed over these layers. It must be noted that the objective of these experiments were to replicate the field state of peat layers. Thus the use of actual field cored samples was critical as it was not possible to attain the structure of peat in field by repacking. The undisturbed samples were inserted in a frozen state using a metal sleeve guide forced inside the drum by slightly compressing the neoprene foam.

The drums were then moved to the upper chamber of the biome using a crane and placed on four 81 cm x 81 cm load cells for continuous weighing. The upper floor was adjusted such that each Mesocosm was 45 cm in the lower chamber and 75 cm in the upper chamber. The Mesocosms were then populated at different depths with 30 cm long time domain reflectometry (TDR) probes (CS610's and CS635's multiplexed using SDMX's, and connected to TDR100) for soil water content, temperature sensors (107B's multiplexed using a AM16/32B), heat flux plates (HFT3) at surface (all sensors from Campbell Scientific, Logan, UT, USA). In addition, ports were installed for gas and soil water sampling. Sensor and sampling port spacing increased with depth with a 5-10 cm

separation in the upper 25 cm, and 12-15 cm in the lower 40 cm and permafrost layer monitored separately. The temperature sensors were inserted such that the tip was 24 cm from the container walls. All sensors were connected to a CR1000 datalogger (Campbell Scientific, Logan, UT, USA) and data was collected every 15 minutes. The TDR was calibrated using undisturbed peat samples from the same site (see Chapter 2). The outside of the containers were then insulated using multiple layers of reflective bubble foam (Reflectix, Inc., Markleville, IN), and one layer of 5.08 cm thick fiber glass insulation (Fibrex Coreplus pipe insulation, Fibrex, Inc., Easley, SC). The gaps between the upper and lower chambers were closed 5.08 cm thick extruded polystyrene rigid insulation, completing the Mesocosm setup. Further details of the experimental setup with a line diagram and pictures are given in the appendix.

### **3.5. Evaluation**

Initial temperature profiles were established over a period of 75 days by maintaining the air temperature at 4 °C and -2 °C in the upper and lower chambers respectively. The initial soil water content profiles were established by slowly raising the water table by spray misting the peat surface. Once a stable linear temperature profile was established, the air temperature was dropped to create winter conditions (Table 1.1). Figures (3.1) and (3.2) show the initial soil water content profiles, and water table elevations, for two freezing runs initiated on 18<sup>th</sup> December, 2009 and 23<sup>rd</sup> July, 2010 respectively. All Mesocosms had a saturated zone located above the frozen soil layer during the first freezing run. This condition was maintained for the second freezing run

except for Mesocosm # 2 which had unsaturated conditions throughout above the frozen soil layer.

<b>Freezing Run</b>		<b>Air temperature (°C)</b>	
		Upper Chamber	Lower Chamber
<b>First freezing run</b>	Phase I (31 days)	-5	-1.9
	Phase II (16 days)	-10	-1.9
<b>Second freezing run</b>		-7.5	-1.9

**Table 3.1.** Temperatures in the upper and lower chambers during first and second freezing runs.

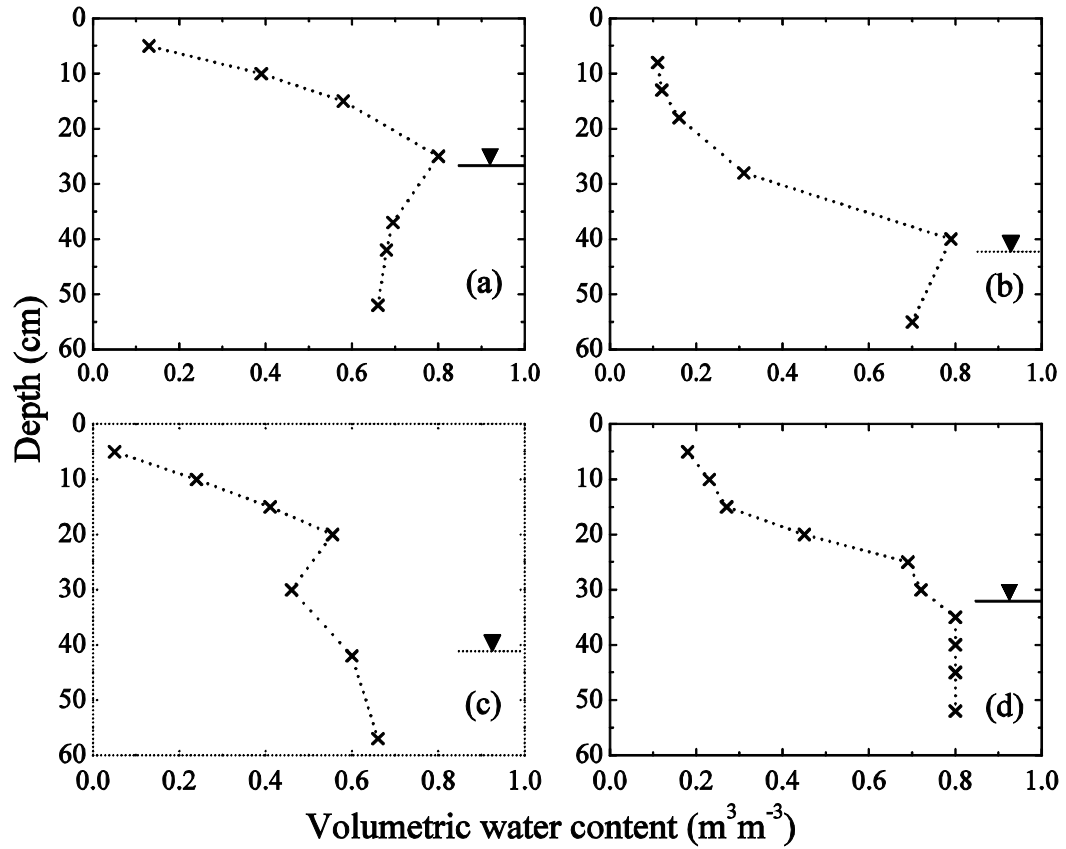


**Figure 3.1.** Initial water content in Mesocosms (a) 1, (b) 2, (c) 3, and (d) 4 for first freezing run. The depth to the groundwater table is shown by free water surface symbol in black.

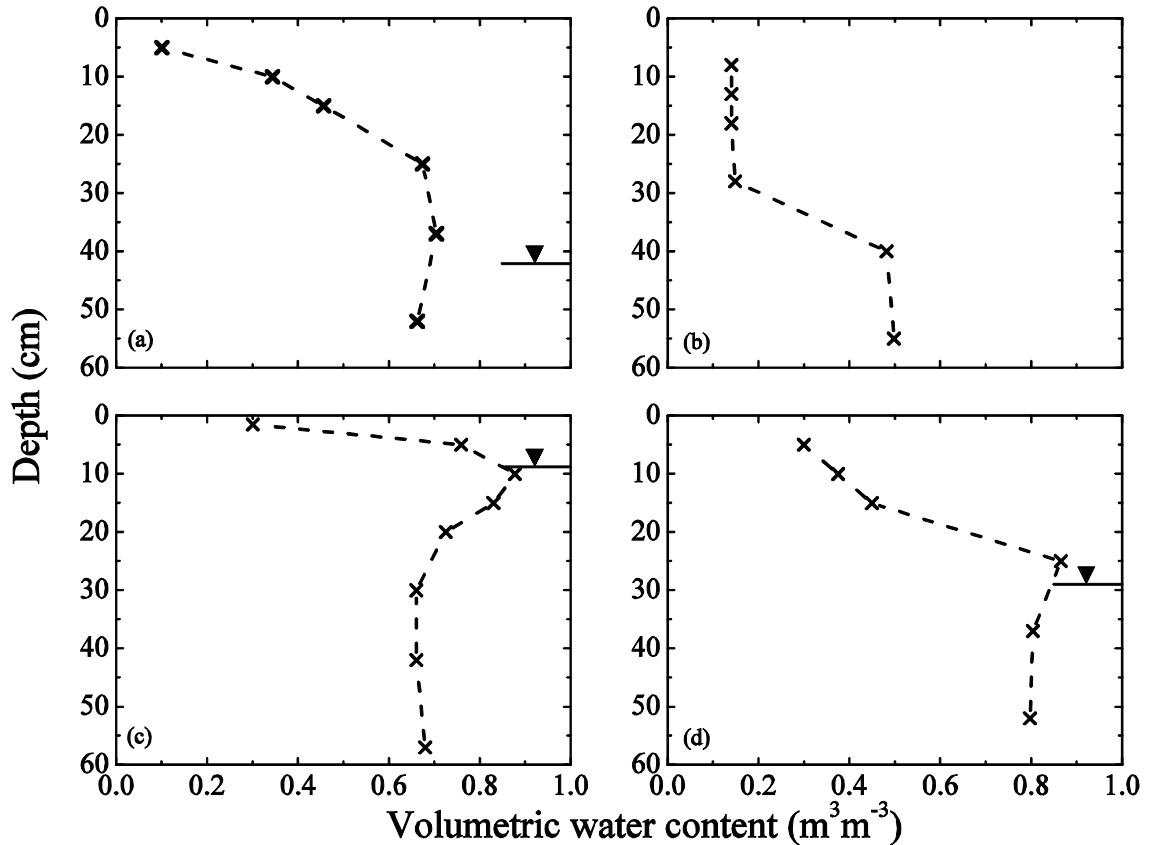


**Figure 3.2.** Initial water content in Mesocosms (a) 1, (b) 2, (c) 3, and (d) 4 for second freezing run. The depth to the groundwater table is shown by free water surface symbol in black. Mesocosm # 2 was unsaturated throughout its depth before the second freezing run.

The temperature profiles for Mesocosms 1 and 3 during the first run clearly show a downward progressing freezing front with time in addition to a very slow upward moving freezing boundary (Figure 3.3). The temperature profiles develop from the top downward with freezing initially taking place at shallow depths near surface. The delay in frost penetration with depth (e.g., Mesocosm #1 between the depths of 8 cm and 55 cm for the first ~100 hours as seen in Figure 3.3a) results in a convex depth versus temperature

profile which mirrors the field response (Figure 3.4). Following this phase of volumetric heat removal these depths remain close to 0°C as the soil water freezes owing to the latent heat-induced zero curtain effect. At around 400 hours, the temperature starts to drop and by 1100 hours only the initially saturated depths are still affected by the zero curtain. Figures (3.5) and (3.6) show the temperature profile and liquid water content time series for Mesocosm #2 during the first freezing run. The temperature profile again follows a similar development trend as for Mesocosms 1 and 3. The unfrozen water time series (Figure 3.6) shows the time lag in freezing with depth. The TDR probes are inserted in all Mesocosms such that the probe rods run laterally from the neoprene liner-soil interface to 30 cm inside. If there is pronounced effect of lateral heat removal due to an influence of air temperature in the upper chamber, very little time lag would be expected in the start of freezing at different depths. Thus the observed time lag is another confirmation of the good performance of the outer fibre glass insulation and the inner neoprene liner.

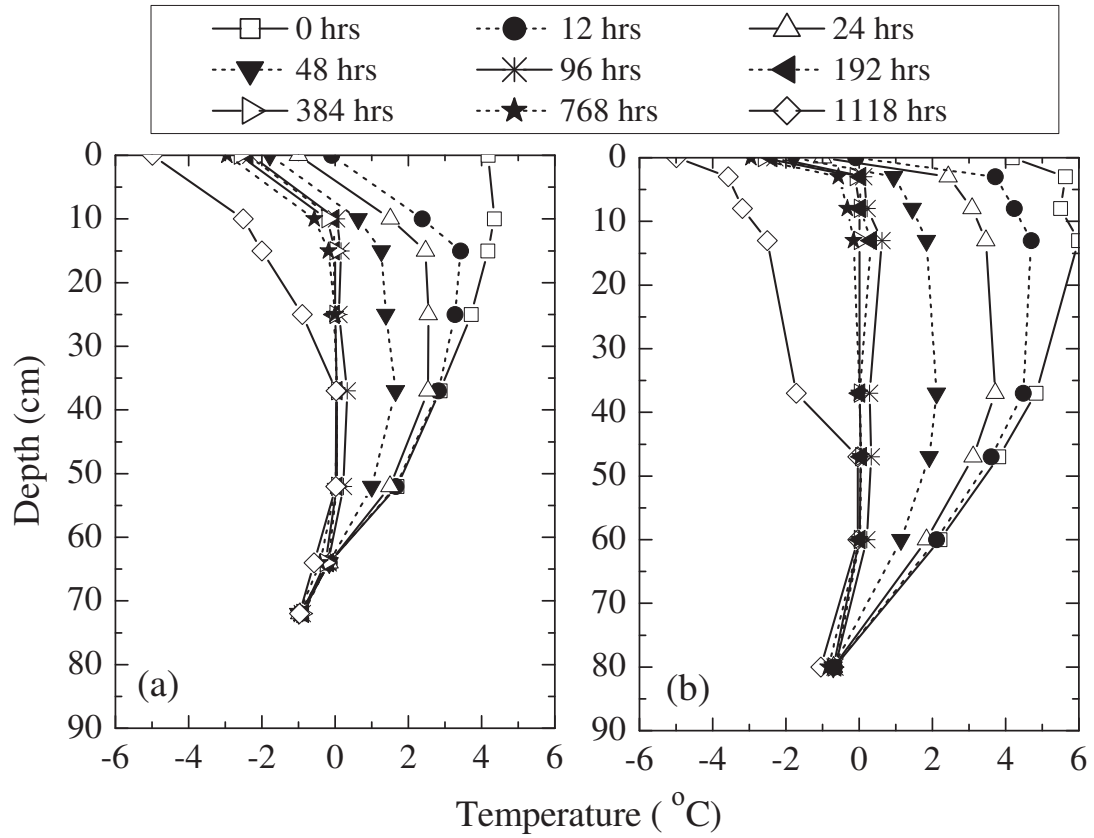


**Figure 3.3.** The temperature profile development for (a) Mesocosm 1 and (b) Mesocosm 3 during the first freezing run.

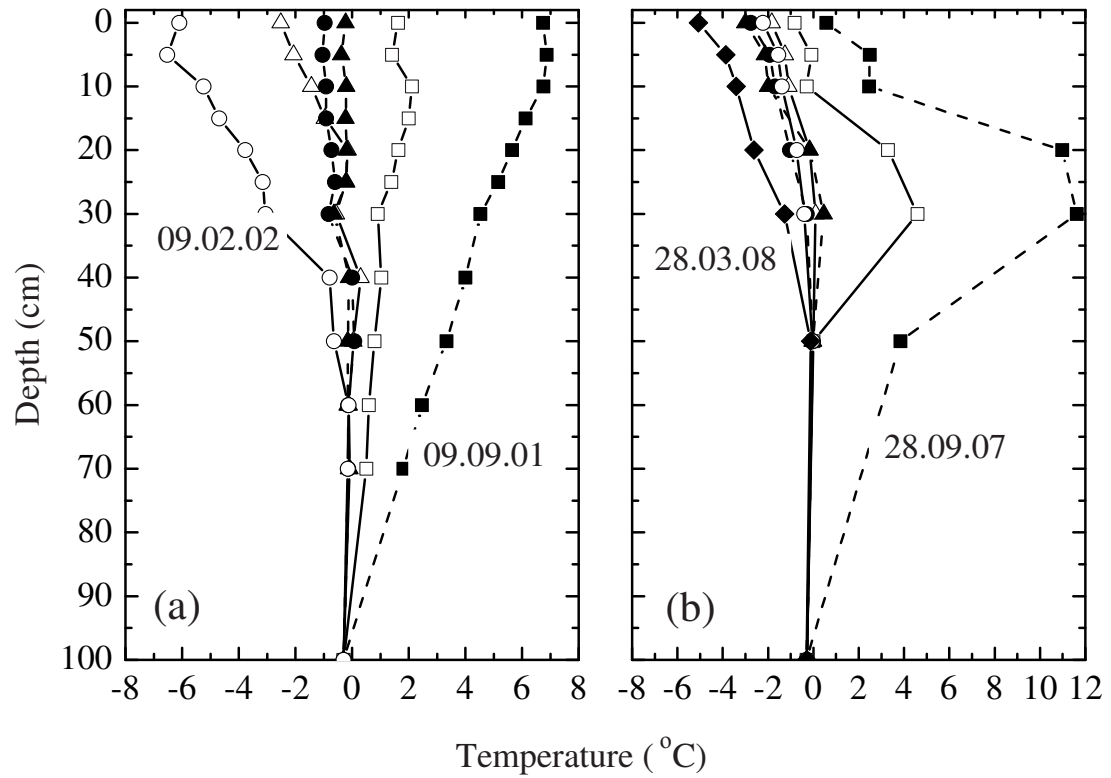


**Figure 3.4.** Temperature profiles recorded at Scotty Creek field site during the winter seasons of (a) 2001-2002 and (b) 2007-2008. The day of recording for the first and last profiles is shown on both graphs. The intermediate profiles are separated by intervals of 30 days. The temperature at 100 cm depth is approximated from borehole temperature records of a nearby (20 km) station from the Norman Wells pipeline study (Smith *et al.*, 2004).

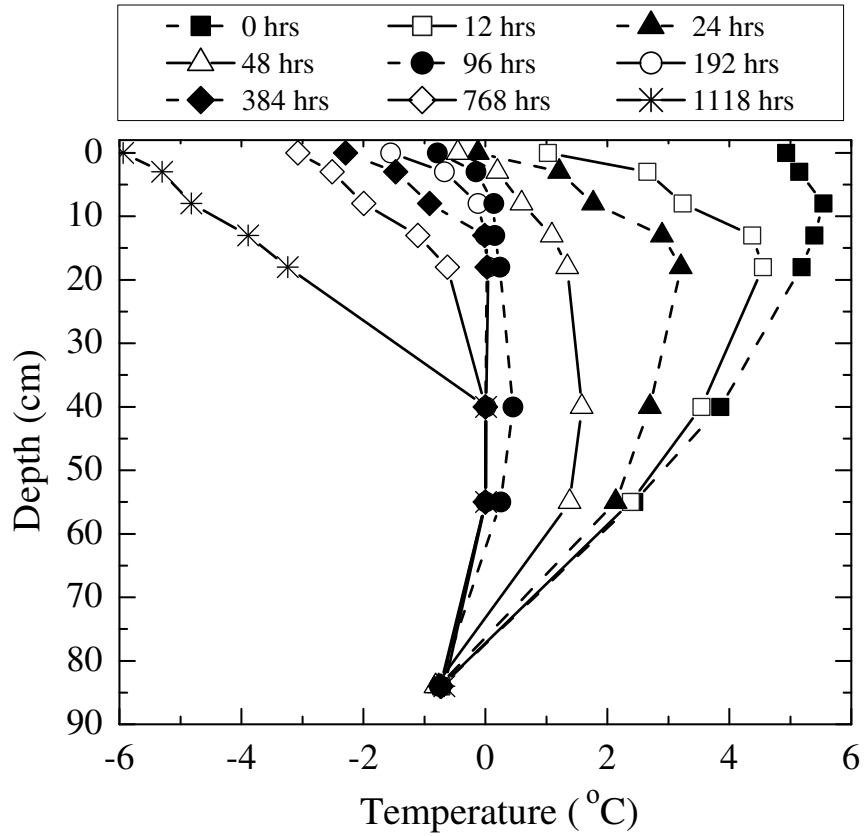


**Figure 3.5.** The temperature profile development for Mesocosm # 2 during the first freezing run.

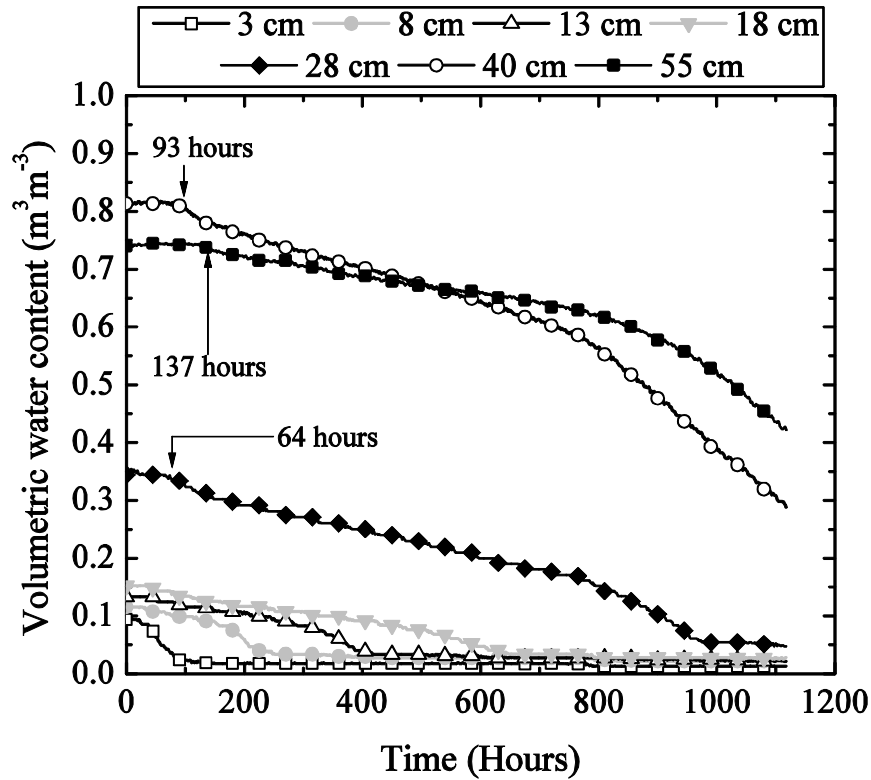


**Figure 3.6.** Unfrozen water content time series for Mesocosms # 2 during the first freezing run. Labels show the time at which freezing commences at three different depths.

While the outer and inner insulation performed well during the initial freezing run of 1118 hours, further refinements were made to prevent potential lateral temperature effects during longer runs with larger vertical temperature gradients. Three additional temperature probes were added to Mesocosm #2 at the start of the second run. These were situated at a distance of 4.5 cm from the container walls, and 8 cm, 28 cm and 55 cm below the top surface. Mesocosm # 2 was chosen because it was the driest and without a water table. Dry soil has a relatively low heat capacity owing to its low water content and therefore the changes in temperature at the edge would be quickly reflected if

there is any interference from air temperature in the upper chamber. A nearly air tight housing with walls made of 2.54 cm thick extruded polystyrene rigid insulation was constructed around Mesocosms in the upper chamber. This left only the tops of the Mesocosms exposed directly to the air in the upper chamber. Dry, compressed air with a temperature of around 5 °C, was circulated through this housing using multiple inlets and vents. Because of its highly porous nature and high water contents, peat temperatures remain close to 0 °C for bulk part of the freezing period. The temperature and pressure of compressed air were varied in order to maintain the temperature of air circulating inside housing close to 0 °C. A schematic of the housing and the compressed air circulation is shown in the appendix (Figure A7). Figure (3.7) shows the central temperature profiles, the same profiles when including the near-edge sensors, and thermal gradients for Mesocosm #2. The comparison shows that the experimental setup is able to maintain reasonable one-dimensional change with very small horizontal temperature gradients as compared to the vertical temperature gradients. The differences between the central temperature profiles and near-edge sensor profiles are within the absolute temperature sensor accuracy of 0.2-0.5 °C. Figure (3.8) shows the comparison between the temperature time series of near-edge sensors and central sensors at 8 cm, 28 cm and 55 cm below peat surface. Overall the near edge-sensor at 8 cm was at times 0.15-0.38 °C warmer than the central sensor, at 28 cm was at times 0.1-0.27 °C colder than the corresponding central sensor, while at 55 cm was within  $\pm 0.07$  °C of the temperature readings of the central sensor at the same depth. These differences could be because of combination of sensor errors, variable lateral peat pore water distribution, and heat

loss/gain at different times and depths. Although lateral heat loss cannot be completely stopped in systems such as described in this paper, the evaluation of the experimental setup shows that it performs fairly well for the intended research purpose.

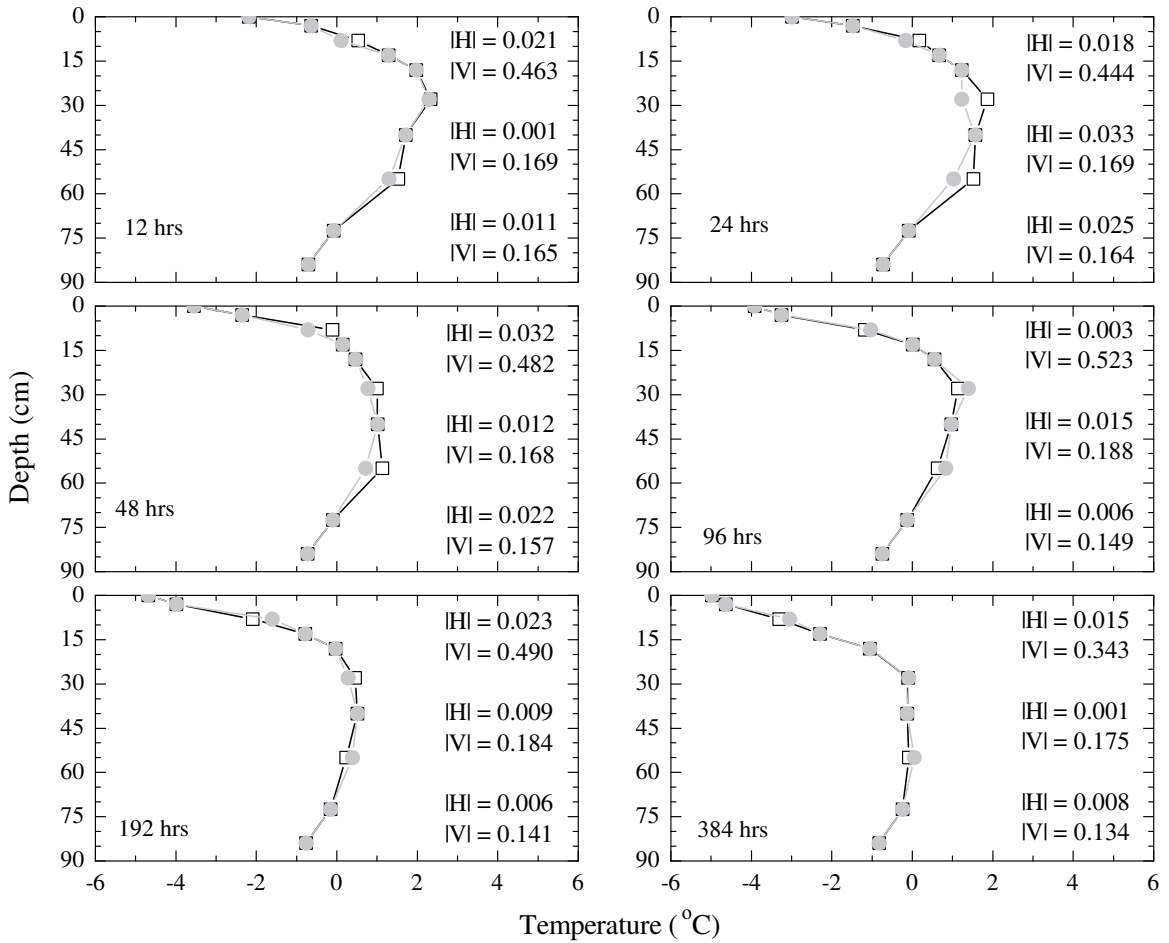


**Figure 3.7.** Comparison between temperature profiles for central location (grey circles) and near-edge sensors (white squares). The numbers on the right are the calculated absolute values of horizontal (|HI|) and vertical (|VI|) gradients in °C cm<sup>-1</sup> at 8 cm, 28 cm and 55 cm respectively.

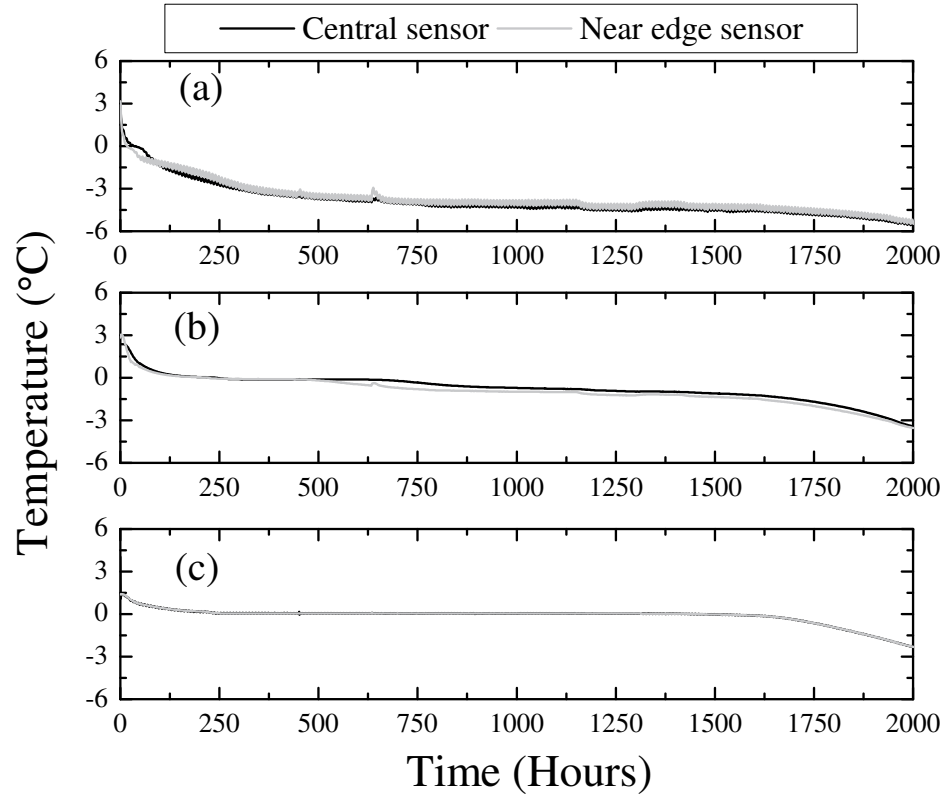


**Figure 3.8.** Comparison between temperature time series of near-edge and central sensors located at (a) 8 cm, (b) 28 cm and (c) 55 cm below peat surface.

### 3.6. Implications

The ability to replicate active layer-permafrost field processes in laboratory depends both on a proper field sampling methodology and an advanced climate chamber, and experimental setup, which can create realistic boundary conditions. The sampling methodology must allow for the collection of a representative volume such that the natural variability and soil structure (in this case peat) is preserved. However, maintaining representative boundary conditions is much more difficult with larger sample sizes. While previous freeze-thaw laboratory-scale studies have only been able to work

with much small samples (8-25 cm diameter x 10-100 cm deep), this study represents a successful extension to the Mesocosm scale. Furthermore, critical to replicating field conditions is the ability to physically represent the permafrost layer, and allow this layer to influence active layer processes if conditions dictate. Previous works have relied on cold plates at sample top and bottom to drive freeze-thaw cycles.

The data generated on peat soils in these experiments can be used to further the fundamental understanding of freeze-thaw processes in general. The less understood influence of individual climatological factors as well as soil moisture states is being currently studied. Study of gas flux during thaw seasons, insulation effects of snow cover, freezing induced water redistribution, and the effects of climate change and canopy cover changes on permafrost deepening are being investigated in a realistic laboratory environment. Changing climate is predicted to impact the northern latitudes more with the current permafrost covered areas expected to see soil zones vastly increase in biogeochemical and microbiological activity (e.g., Serreze *et al.*, 2000; IPCC, 2007; Zhang *et al.*, 2008). The success of the current experimental setup provides an opportunity to understand the biogeochemical and microbial response to climate change scenarios predicted for the organic covered permafrost terrain. These studies will provide verification based on physical experimental data of the numerical predictions to increase the reliability of numerical methods currently in use. The numerical models verified in this manner can be scaled-up and used for field conditions to obtain more consistent estimates of runoff and permafrost response to current and future climates.

### 3.7. References

- Aldrich, H. P., and H. M. Paynter (1966). Depth of frost penetration in non-uniform soil, *CRREL Special Report 104*, US Army Cold Regions Research and Engineering Laboratory, Hannover, 148 pp.
- Bardy, E., J. Mollendorf, and D. Pendergast (2005). Thermal conductivity and compressive strain of foam neoprene insulation under hydrostatic pressure, *Journal of Physics D-Applied Physics* **38**, 3832-3840.
- Buckingham, E. (1907). Studies on the movement of soil moisture, *USDA, Bureau of Soils, Bull. 38*, Washington D.C.
- Cary, J. W., and H. F. Mayland (1972). Salt and water movement in unsaturated frozen soil, *Soil Science Society of America Proceedings* **36**, 549-555.
- de Vries, D. A. (1963). Thermal properties of soils, in *Physics of plant environment*, W. R. van Wijk (Editor), North-Holland Pub. Co., 210-235.
- Dirksen, C. (1964). Water movement and frost heaving in unsaturated soil without an external source of water, Ph.D. Thesis, Cornell University, United States.
- Dirksen, C., and R. D. Miller (1966). Closed-system freezing of unsaturated soil, *Soil Science Society of America Proceedings* **30**, 168-173.
- Fukuda, M., A. Orhun, and J. N. Luthin (1980). Experimental studies of coupled heat and moisture transfer in soils during freezing, *Cold Reg.Sci.Technol.* **3**, 223-232.
- Guymon, G. L., R. L. Berg, and T. V. Hromadka (1993). Mathematical model of frost heave and thaw settlement in pavements, *CRREL Special Report 93-2*, US Army Cold Regions Research and Engineering Laboratory, Hannover, 130 pp.

- Harlan, R. L. (1973). Analysis of coupled heat-fluid transport in partially frozen soil, *Water Resour.Res.* **9**, 1314-1323.
- Hoekstra, P. (1966). Moisture movement in soils under temperature gradients with cold-side temperature below freezing, *Water Resour.Res.* **2**, 241-250.
- IPCC (2007). Climate Change 2007: The Physical Science Basis. Contribution of Working Group I to the Fourth Assessment Report of the Intergovernmental Panel on Climate Change [Solomon, S., D. Qin, M. Manning, Z. Chen, M. Marquis, K.B. Averyt, M. Tignor and H.L. Miller (eds.)]. Cambridge University Press, Cambridge, United Kingdom and New York, NY, USA.
- Jame, Y. (1977). Heat and mass transfer in freezing unsaturated soil, Ph.D. Thesis, The University of Saskatchewan, Canada.
- Lawrence, D. M., and A. G. Slater (2005). A projection of severe near-surface permafrost degradation during the 21st century, *Geophys.Res.Lett.* **32**, L24401, 5 PP.
- Meyer, T., Y. D. Lei, and F. Wania (2006). Measuring the release of organic contaminants from melting snow under controlled conditions, *Environ.Sci.Technol.* **40**, 3320-3326.
- Millette, J. A., and G. Demers (1984). The development of a large core sampler for organic soils, *Can.Agric.Eng.* **26**, 81-83.
- Mizoguchi, M. (1990). Water, heat and salt transport in freezing soil, Ph.D. Thesis, University of Tokyo, Tokyo.
- Philip, J. R., and D. A. de Vries (1957). Moisture movement in porous materials under temperature gradient, *Transactions, American Geophysical Union* **38**, 222-232.

- Quinton, W. L., M. Hayashi, and S. K. Carey (2008). Peat hydraulic conductivity in cold regions and its relation to pore size and geometry, *Hydrol.Process.* **22**, 2829-2837.
- Serreze, M. C., J. E. Walsh, F. S. Chapin, T. Osterkamp, M. Dyurgerov, V. Romanovsky, W. C. Oechel, J. Morison, T. Zhang, and R. G. Barry (2000). Observational evidence of recent change in the northern high-latitude environment, *Clim.Change* **46**, 159-207.
- Smith, S.L., M. M. Burgess, D. Riseborough, T. Coultish, J. Chartrand (2004). Digital summary database of permafrost and thermal conditions - Norman Wells pipeline study sites. *GSC Open File 4635*.
- Staehli, M., and D. Stadler (1997). Measurement of water and solute dynamics in freezing soil columns with time domain reflectometry, *Journal of Hydrology* **195**, 352-369.
- Zhang, Y., W. J. Chen, and D. W. Riseborough (2008). Transient projections of permafrost distribution in Canada during the 21st century under scenarios of climate change, *Global Planet.Change* **60**, 443-456.
- Zhou, J., J. L. Heitman, R. Horton, T. Ren, T. E. Ochsner, L. Prunty, R. P. Ewing, and T. J. Sauer (2006). Method for maintaining one-dimensional temperature gradients in unsaturated, closed soil cells, *Soil Sci.Soc.Am.J.* **70**, 1303-1309.

# CHAPTER 4. EFFECTS OF FREEZING ON SOIL TEMPERATURE, FROST PROPAGATION AND MOISTURE REDISTRIBUTION IN PEAT

## 4.1. Introduction

Wetland-dominated terrain underlain by discontinuous permafrost covers extensive parts of northern North America and Eurasia. The hydrologic response of these areas is poorly understood, in part due to the lack of understanding of role of individual climatological and soil related factors (e.g., initial moisture conditions) on active layer freeze-thaw processes. The active layer overlies the permafrost and undergoes seasonal freezing and thawing. Subzero soil temperatures result in higher capillary pressure gradients between warmer and colder regions of frozen soils (Phillip and de Vries, 1957). At the onset of winter water from deeper horizons moves toward the freezing front near the ground surface (Dirksen and Miller, 1966; Guymon and Luthin, 1974). Water carries heat and therefore alters both thermal and hydraulic properties of soil during redistribution. Although these processes have been extensively studied in mineral soils (e.g., Dirksen, 1964; Jame, 1977; Hansson, 2004), by comparison only a few studies have examined moisture redistribution in organic soils (e.g., Carey and Woo, 2005; Quinton *et al.*, 2005). Peat can have bulk densities ( $\rho_b$ ) as low as  $0.035 \text{ kg m}^{-3}$  and porosities exceeding 96% by volume. These characteristics are common in the peat deposits at or near the ground surface (e.g., Schlotzhauer and Price, 1999; Quinton *et al.*, 2009). The

high porosities results in significant changes in the thermal and hydrological properties of peat as soil water content varies (de Vries, 1963; Smerdon and Mendoza 2010).

In organic-covered permafrost terrain, the topography of the relatively impermeable frost table plays an important role in controlling spring runoff (Wright *et al.*, 2009). It is broadly understood that factors such as climate, canopy cover, ground slope, and soil moisture and thermal properties of soil play critical roles in development or degradation of permafrost. Redistribution of moisture within the active layer during the winter months plays an important role in determining the position of the impermeable frost table at the onset of end-of-winter snowmelt event. The mechanisms that drive this redistribution of moisture are poorly understood (Quinton and Hayashi, 2008). For example, observations of Quinton and Hayashi (2008) suggest that at onset of winter, the water table is typically deeper than 0.5 m below ground, while at the start of spring melt, the upper surface of the frozen, saturated soil is typically about 0.1 m below the ground surface. How this condition developed during the winter period remains unclear. Field investigations by Quinton and Hayashi (2008) suggest that the amount of water supplied to the soil during the spring melt event in addition to the cumulative amount of meltwater supplied during over-winter melt events, is sufficient to saturate the ~0.4 m thick soil zone between the water table position at the time of freeze-up and the frost table position at the end of winter. The role latent heat plays in the propagation of frost has been examined (e.g., Harris *et al.*, 2008), yet the effect of different soil moisture conditions on frost propagation and frost induced water redistribution remains unclear. Soil moisture profile at the onset of winter also governs the ice content in the surface layer of the

organic soils. The rate of thaw propagation is affected by the initial soil ice content. Once thaw reaches a certain depth infiltration into organic soils becomes unlimited (Gray *et al.*, 1985; Gray *et al.*, 2001). Field studies have greatly contributed to advancing the understanding of freeze-thaw processes in organic terrains (e.g., Quinton *et al.*, 2005; Carey and Woo, 2005). However, seasonal limits on the accessibility of field sites mean that laboratory and numerical studies are required to develop and complement the fundamental understanding of freeze-thaw and moisture distribution processes that occur throughout the year. Mathematical theories and improved numerical approaches (e.g., Hansson *et al.*, 2004; Dall'Amico, 2010) are still being developed to increase the efficiency of modeling approaches.

Soil column and lysimetric experiments, under controlled laboratory conditions, produce data that can be used to verify these models. Examples of column experiments to study coupled water and heat movement in frozen mineral soils can be found in literature (e.g. Dirksen, 1964; Hoekstra, 1966; Jame, 1977; Guymon *et al.*, 1993, Staehli and Stadler, 1997; Gergely 2007). However, two major limitations in using this experimental data involve realistic boundary conditions and soil heterogeneity. Soil column freeze-thaw experiments have been traditionally conducted with cold plates at least at one end (e.g., Mizoguchi, 1990; Jame, 1977; Staehli and Stadler, 1997; Gergely 2007). In these experiments the other end of the column was either thermally insulated, in contact with a warm/cold plate, or exposed in a freezer/cold room. This does not create realistic replication of field permafrost conditions or the bi-directional freezing of the active layer, and hence, the influence of subsurface thermal properties on near surface energy balance

is not the same. Laboratory studies using uniformly packed soil columns subjected to simplified boundary conditions have long been used to verify numerical schemes and mathematical theories (e.g., Jame and Norum, 1980; Hansson *et al.*, 2004; Painter, 2010). Zhang *et al.* (2010) point to limitations of schemes verified with such data when applied to non-uniform/ layered soil conditions, or large flux conditions such as snow melt infiltration. Data for such verification cases is scarce and experiments under controlled laboratory settings need to be aimed at observing freeze-thaw processes that emulate field conditions as closely as possible (e.g., undisturbed soil cores) with realistic boundary conditions.

Innovative experimental design is required to isolate the influence of individual climatological factors, soil moisture conditions and soil properties on soil freezing and thawing. This study uses four mesocosms that are thermally insulated on the sides and contain a basal layer of peat that is continuously frozen to simulate permafrost (proxy permafrost). The air above the Mesocosms was maintained at temperatures below 0° C so that the unfrozen peat above the simulated permafrost could be subjected to bidirectional, one-dimensional freezing. The influence of initial soil moisture on freezing processes was studied by maintaining the four Mesocosms at different water contents at the start of freezing. The experiments were specifically aimed at

(1) observing the process of freezing-induced soil water redistribution, and the role of the initial soil water content in movement of water towards the freezing fronts. Correlating the freezing-induced soil water redistribution to the over-winter moisture redistribution

observed in the field is needed to understand the over-winter moisture redistribution processes that result in the saturation of most of the active layer by the end of winter;

(2) understanding if the initial soil moisture profile governs the ice content in the peat near the ground surface, which has implications for the partitioning of snowmelt water into infiltration and runoff.

(3) understanding the effects of initial water content on (a) soil freezing characteristics; and (b) soil thermal properties and frost propagation.

(4) organizing the observations of this study into a simple conceptual model to describe the processes of freezing front movement and freezing induced water redistribution.

In addition to the above mentioned objectives, the contribution of water from the partially frozen transition zone between the active layer and proxy permafrost to the overlying active layer was investigated using deuterium isotope labelling. This was done to observe if the water from the partially frozen transition zone remains immobile during freezing of the overlying active layer.

## **4.2. Methodology**

### **4.2.1. Experimental setup**

The experimental setup consisted of four peat Mesocosms (M1, M2, M3 and M4), each ~110 cm deep and 56 cm in diameter. All Mesocosms consisted of a ~45 cm thick proxy permafrost layer prepared by packing unprocessed humified peat to a bulk density

of  $\sim 250 \text{ kg m}^{-3}$ . Once prepared, this layer was completely saturated and allowed to freeze at  $-6 \text{ }^\circ\text{C}$ . Intermediate layers of unprocessed humified peat were then packed in each Mesocosm (bulk density varying from  $\sim 250 \text{ kg m}^{-3}$  to  $\sim 125 \text{ kgm}^{-3}$ ) to a thickness that allowed  $\sim 110 \text{ cm}$  deep Mesocosms to be formed when the undisturbed field sampled cores were placed over these layers (Table 4.1). The unprocessed humified peat used for proxy permafrost and intermediate layers was obtained from the Upsala, Ontario operations of Peat Resources Ltd. The undisturbed cores were extracted from Scotty Creek watershed, Northwest Territories, Canada located in the wetland-dominated, discontinuous permafrost region. Details of the site location, landform types and site characteristics can be found in Quinton *et al.* (2008), and details of coring methodology can be found in the appendix. Dry bulk densities and porosities for Scotty Creek peat were reported by Hayashi *et al.* (2007) and are shown in Figures 4.1a and 4.1b. The vertical hydraulic conductivity of saturated peat was measured for different depths in the laboratory using the cube method (Figure 4.1c). The samples contained no mineral material and the ash content determined using methods prescribed in ASTM D2974 - 07a was only 2% of dry weight. Water retention characteristics for the peat layers were reported by Quinton and Hayashi (2005) as shown in Figure 4.1c. In general, deeper peat layers hold more water at higher tension. For peat from the same site, Rezanezhad *et al.* (2009) found the degree of humification on the von Post scale to change from H3 just below surface vegetation to H5 at a depth of 65 cm.

Mesocosm	Undisturbed peat (top of core)	Repacked layer* (middle of core)	Repacked frozen layer (bottom of the core)
M1	42	18	45
M2	50	15	45
M3	17	51	45
M4	57	8	45

\*unprocessed, humified peat from Upsala, Ontario

**Table 4.1.** Details of the thickness (cm) of peat layers in each Mesocosm.

The Mesocosms were setup in the Earth Science module (BESM) of the Biotron Institute for Experimental Climate Change at the University of Western Ontario. The BESM is a two level biome with four dedicated compressors, two each for the upper and lower chambers with an air temperature control range of -40 °C to +40 °C. By situating the Mesocosms between these two chambers it was possible to maintain a frozen state in the lower ~45 cm of the core while allowing for freezing and thawing of the overlying peat. Light intensity, rain, relative humidity, wind speeds, and CO<sub>2</sub> concentrations can be controlled independently in upper chamber. Further details on the BESM facility can be found in Chapter 3.

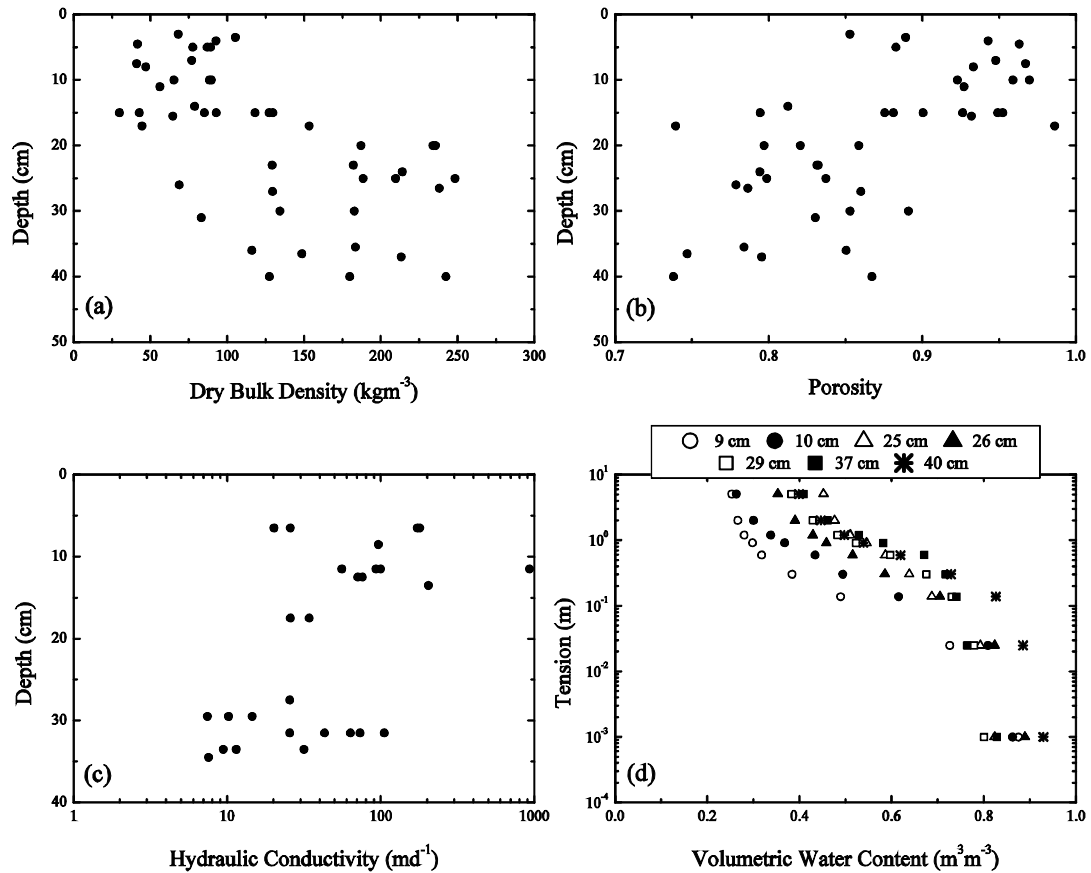


**Figure 4.1.** Depth variation of (a) Bulk density (Hayashi *et al.*, 2007), (b) porosity (Hayashi *et al.*, 2007), (c) vertical hydraulic conductivity, and (d) soil water retention curves (Quinton and Hayashi, 2005) for peat from Scotty Creek watershed. The different symbols in (d) represent the samples taken at different depths as shown in legend.

Mesocosms were instrumented at different depths with time domain reflectometry (TDR) sensors (TDR100, CS610 and CS635 probes, Campbell Scientific, Inc., Logan UT) and temperature sensors (107BAM, Campbell Scientific, Inc., Logan UT). A heat flux plate each (HFT3, Campbell Scientific, Inc., Logan UT) was inserted near the soil's surface in M2 and M3. Sampling ports were drilled in the sides of the Mesocosms at different depths to allow soil gas and water sampling. The Mesocosms were placed on

four 81 cm x 81 cm load cells (KC600S, 10 g precision over 600 kg, Mettler Toledo Canada, Mississauga, ON) for continuous weighing such that the bottom ~45 cm of the Mesocosms were in lower chamber and the remainder protruded into the upper chamber. The sides of the Mesocosms were insulated using a combination of neoprene foam and mineral fibre insulation. The lower chamber was maintained at -1.9 °C to keep the bottom ~45 cm of the cores continuously frozen while the air temperature was varied in the upper chamber. Figure 4.2 shows a schematic of the experimental setup with detailed explanation of various components. Soil dielectric permittivity, temperature, heat flux and weight were recorded every 15 minutes.

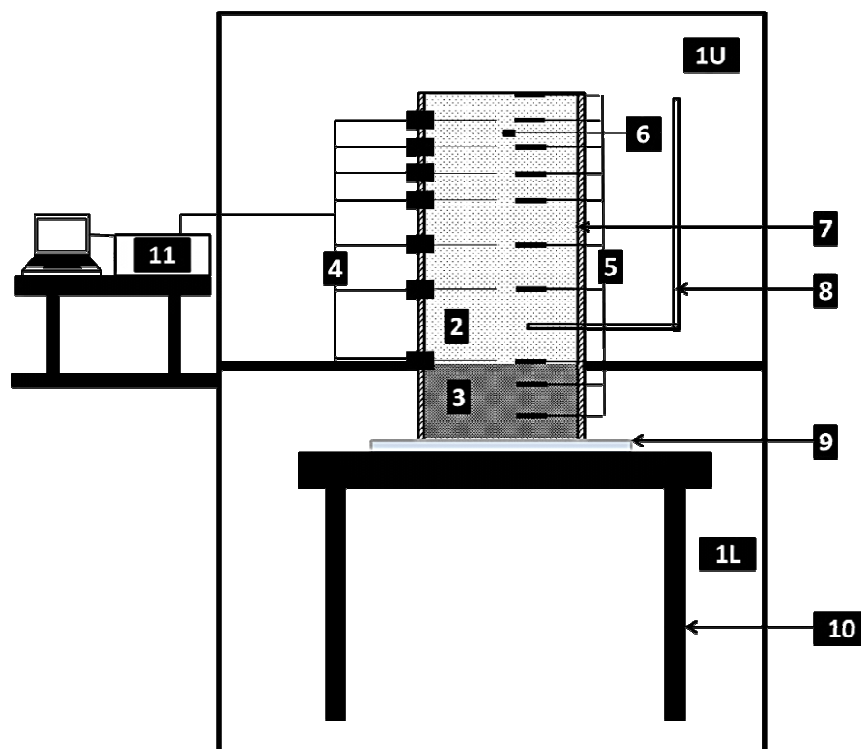


**Figure 4.2.** Line diagram showing the experimental setup. **1U**: Upper level chamber of the BESM; **1L**: Lower level chamber of the BESM; **2**: 65-75 cm deep unfrozen layer; **3**: 45 cm bottom frozen layer (fully saturated before freezing); **4**: TDR probes connected to

11 through low-loss coaxial cables; **5**: temperature probes connected to 11; **6**: heat flux plate; **7**: LDPE container lined with neoprene from inside and insulated from outside; **8**: stand pipe for water level measurements; **9**: weighing scale; **10**: custom made stand to support the entire experimental setup; **11**: multiplexers and datalogger connected to a personal computer.

#### **4.2.2. Experimental conditions**

Two freezing runs were conducted. In the first run, the Mesocosms were subjected to air temperature in the upper chamber of -5 °C for 31 days and then -10 °C in the following 16 days. This first run was aimed at understanding the freezing characteristics in general and tracing the water movement from deeper sources (e.g., from proxy permafrost-active layer transition zone to the overlying active layer saturated zone). All four Mesocosms had an unfrozen, saturated layer at the commencement of the first freezing run with water table depths of 27-, 43-, 43- and 32 cm below the surface respectively. To establish saturated layers within the Mesocosms, water was sprayed daily (twice a day in different amounts) on the surface and the Mesocosms were allowed to equilibrate for at least 30 days. After 47 days of freezing, it took 75 days to thaw the active layer down to the top of the proxy permafrost layer. The air temperature in the upper chamber was maintained constant at 15 °C and lights were kept on such that the soil surface level received an energy input of  $160 \text{ Wm}^{-2}$ . A further 75 days were required to establish the initial conditions for the second freezing run. The air temperature in the upper chamber was maintained at -7.5 °C for 93 days during the second freezing run. The air temperature in the lower chamber was kept constant at -1.9 °C. Most of the data from first freezing run, except the isotope analysis, could not be used because of sequential

failure of temperature sensors during this run. Therefore, the discussion of water movement from the transition zone is based on isotope profiling carried out during the first freezing run while soil freezing characteristics and influence of initial water content on soil water redistribution and frost propagation was examined from the data of the second freezing run.

### 4.2.3. TDR calibration

A detailed calibration of the TDR100 was performed at a constant temperature (30 °C) using undisturbed peat samples from the Scotty Creek field site (see Chapter 2). In an independent test, the temperature dependency of the observed apparent dielectric permittivity ( $\epsilon$ ) of unfrozen peat-air-water mixture at three different volumetric water contents ( $\theta$ ) was also determined (Figure 4.3a). It can be seen that  $\epsilon$  is significantly affected by temperature at higher water contents. Figure 4.3b shows the relationship between temperature and  $\epsilon$  for water (unfrozen and frozen states) in the -10 °C to +16 °C range. The same relationship was observed by Wohlfarth (2010). Neither peat nor air shows any variation in  $\epsilon$  with changing temperature (Figure 4.3c). The increase in  $\epsilon$  with decreasing temperature for the peat-air-water mixture can be thus solely attributed to the temperature- $\epsilon$  relationship of water. The apparent dielectric permittivity of ice remains close to 3.14 without any dependency on decreasing temperature in the observed range (Figure 4.3b). Maxwell De-Loor's (MDL) mixing model can efficiently handle the temperature effects on the  $\epsilon$ - $\theta$  relationship (Nagare *et al.*, 2011). Because a temperature correction is required for the empirical equation, the MDL model was used to estimate

water content from observed  $\epsilon$  in the mesocom experiments after calibrating it with the empirical equation at 30 °C. Bound water was not taken into account and the influence of ice on apparent dielectric permittivity was not considered owing to the inability of estimating pore ice content. Also, probe length differences between TDR probes and soil temperature sensors could be important as temperature differences along the TDR waveguides can induce temperature effects in water content measurements. However given the close comparison between near edge and central temperature sensors, it appears that such effects would have been minimal during this study. The measuring volume for

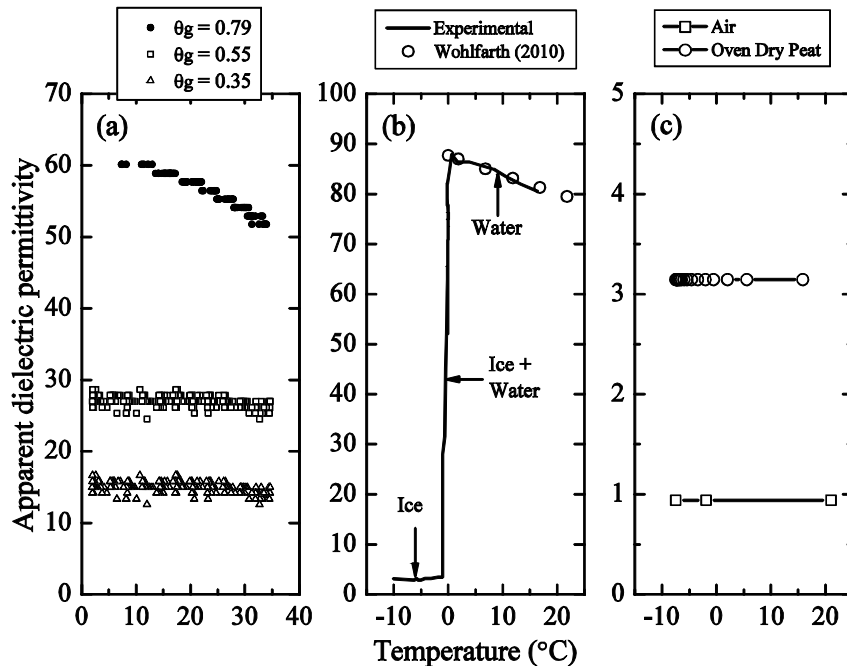


**Figure 4.3.** (a) Effect of temperature on apparent dielectric permittivity measurements in peat. The gravimetric water content ( $\theta_g$ ) did not change over the duration of test. Effect of temperature on observed apparent dielectric permittivity of (b) water, and (c) air and oven dried peat as determined using TDR100. The relative permittivity of oven dried peat was derived from the bulk apparent dielectric permittivity using a 2-phase mixing formula.

temperature sensor is relatively much smaller than that for the TDR probes. This can result into differences in timing of freezing of water around the temperature sensor as compared to TDR probes. However, such differences are ignored in this study and it is assumed that water content in the lateral plane is uniform. Time domain reflectometry measurements below 0 °C can be affected by a number of factors. These include the effect of pore ice on relative permittivity of unfrozen soil water (Van Loon, 1991) and effect of presence of ice on bulk relative permittivity of soil. However, such effects were not considered in this study due to the unavailability of data.

#### **4.2.4. Final total water content**

Final total water content (ice + liquid water) was measured at the end of the second freezing run for all four Mesocosms. Cores were extracted from the frozen Mesocosms using a custom designed coring tool (30 cm long thin walled stainless steel tube; 2.03 cm inner diameter) powered by an electric drill. Two cores each from M2 and M4 were sampled from depth intervals 0-25 cm and ~25-45 cm by slowly drilling into the samples in two depth increments. Two cores between depth intervals 0-25 cm and ~25-36 cm could be extracted from M1. The final water content in M3 could be determined only for the upper 9.1 cm, as efforts to core deeper in this Mesocosm did not succeed due to high ice contents. The cores were cut while frozen into smaller sections, weighed and oven dried at 87 °C until no further change in weight was recorded. The dry samples were weighed again for gravimetric measurement of the final total water content. A limitation of taking much smaller cores is that it may not give a true representative final water

content. Moreover, these cores were taken very close to the edge of the drum holding the samples. This may have led to further errors due to edge effects and probably a different water movement regime near the edges. Also, lateral movement could have led to differences in water contents spatially in the sample. Usually it is best to cut the entire core to know the final water content. Therefore, the final water content obtained using the cores is used only for process based discussion and no quantification is provided.

Soil pore pressure in freezing peat was not directly measured as soil water content (via TDR measurements) was measured and related to soil pore pressure using soil moisture curves (Figure 1d) for unfrozen soils and soil freezing curves (discussed in later sections) for frozen soils.

#### **4.2.5. Isotope profiling experiment**

Deuterium-enriched water was used as a tracer to monitor the upward movement of water from the ice rich transient layer during the first freezing run. The ~45 cm thick permafrost zone (Figure 4.2) was prepared by packing unprocessed humified peat, saturated with deuterium enriched water, to a density of  $\sim 250 \text{ kg m}^{-3}$  in each Mesocosm. This peat was then frozen at  $-6 \text{ }^\circ\text{C}$  until a thin ice crust formed on the surface of this layer. A repacked middle layer, thickness for which varied from 8 cm to 51 cm in different Mesocosms, was then placed on top of the proxy permafrost, and on top of it was placed the undisturbed peat core (for full description see Chapter 3).

Oxygen and hydrogen isotope values were determined using a Picarro Cavity Ring-Down Spectrometer (CRDS) Isotopic Water Analyzer (Model L1102-*i*) with a PAL

autosampler. Two ml of water were placed in vials and water aliquots of ~1.8  $\mu$ l were injected into the evacuated evaporator, kept at 140°C. Six injections were repeated for each sample and only signals of 17000-23000 ppmV H<sub>2</sub>O in the gas stream were considered good injections. Results from the first 3 injections were discarded and the oxygen- and hydrogen-isotopic value reported for one sample is the average of data obtained for the last 3 good injections. All isotope values are reported in the delta-notation:  $\delta = (R_{\text{sample}}/R_{\text{standard}} - 1) \times 1000$  in parts per thousand or per mil (‰); where R = D/H or <sup>18</sup>O/<sup>16</sup>O. All measurements are reported relative the international standard VSMOW. Laboratory standards, calibrated to VSMOW, were measured with each set of samples. LSD and HEAVEN were used to provide a calibration curve and EDT and MID were used to assess accuracy. Over this study, a  $\delta^{18}\text{O}$  value of  $-7.3 \pm 0.09$  ‰ (n=16) was obtained for EDT, which compares well with its accepted value of  $-7.3$  ‰, and a  $\delta^{18}\text{O}$  value of  $-13.1 \pm 0.06$  ‰ (n=8) was obtained for MID, which compares well with its accepted value of  $-13.1$  ‰. A  $\delta\text{D}$  value of  $-55 \pm 0.5$  ‰ (n=16) was obtained for EDT (accepted value =  $-56$  ‰), and a  $\delta\text{D}$  value of  $-108 \pm 0.4$  ‰ (n=8) was obtained for MID (accepted value =  $-108$  ‰). The standard deviation ( $1\sigma$ ) for duplicate analysis of unknown samples was better than  $\pm 0.1$  ‰ for  $\delta^{18}\text{O}$  and  $\pm 0.6$  ‰ for  $\delta\text{D}$  values.

During the experimental set-up waters were extracted from the saturated peats via high speed centrifugation of small peat samples in order to obtain the  $\delta\text{D}$  values that result from the mixture of the original soil moisture and the D-enriched labeled water. Analysis of peat water from the proxy permafrost layers showed that they were highly

enriched in deuterium ( $\delta D = 566 \text{ ‰}$ ,  $656 \text{ ‰}$ ,  $669 \text{ ‰}$ , and  $621 \text{ ‰}$  in M1, M2, M3, and M4). The crustal ice was enriched in deuterium resulting in  $\delta D$  values of  $559 \text{ ‰}$ ,  $620 \text{ ‰}$ , and  $502 \text{ ‰}$  in M2, M3, and M4 respectively. A 10 ml disposable syringe was used along with a 30 cm long needle to sample laterally from the inner core of the saturated zone of active layers in each Mesocosm. Water samples were taken from different pockets by varying the length of lateral needle penetration in order to avoid drying the soil in one location. Water was sampled at three different depths (40 cm, 50 cm and 60 cm) in the saturated zone of the active layer in all three Mesocosms from the start of the freezing run until late into the freezing period when no water could be withdrawn. An additional 14 samples from the three Mesocosms were collected at these depths while the peat was thawing.

### **4.3. Results and discussion**

#### **4.3.1. Initial conditions**

The influence of water content at the start of the freezing run on active layer freezing processes was studied during the second freezing run. A leak developed in Mesocosm 2 at the end of first freezing run. Rather than take this Mesocosm out of the experiments, it was allowed to drain to the level of the leak and used to simulate dryer moisture condition. Figure 4.4 shows the initial water content profiles in all four Mesocosms at the start of the second freezing run. Initial water content is the unfrozen water content at the start of the freezing run estimated from TDR observations. Mesocosms 1 and 4 were variably wetted (unsaturated zone over saturated zone) at the

start of this freezing run with the water tables located at 42 cm and 27 cm below the ground surface respectively. Mesocosm 2 was unsaturated throughout the depth with no saturated zone, while the water table was located at ~5.5 cm in Mesocosm 3 at the start of the freezing run. A linear initial temperature profile in each Mesocosm was achieved by maintaining the air temperatures in lower and upper chambers at -1.9 °C and 3 °C respectively until a relatively stable linear profile was achieved.

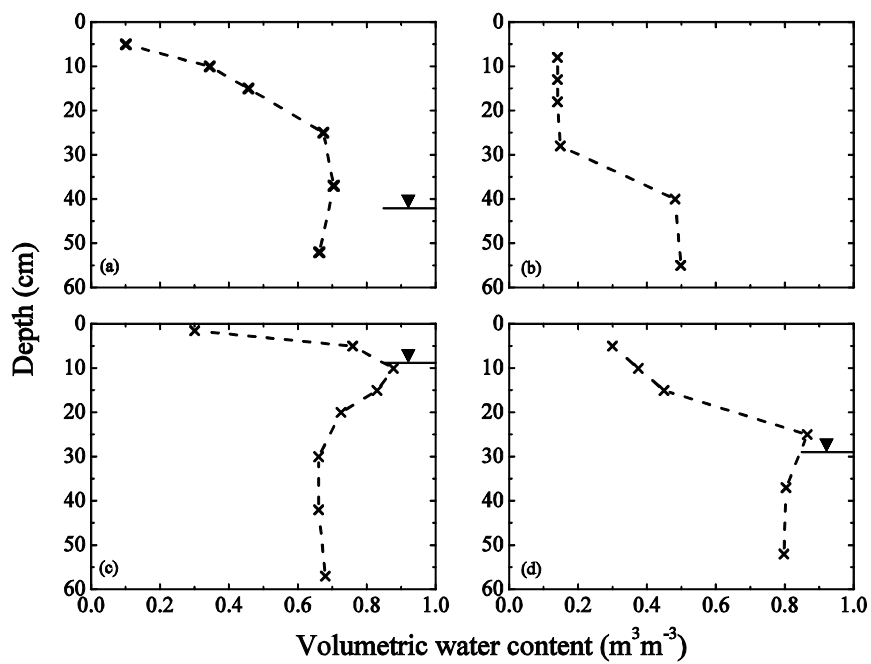


**Figure 4.4.** Initial water content in Mesocosms (a) 1, (b) 2, (c) 3, and (d) 4 for second freezing run. The depth to the groundwater table is shown by free water surface symbol. Mesocosm # 2 was unsaturated throughout the depth for before the second freezing run.

#### 4.3.2. Soil freezing characteristics

Soil freezing characteristics (SFCs) at different depths were determined from observed liquid water content and soil temperature data collected during the second

freezing run. Water in M1, M2, M3 and M4 started to freeze at  $-0.08\text{ }^{\circ}\text{C}$ ,  $0\text{ }^{\circ}\text{C}$ ,  $-0.05\text{ }^{\circ}\text{C}$  and  $-0.08\text{ }^{\circ}\text{C}$  respectively, and represent the temperatures at which peat water starts to freeze (freezing point before further depression) in each Mesocosm in the discussion to follow (Figure 4.5). It is evident that some water remained unfrozen even after 2000 hours (83 days) of freezing (Figure 4.6a) with residual liquid water contents between  $0.05\text{ m}^3\text{ m}^{-3}$  and  $0.13\text{ m}^3\text{ m}^{-3}$  continuing to exist even at  $-5\text{ }^{\circ}\text{C}$ . Shallower depths are left with less residual water than deeper ones for the same freezing temperatures. Similarly, depths with higher initial water contents are left with slightly larger amounts of residual water at similar temperatures. One reason for the differences in residual water content with depth could be the effect of pore size on unfrozen water content and TDR measurements. Time domain reflectometry measurements in frozen soils (e.g. Watanabe *et al.*, 2011) show that relatively larger amounts of residual water is left in soils with smaller pores than in soils with larger pore sizes (e.g., silt loam v.s. sand). Pore size in peat decreases with depth and this could be a potential reason for differences in the residual water contents at different depths in the Mesocosms.

A few SFCs in all Mesocosms appear to be affected by water redistribution at some stage for temperatures below freezing (Figure 4.7). However, overall the other SFCs appear to follow a common path during freezing. As theorized by Low *et al.* (1968), liquid water content in frozen soils must have a fixed value for each temperature at which the liquid and ice phase are in equilibrium, regardless of the amount of ice present. It is convenient to define a single soil freezing curve for a particular soil type in order to simplify the relationship between soil temperature and liquid water content. An

example of a single curve defining the temperature-liquid water content relationship based on the van Genuchten model (van Genuchten, 1980) is shown in Figure 4.8. The curve was obtained by fitting into the soil temperature and liquid water content data other than those shown in Figure 4.7. This approximation of the SFCs in a single curve is important for numerical studies as it simplifies the constitutive relationship between soil temperature and liquid water content.

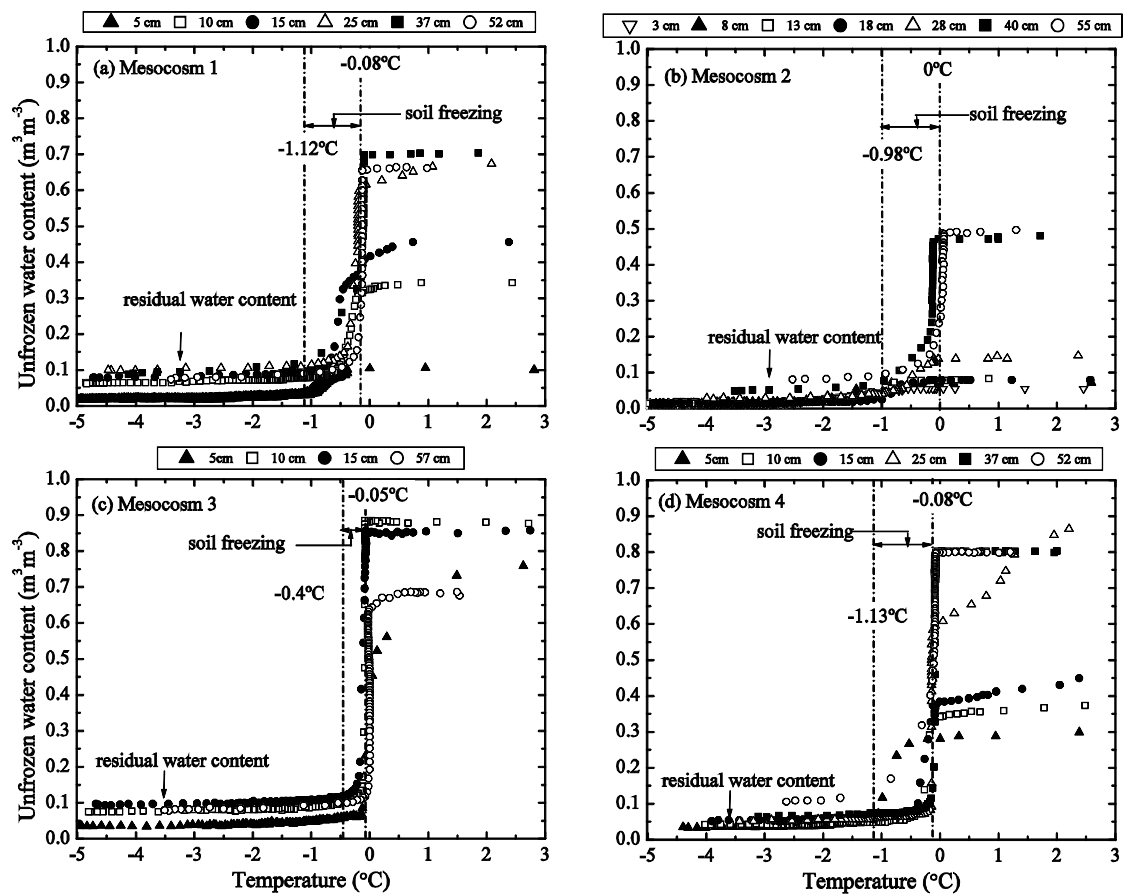


**Figure 4.5.** Soil freezing characteristics of all four Mesocosms obtained from observed unfrozen water and soil temperature data.

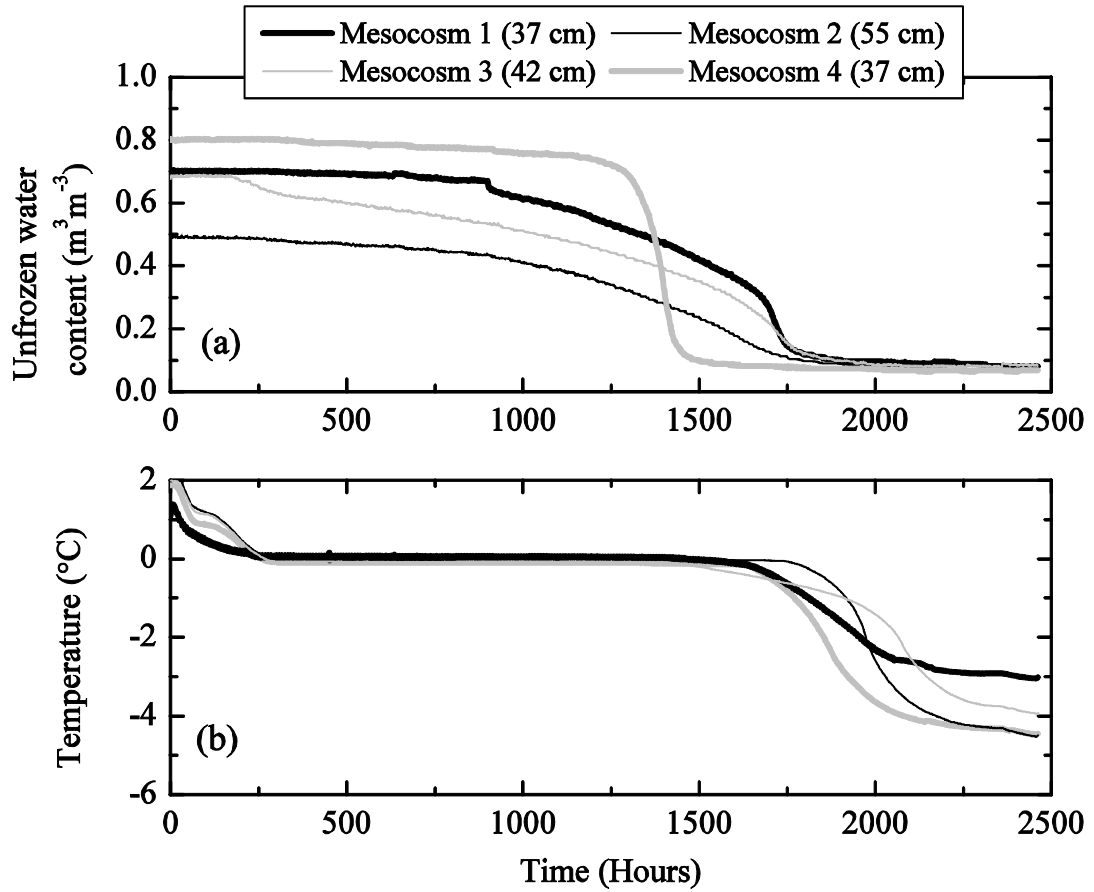


**Figure 4.6.** (a) Soil unfrozen water content and (b) temperature time series at selected depths in the four Mesocosms. The depths were selected such that initial water content was greater than  $0.5 \text{ m}^3\text{m}^{-3}$ .

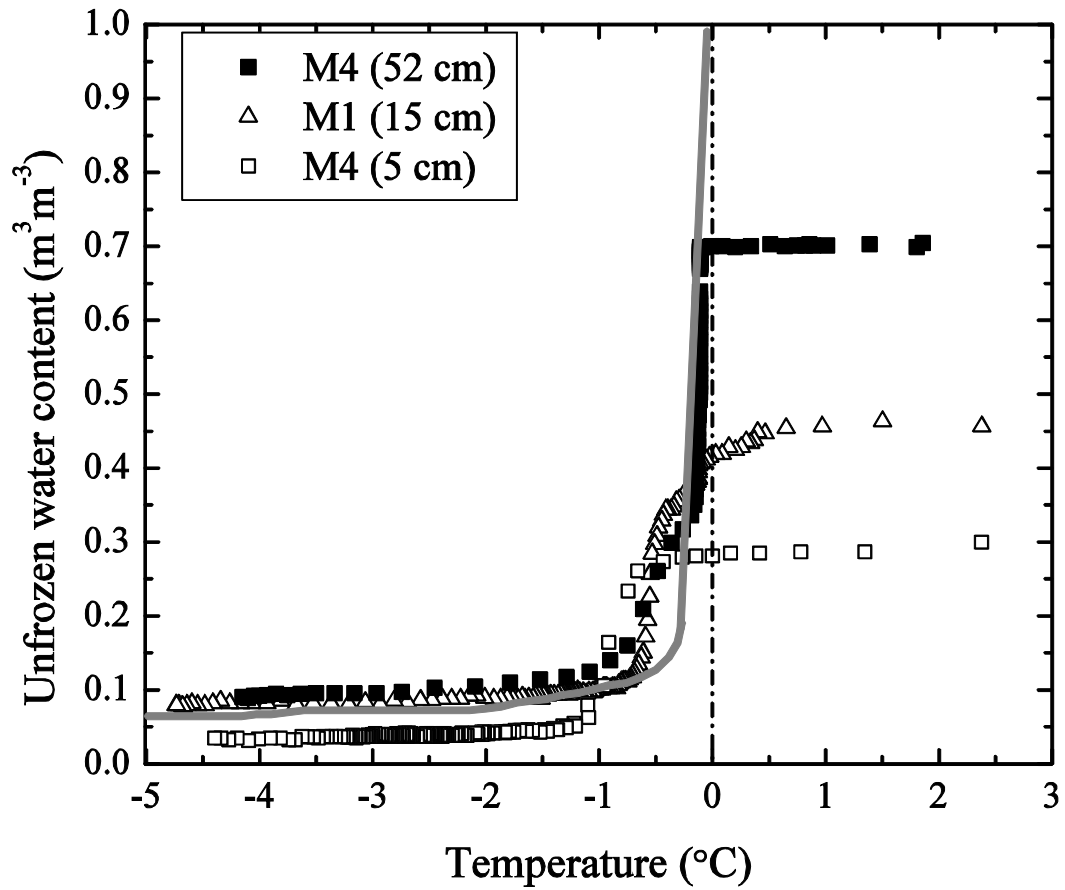


**Figure 4.7.** Soil freezing curves in different Mesocosms (M1, M3 and M4). The effect of water redistribution on the shape of SFC is seen in form of deviation from an initial path the curves traverse (shown approximately by a thick gray line). The depth at which soil temperature-liquid water content relationship was observed is shown in parenthesis.

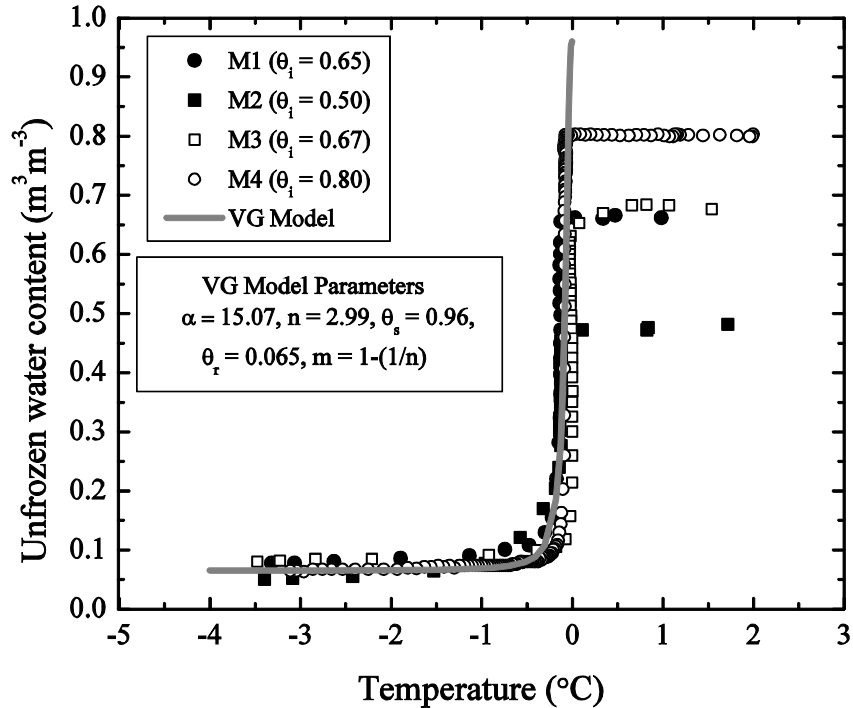


**Figure 4.8.** Soil freezing curves chosen from four different Mesocosms and initially at different water contents ( $\theta_i$ ). A best fit defined by van-Genuchten model (VG Model, van Genuchten, 1980) is also shown along with the VG Model parameters. The SFC's were chosen from each Mesocosm such that  $\theta_i \geq 0.5 \text{ m}^3 \text{ m}^{-3}$ .

#### 4.3.3. Frost induced water redistribution within the active layer

Soil water redistribution during the second freezing run in each Mesocosm was inferred based on initial and final total water contents and SFCs at different depths.

##### 4.3.3.1. Variably wetted conditions with a water table at depth

###### (Mesocosms 1 and 4)

In both M1 and M4 the zone near and above the water table loses water because of movement upwards towards the freezing front before the soil temperature falls below

the freezing point. This movement is evident from the reduction of water content at 15 cm and 25 cm depths prior to soil freezing (Figures 4.5a and 4.5d). Before the arrival of freezing front, the reduction in water content ranges from  $\sim 0.27 \text{ m}^3 \text{ m}^{-3}$  at 25 cm depth in M4 to  $\sim 0.07 \text{ m}^3 \text{ m}^{-3}$  in M1. This difference appears to have resulted from the higher water content in the top 10 cm of M4 and therefore higher hydraulic conductivity than in M1. Figure 4.9 shows the effect of freezing on water redistribution in Mesocosm M4. The freezing front descends from the surface and arrives at 5 cm in M4 after  $\sim 69$  hours. At this time, the slope of the SFC at 25 cm depth becomes steeper illustrating a higher rate of moisture flow toward the overlying peat. Freezing reduces the soil pore pressures significantly due to changes in surface tension, temperature sensitivity of contact angles and the increase in volume as water transforms to ice (Philip and de Vries, 1957; Grant and Bachmann, 2002) creating large pore pressure gradients between the colder and warmer regions. Peat is characterized by larger pore size as compared to mineral soils (e.g. silt) wherein the phenomenon of freezing induced water movement has been observed in the past. However, peat is also characterized by large variation in pore size associated with peat structure (Smerdon and Mendoza, 2010). Peat can exhibit strong dual porosity wherein smaller pores can facilitate water movement by capillary action. The loss of water from 25 cm depth interval in M4 prior to 69 hours (and beyond) must have resulted from potential gradients created between the surface, where the temperature drops below zero within first few hours, and deeper depths. A reduction in water content was observed in both M1 and M4 prior to the temperature falling to freezing point. However, it appears that hydraulic conductivity differences due to differences in initial

water contents in the upper 10 cm of these two Mesocosms play a role during upward movement of water from 15 cm depth. No water movement is observed from 15 cm depth in M1 until 43 hours into the freezing run, while water movement from the same depth in M4 starts within the first hour of the ground surface freezing (Figure 4.10a). Water from 15 cm depth in M1 migrates upwards only after the downward propagating freezing front has reached between 5 cm and 10 cm creating a hydraulic gradient steep enough for water movement to occur. The shapes of the SFCs at 37 cm in M1 and 52 cm in M4 indicate that water migration continues late into the freezing run and that these depths are gaining and losing water as the upper freezing front moves downward.

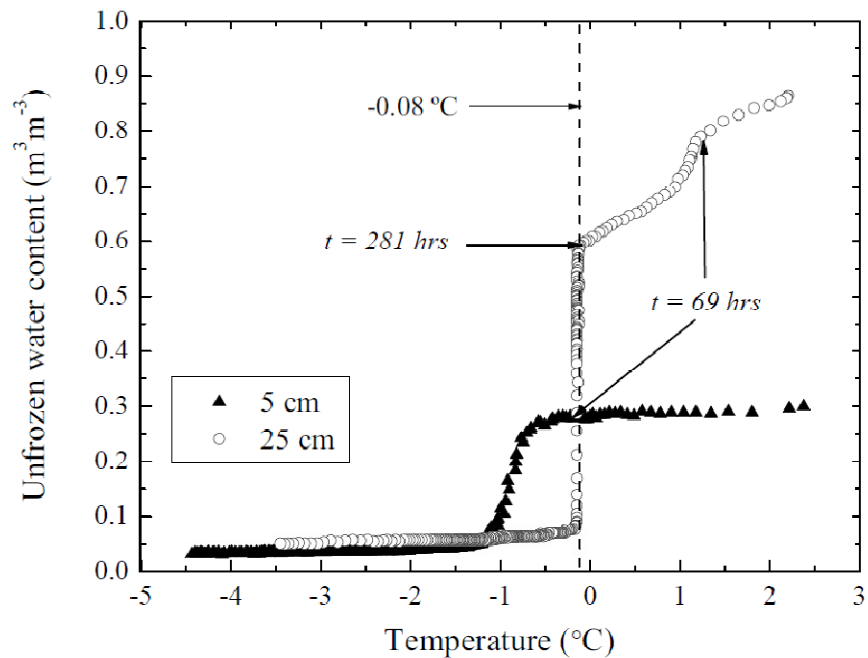


**Figure 4.9.** Water movement towards freezing front: soil freezing characteristics of Mesocosm 4 shows change in slope of the curve at 25 cm depth exactly when the freezing front reaches 5 cm depth.

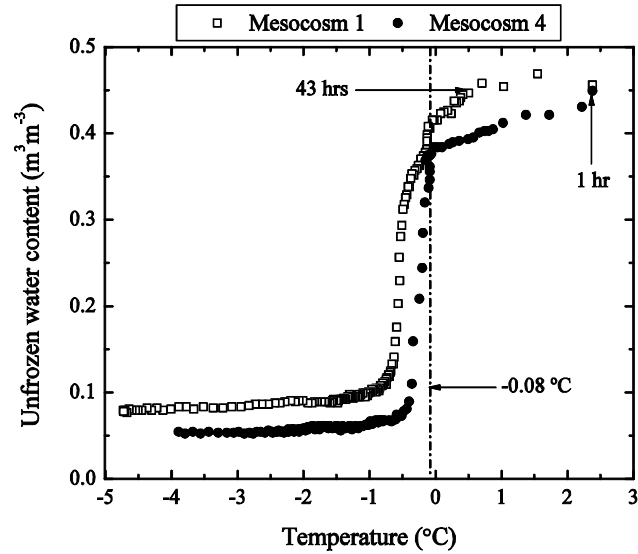


**Figure 4.10.** Comparison between the SFCs of Mesocosms 1 and 4 at 15 cm depth. This depth in both Mesocosms loses water before the soil temperature drops below freezing point, however M4 starts to lose water much earlier (1 hour) than M1 (43 hours). Both Mesocosms were exposed to air temperature of  $-7.5\text{ }^{\circ}\text{C}$  at the surface at time = 0 hours.

#### 4.3.3.2. Dry conditions (Mesocosm 2)

Mesocosm 2 was the driest among the four at the start of second freezing run with only residual water contents in upper 30 cm ( $\sim 0.15\text{ m}^3\text{ m}^{-3}$  at 28 cm, Figure 4.4b), had no saturated layer and had a degree of saturation of  $\sim 50\%$  at 55 cm. No reduction of water content was observed in M2 at temperatures above freezing (Figure 4.5b). This can be attributed to extremely low hydraulic conductivities in the dry zone. The frost penetration in the upper 30 cm of this Mesocosm was relatively rapid and steeper hydraulic gradients appear to have been created.

#### 4.3.3.3. Saturated conditions (Mesocosm 3)

At the start of the freezing run, the water table in M3 was at ~5.5 cm. It is difficult to infer any water movement for this Mesocosm from SFC alone, except at 5 cm depth, where water loss commenced prior to the temperature falling below freezing.

There is a good match between the arrival time of the freezing front at a shallower depth and migration of water from a deeper depth as seen in Figure 4.9. This illustrates the importance of soil freezing on the matric potential at least in the initial freezing period (e.g., water removal prior to freezing front reaching 25 cm depth in M4 continued for first 281 hours as seen in Figure 4.9). The generalized Clausius-Clapeyron equation (CCE) is used to convert from temperature to matric potential in frozen soils. There have been very few efforts (e.g., Williams, 1967; Guymon *et al.*, 1993) to measure soil matric potential in frozen soils owing to the difficulties in using the existing measuring techniques. While there are very few experimental works verifying the use of CCE in frozen soils, Williams (1967) show a close match between the observed and predicted values of matric potential in a Leda Clay-water-ice system. The effect of temperature on matric potential needs to be further examined and extended to peat in order to improve the numerical support in cold regions water balance studies.

The final water content profiles indicate an upward water movement in all Mesocosms (Figure 4.11), although the rates of water flow appear to have varied among the Mesocosms owing to the differences in initial moisture profiles and moisture dependant hydraulic conductivities. The role of hydraulic conductivity is evident from the

differences in the final total water content profiles of M1 and M4. M1 had less water in the upper 10 cm and water accumulated behind this low permeability zone. In comparison, there was a more gradual change toward the final water content profile of M4. Most water can be observed to be lost from the zone just above water table in both M1 and M4. The role of hydraulic conductivity can also be seen from the comparison between the soil freezing curves of M1 and M4 at 15 cm depths (Figure 4.10). Water coming from the deeper depths accumulated just above the 15 cm depth in M1 (Figure 4.11a). The shape of the SFC at 15 cm in this Mesocosm appears to be somewhat affected by the water coming from deeper depths. In comparison, the SFC at 15 cm in M4 was not affected as much because water may have moved through this zone at a much faster rate owing to comparatively higher hydraulic conductivity in the zone above.

The movement of water towards freezing front appears to have been dominated by liquid water movement under potential gradients at least in the initial freezing period. However, there is enough indication that moisture movement also took place in vapour form. The weights of the Mesocosms continued to drop during the freezing period. This indicates that water was escaping from the Mesocosms during freezing. This is an evidence of water transport in vapour form from warmer regions with high water contents towards colder regions with relatively low water contents. The modes of transport and quantification of contribution from liquid water movement and vapour transport are a topic of further investigation and will be discussed in a separate publication in near future.

One critical issue in field studies is to understand the role of over-winter snowmelt events, and the origin of water participating in the freezing of active layer over the winter season. Figure 4.12 shows the water content values observed at the Scotty Creek research site at beginning and end of winter season of 2002-2003. Initial moisture conditions for the field were not measured below 40 cm. The depth to permafrost at the onset of winter was 70 cm. This site is underlain by sporadic/discontinuous permafrost (Smith *et al.*, 2004; Quinton and Hayashi, 2005).

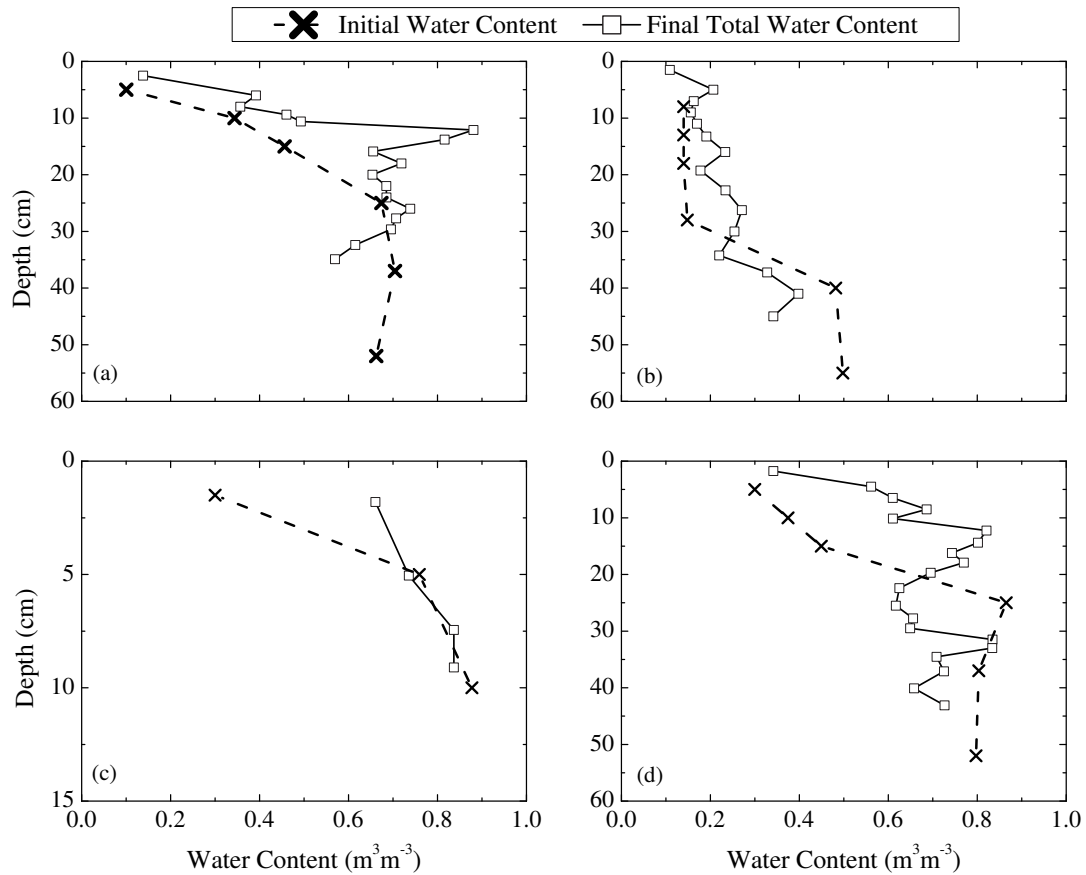


**Figure 4.11.** Initial (liquid) and final (total) water content after 2000 hours of freezing in Mesocosms (a) 1, (b) 2, (c) 3, and (d) 4. Please note the different Y-axis limits in (c).

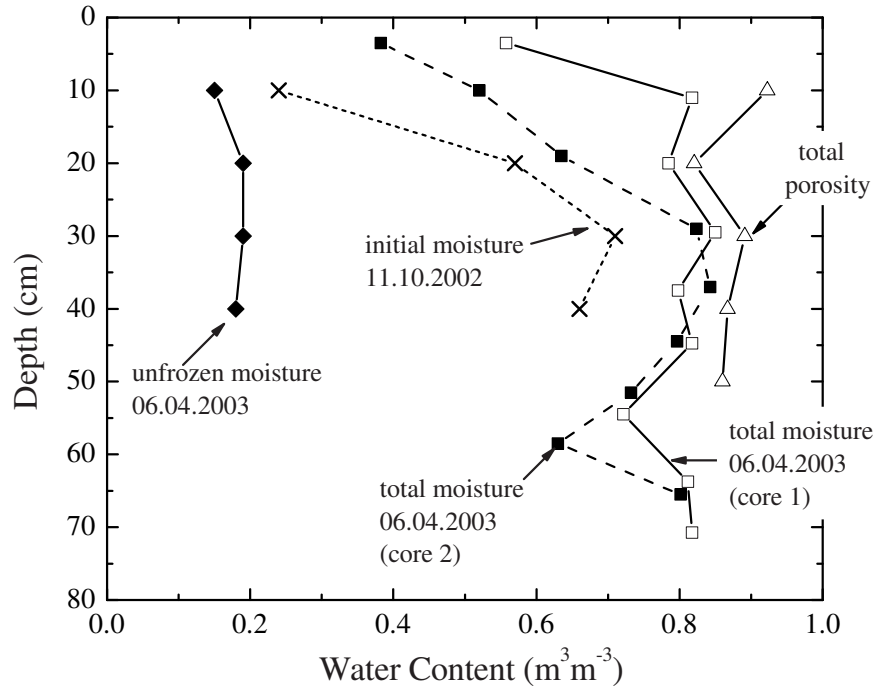


**Figure 4.12.** Observed initial (liquid) and final water contents (liquid + ice) at Scotty Creek field site for winter of 2002-2003 (Quinton and Hayashi, 2008). The initial and unfrozen moisture content readings are from a soil pit being measured using a water content reflectometer. Two frozen cores were sampled at the end of winter season near the soil pit and total (liquid + ice) water content was determined gravimetrically.

It is evident that a large amount of water moved into 0 - 40 cm depths at the end of the winter (Figure 4.12). Comparing Figures 4.11 and 4.12 indicates that it is possible that water from deeper zones at initial high water contents moved upward towards the freezing front during the winter season and resulted into the final profiles in Figure 4.12. The measurements in Figure 4.12 indicate a 41.85 mm change in storage in the upper 40 cm depth (assuming average 85% total porosity). A change of storage of 33.65 mm and 42.11 mm in upper 29 cm and 21 cm in M1 and M4 respectively was inferred from the initial and final profiles (Figure 4.11). It must be noted that the initial water content in

upper 40 cm depth in both Mesocosms (Figure 4.4) was higher than the initial water content in the field (initial moisture in Figure 4.12). Also, the water table was within upper 42 cm depth in both Mesocosms and the air temperature at the surface was constantly at -7.5 °C. All these conditions may have resulted into relatively larger amount of water movement towards the freezing front in the Mesocosms than in the field. This is an important observation as it suggests that temperature gradients drive an upward flux of water from deeper regions of the soil into the upper 10 cm zone where it can be supplemented by an intermittent downward flux of snowmelt water over the winter period. This combination of freezing induced upward migration of water supplemented by an intermittent downward flux of snowmelt water over the winter period results into raising the upper surface of the frozen, saturated soil typically within about 0.1 m below the ground surface.

#### **4.3.4. Water movement from the transition zone**

Deuterium was used as a tracer to observe upward water movement from the proxy permafrost-active layer transition zone towards the downward moving freezing front. Water was sampled in the three Mesocosms with active saturated zones (M1, M3 and M4) throughout the first freezing run. Figure 4.13 shows the  $\delta^{18}\text{O}$  -  $\delta\text{D}$  relationship of the soil waters during the entire sampling period. First, it is important to understand the variability in the isotopic composition of pore water in the three Mesocosms. In Figure 4.13, soil waters that plot below the global meteoric water line (GMWL) represent the initial isotopic composition before being affected by mixing/diffusion with the water

coming from the transition zone. These isotope compositions represent a mixture of latent pore water present in the peat and the tap water added during the initial Mesocosm saturation and compaction efforts. The peat in M1 retained the most latent pore water during sampling of the cores. Precipitation in northern regions typically has lower  $\delta^{18}\text{O}$  and  $\delta\text{D}$  values than precipitation at lower latitudes and it is not surprising to see soil water depleted in D and  $^{18}\text{O}$  in M1. Tap water in London Ontario used to saturate the peats at the BESM comes from Lake Huron and Lake Erie and has a  $\delta\text{D}$  value of  $-50\text{‰}$  and a  $\delta^{18}\text{O}$  value of  $-7\text{‰}$ . The distribution of soil water  $\delta$  – values from the 40 and 50 cm depth in M1 along the GMWL (Figure 4.13a) reflects variable mixing of these two sources of water (arctic pore water and London Ontario tap water). The peat in M4 was flushed multiple times before the start of the freezing experiment and pore water was replenished with tap water. Hence, the  $\delta^{18}\text{O}$  and  $\delta\text{D}$  values of water within the upper active layer (40 cm depth) are similar to tap water and average  $-8.1 \pm 0.2\text{‰}$  and  $-59 \pm 0.9\text{‰}$ , respectively (Figure 4.13c). The majority of peat within Mesocosm 3 was repacked with peat from Upsala, Ontario with a 17 cm undisturbed peat layer at the top. The upper portion of the M3 column sat in the upper chamber of BESM operated at 60 % relative humidity and 16 °C air temperature for more than 4 months. Over this time the repacked peat water was subjected to evaporation and was replenished with tap water from time to time. Preferential loss of  $^{16}\text{O}$  and H during evaporation leaves the remaining water enriched in  $^{18}\text{O}$  and D, with a greater enrichment in  $^{18}\text{O}$  relative to D. Hence, the  $\delta\text{D}$  and  $\delta^{18}\text{O}$  values of peat water sampled from the 40 cm and 50 cm depths of M3 plot are shifted to the right as compared to M1 and M4. The narrow distribution of  $\delta^{18}\text{O}$

values ( $-4.3 \pm 0.2 \text{‰}$ ) of the pore waters from the upper layers (40 and 50 cm depth) of M3 suggest that the pore waters are well mixed (Figure 4.13b).

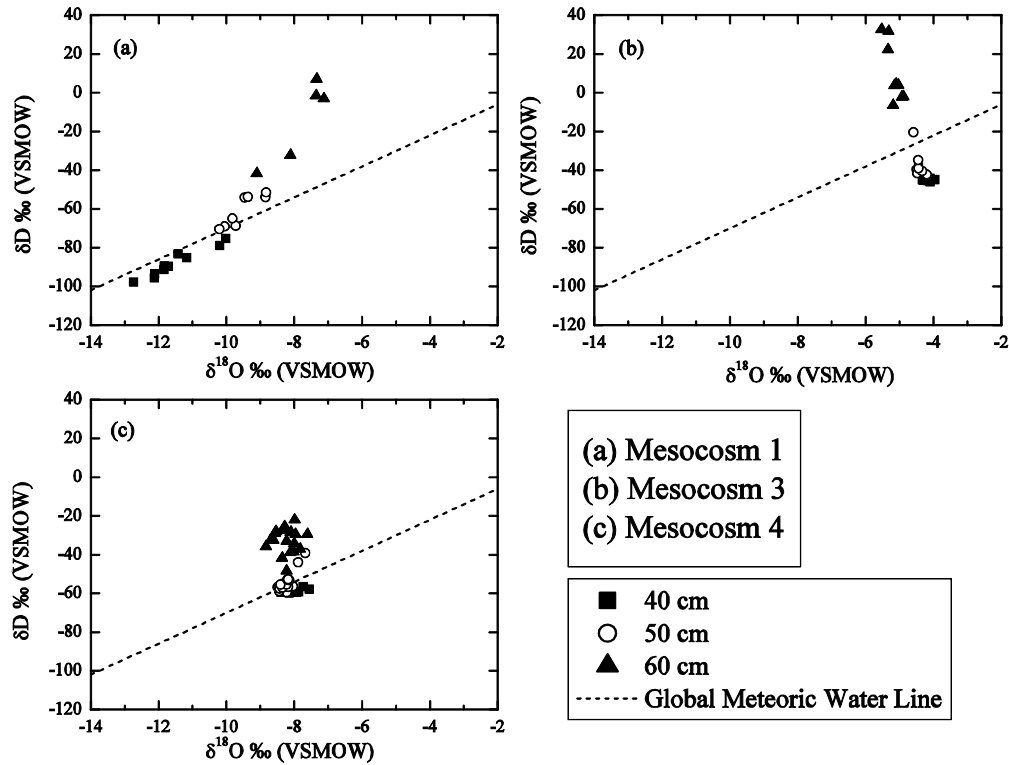


**Figure 4.13.**  $\delta^{18}\text{O}$  vs  $\delta\text{D}$  plot of water samples collected in saturated zones of M1, M3 and M4 during first freezing run. The global meteoric water line is also shown for comparison. Note that the frozen layer was enriched only in Deuterium and the shift seen in Mesocosms 3 and 4 reflect enrichment in Deuterium with time.

Soil waters sampled throughout the freezing run from the 60 cm depth of the active layer in all Mesocosms plot above the meteoric water line in Figure 4.13. These waters contain a small proportion the deuterium tracer from the proxy permafrost layer. Throughout the experiment the  $\delta^{18}\text{O}$  values of these waters are similar to tap water ( $\delta^{18}\text{O} = -7.8 \pm 0.8 \text{‰}$  for M1 and  $-8.2 \pm 0.3 \text{‰}$  for M4) or slightly evaporated tap water ( $\delta^{18}\text{O} = -$

$5.2 \pm 0.2 \text{ ‰}$  for M3). The  $\delta^{18}\text{O}$  values of the 60 cm pore waters in M3 ( $\delta^{18}\text{O} = -5.2 \pm 0.2 \text{ ‰}$ ) are lower than found in the upper layers of the column. Given that the  $\delta^{18}\text{O}$  values of water at 60 cm were less enriched than water in the overlying layers, this could also suggest mixing between an evaporated water with  $\delta^{18}\text{O}$  values typical of shallower depths ( $\delta^{18}\text{O} = -4.3 \text{ ‰}$ ) and the ice that formed on the top of the frozen layer before the remaining peat was added to the Mesocosm ( $\delta^{18}\text{O} = -5.4 \text{ ‰}$  in M3). Likewise the absence of a  $^{18}\text{O}$ -depleted Arctic precipitation signal in the 60 cm depth of M1 could suggest an increased concentration of tap water pooling at this depth during initial peat saturation, or mixing between the residual Arctic pore water, tap water and water from the proxy permafrost layer ( $\delta^{18}\text{O} = -3.3 \text{ ‰}$ ). It is not unreasonable to assume that tap water added during the experimental set up would pool at the bottom (60 cm) of the active layer as the pore waters from the 50 cm depth that plot on the MWL have a greater proportion of tap water than the pore water at 40 cm depth (Figure 4.13a).

Figure 4.14 shows the time series of the  $\delta\text{D}$  values of peat water at various depths for M1, M3 and M4. Water within all three Mesocosms was enriched in deuterium at 60 cm at the beginning of the experiment. This is most likely the result of mixing of lower pore waters with the ice layer on the top of the frozen layer (ice  $\delta^{18}\text{O} = -1.3$  to  $+2.4 \text{ ‰}$ ;  $\delta\text{D} = 502$  to  $621 \text{ ‰}$ ). Over the length of the experiment a large variability with no clear trend in  $\delta\text{D}$  values was observed for the mixing zone (60 cm depth) of M1 (Figure 4.14a). Hence, for this study, the presence of deuterium enrichment in the pore water at 50 cm in the active layer will be considered most indicative of vertical water movement from the

transition zone. The variations in  $\delta D$  values at a given depth likely resulted from pore water heterogeneity, and variable water movement, as sampling occurred in different regions within the mixing zone. In M1, the  $\delta D$  values of pores water in the 50 cm depth are also enriched at the beginning of the experiment, but do not evolve with time. However, it is difficult to infer if water from the transition zone moved to shallower layers in M1 over time or if the elevated  $\delta D$  values result only from heterogeneity caused by mixing between the original pore waters and the ice above the proxy permafrost when the peat was layered. Mesocosm 3 had the highest deuterium enrichment in the mixing zone (60 cm) and the enrichment increased with time. Yet no appreciable change in  $\delta D$  values can be seen at 40 cm and 50 cm depths, except for the last sample of pore water collected from 50 cm depth when the peat was thawing. In contrast, there is a constant upward trend in increasing  $\delta D$  values observed at 50 cm in M4. M4 had warmer proxy permafrost ( $-0.45$  °C) during the first freezing run. This could have resulted in higher liquid water content in the transition zone with more water moving upward through the mixing zone and higher. The increase in  $\delta D$  values of pore waters at 50 cm depth during the thaw period in this Mesocosm also suggest that at least some water moved towards the higher depths from the transition layer (Figure 4.14c). A mass balance calculation using the average  $\delta D$  values of pore waters from the 50 cm depth that plot below the MWL for that Mesocosm as the original pore water values and the  $\delta D$  values of the frozen layer pore water values, suggests that this reflects an average of 0.5%, 3.1% and 2% of water contributed from the proxy permafrost layer to the 50 cm depth in M1, M3 and M4, respectively, over the length of the experiment. This is negligible amount of

water and therefore it appears that the transition zone contribution is not important. This means that the saturated layer above the proxy permafrost layer plays the most important role in water redistribution during soil freezing.

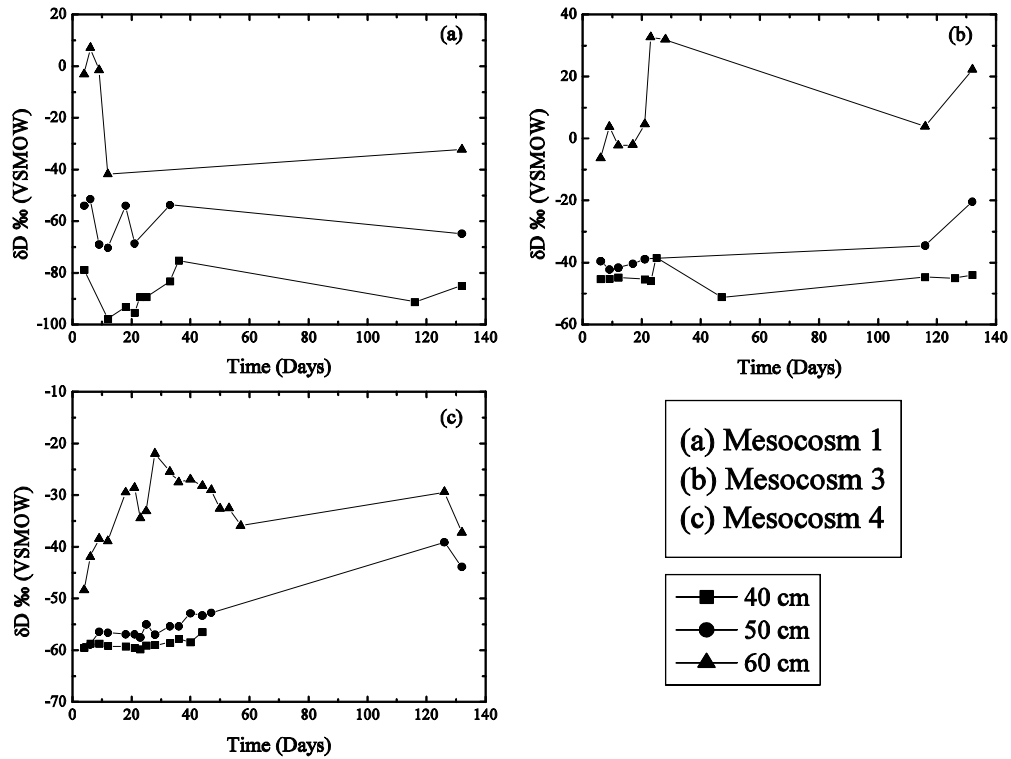


**Figure 4.14.** Time series of  $\delta D$  signatures of water sampled within the saturated zones of M1, M3 and M4. Please note the different scales on y-axis. Data points after 70 days represent water sampled during thawing period.

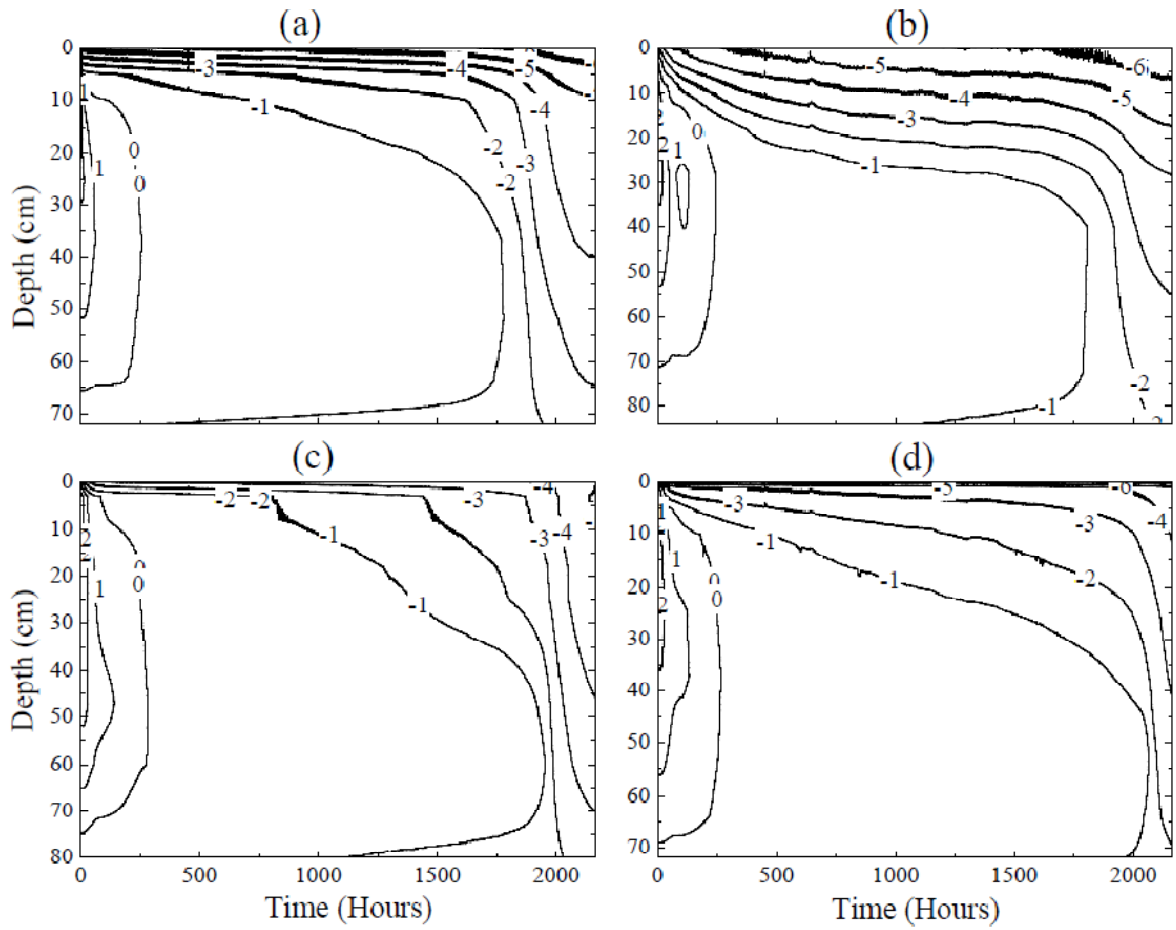
#### 4.3.5. Soil temperature and frost propagation

Figure 4.15 shows the isothermal maps for all four Mesocosms plotted from temperature measurements during the second freezing run. Bi-directional freezing, with a relatively fast moving downward and a slower moving upward freezing front, can be observed in all four Mesocosms. The freezing front propagates faster and deeper in upper

dry ~35 cm of M2 due to minimal latent heat release. Freezing slows down considerably below this depth due to relatively high saturation and latent heat effects. Strong thermal gradients can be seen near surface in the wetter M1, M3 and M4 Mesocosms indicating presence of high amounts of water near the freezing front. In all four Mesocosms, the frost propagation is controlled by competing roles of thermal conductivity, heat capacity and latent heat. The slow progression of the freezing front in M2 below the upper 30 cm is due to a combination of latent heat, and low thermal conductivity owing to drier peat and higher air volume relative to M1, M3 and M4. The role of thermal conductivity in the ground heat removal can be seen from the difference in ground heat flux (from heat flux plates) observations between Mesocosms M2 and M3 (Figure 4.16a). It can be seen that the heat removed from the saturated Mesocosm M3 is consistently higher than from the dry M2. Most water in Mesocosms M1, M3 and M4 freezes around ~2000 hours (Figure 4.6a) after which the freezing front propagates deeper and at a higher rate. The critical effect of latent heat on soil temperature can be seen from the shape of isolines in Figure 4.15. Almost all water appears to freeze after approximately 1700 hours in all Mesocosms. Around this time, the isolines suddenly become vertical indicating that latent heat is no more contributing to a zero curtain effect. Thus, latent heat plays a significant role in keeping the soil warm for very long periods during freezing, yet higher water contents result in colder horizons at depth owing to higher thermal conductivity and lower heat capacity during late freezing periods.

The effect of differences in sub-surface thermal properties on near surface thermal regimes can be seen from comparison between the Mesocosms with colder (M1) and

warmer (M4) proxy permafrost. Figure 4.16b shows the time series of temperature changes of near surface depths in these Mesocosms. Both M1 and M4 were variably saturated throughout the depth with water tables located at 42 cm and 26 cm below the ground surface at the start of freezing. Mesocosm 4 was relatively wetter than M1 in the upper 10 cm when freezing commenced, and had a warmer proxy permafrost ( $-0.35\text{ }^{\circ}\text{C}$ ) than M3 ( $-0.88\text{ }^{\circ}\text{C}$ ). Although both Mesocosms were subjected to the same air temperature in the lower chamber, the differences in temperatures of the proxy permafrost were probably due to differences in water contents. The colder proxy permafrost resulted in a greater ice content in M1 compared to soils at similar depths in M4. The comparison of temperature at similar depths in these two Mesocosms reveal that the temperature time series of M4 always lags M1 in reaching the  $-0.08\text{ }^{\circ}\text{C}$  line (freezing point for these two Mesocosms). A higher ice content in M1 resulted in a higher thermal conductivity and lower heat capacity than M4 and thus results in quicker heat loss.



**Figure 4.15.** Isolines of equal temperature across depth and time for (a) M1, (b) M2, (c) M3 and (d) M4.

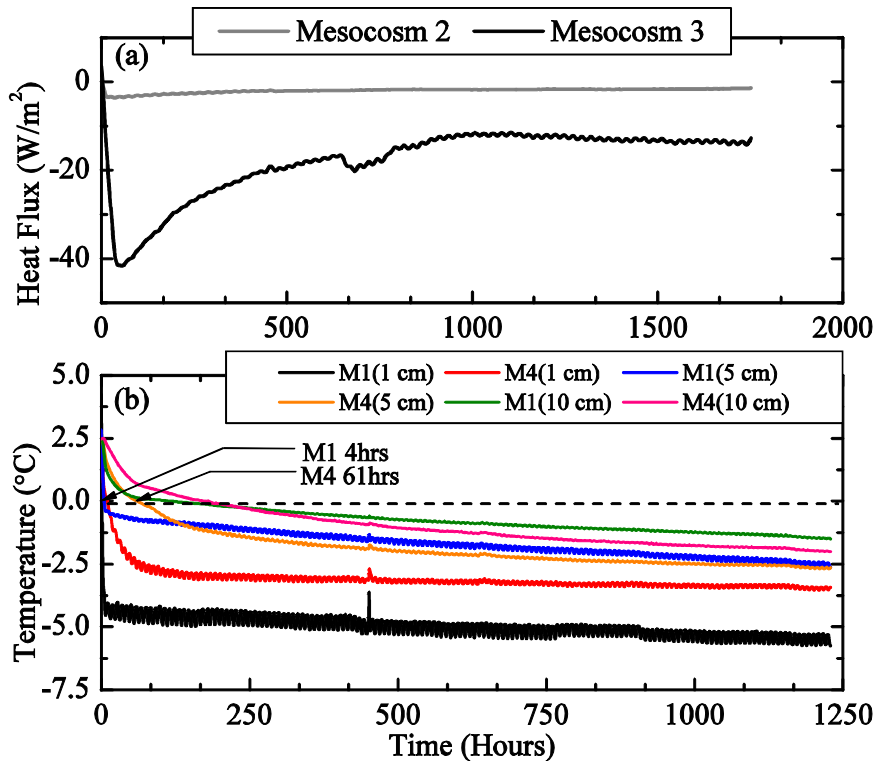


**Figure 4.16.** (a) Observed ground heat flux in fully saturated M3 and dry M2 (at the start of freezing), and (b) Temperature time series for near surface sensors in Mesocosms M1 and M4. Note that the differences in time intervals.

The results of this study are used to describe the evolution of frost table topography for a peat plateau through a simple conceptual model (Figure 4.17). The model is hypothetical, but it provides a useful framework for discussion. At the onset of winter, the organic active layer resembles a variable moisture landscape with regions of full saturation under the topographic depression, low moisture content (at the top with a dry surface layer), and relatively wetter unsaturated zone below the dry surface layer and under the mound. The water table more or less resembles the surface topography. When the air temperatures drop below freezing, the freezing front migrates at variable rates in the different regions. The rate of migration in early winter is maximum in the dry surface

layer because there is very little moisture to slow down the descend (Figure 4.17b). In comparison the rate of freezing front movement is slowest under the topographic depression where peat is fully saturated. Water from the regions just above the water table moves upward in response to the pressure head gradient created between the colder and warmer regions drawing the water table downward. Water also moves in form of vapour during this period, however liquid water movement under pressure head gradients is possibly the dominant process of water movement in initial periods. As the winter progresses, so does the freezing front drawing more water from regions of higher saturation creating a continuous zone of increased saturation just below it (Figure 4.17c). Much more water is accumulated behind the freezing front in regions where the initial water content in unsaturated zone was relatively high (e.g., under the mound higher rate of water flow is shown by longer arrow). This happens because of the higher hydraulic conductivity of the wetter unsaturated zones as compared to the drier ones. In comparison, the initially dry surface layer remains on lower side of saturation because the low hydraulic conductivity in this layer slows down the upward movement of water beyond its interface with the wetter unsaturated zone underneath. By mid-winter (Figure 4.17d), there is no more a saturated unfrozen zone on the entire peat plateau. The entire plateau is unsaturated because of freezing induced water redistribution or partial freezing of soil water. The soil moisture migration (liquid + vapour) towards freezing front continues from areas where there is still substantial liquid water. As the water accumulating behind the freezing front freezes, it also retards the movement of the freezing front (Figures 4.17c and 4.17d). The rate of descend still is slowest below the

topographic depression and the mound where maximum water is accumulating behind the freezing front. By mid to late winter (Figures 4.17e and 4.17 f), most of the water behind the freezing front is frozen, except under the topographic depression and the mound. Elsewhere on the peat plateau, the downward freezing front movement accelerates. By this time, freezing induced water movement has slowed down considerably except near the depression where larger effects of temperature on soil matric potential (because of higher ice content than elsewhere) and initially high hydraulic conductivity still result into comparatively higher rate of upward water redistribution. As most water freezes behind the freezing front, the front migrates much more rapidly owing to increased thermal conductivity and lower release of latent heat. By the end of winter most water redistribution stops and the entire soil profile is now below freezing temperatures with warmest temperatures occurring at depths. The significant water movement upwards in early to mid, late-mid winter periods results into a continuous saturated frozen layer near surface of varying thickness. The thickness is minimum below the dry surface layer and maximum below the topographic depression and the mound. This saturated frozen layer creates a near impermeable frost table near surface with variable thickness of unsaturated zone above it. As spring arrives and snow melts, runoff takes place in different modes in different regions of the peat plateaus. There is unimpeded infiltration into the dry surface layer with lowest ice content. The infiltrating water runs off down-slope along the topography of the frost table through the subsurface. Near the topographic depression and the mound, where the impermeable surface is flush with ground surface, most snowmelt runoff takes place as overland flow along the topographic slopes.

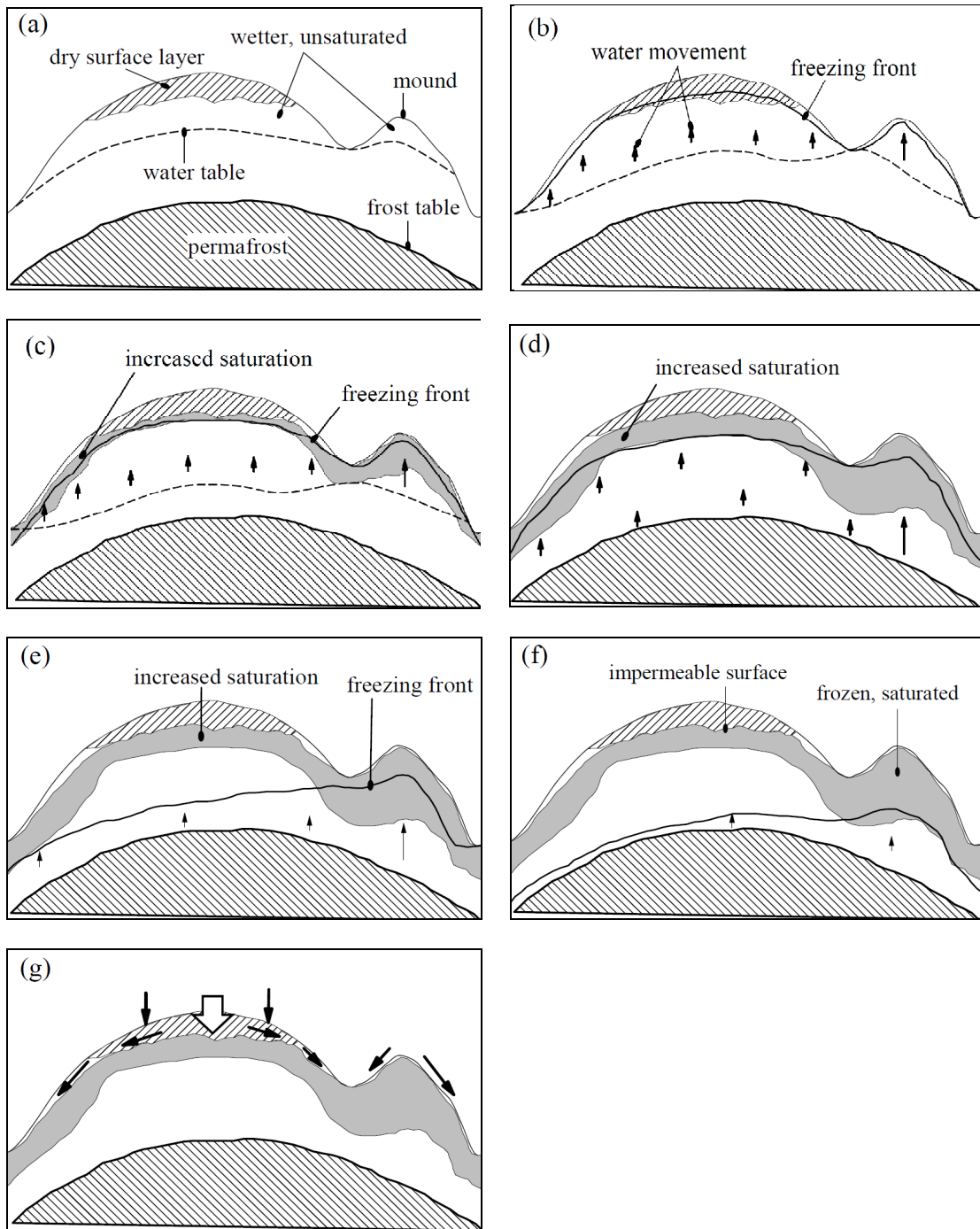


**Figure 4.17.** Conceptual model describing freezing induced water redistribution and frost propagation inside an organic active layer on a peat plateau (a) onset of winter, (b) early winter, (c) early-mid winter, (d) mid winter, (e) and (f) mid-late winter, and (g) end of winter and spring runoff. Variable moisture landscape made up of regions with deeper

unsaturated zones plus dry surface layer (zone of lower hydraulic conductivity) and shallow water table with wetter unsaturated zone (zone of higher hydraulic conductivity) result into variable amount of freezing induced moisture movement and different rates of freezing front movement.

#### **4.4. Conclusions and implications**

Four peat Mesocosms with different initial moisture contents were subjected to freezing to study the impact of soil water content on soil freezing characteristics, freezing induced soil water redistribution, and frost penetration. Water movement from the proxy permafrost transition layer to the active layer during freezing was studied using deuterium tracer in the water originating from the proxy permafrost-active layer transition zone.

It appears that most water in the partially frozen transition zone remains immobile, and therefore negligible amount of water is contributed from the deeper sources during the freezing of active layer. There appears to be very little effect of initial soil moisture on soil freezing characteristics of peat. This implies that liquid water content in frozen peat has a fixed value for each temperature at which the liquid and ice phase are in equilibrium, regardless of the amount of ice present. A single freezing curve can be derived, regardless of initial soil moisture. This simplifies the temperature-liquid water content parameterization required for numerical studies. Initial moisture profiles seem to control the amount of water moving upwards by influencing the hydraulic conductivities in unsaturated soils. Substantial water redistribution appears to have taken place within the active layer during its freezing. This suggests that in favorable conditions

the water moving from deeper depths under temperature gradients, with “complementary” contribution from preceding over-winter melt events, could be sufficient to raise the upper surface of frozen saturated soil within upper 10 cm zone. Effects of temperature and phase change on soil matric potential appear to be the primary cause behind the movement of water towards the freezing front in initial freezing periods, while vapour movement from warmer wetter regions towards colder drier regions also appears to play a role in water movement. Initial water content in the surface layer (~10 cm) appears to control the amount of ice and location of the zone where maximum ice is formed near the surface. It appears that if there is a relatively thick dry layer, then water moving towards the freezing front from below is accumulated relatively at a deeper depth as compared to if the surface layer was moist. Also, the ice content in a dry surface layer would be much lower than a relatively wetter surface layer. This has implications in the timing and mode of runoff during the initial thaw period because an initially dry surface layer would result into unimpeded higher infiltration.

The frost movement in the four Mesocosms with different initial moisture content shows that frost propagation in frozen soils is controlled by a combination of latent heat and thermal properties of the peat-air-water-ice system. Latent heat governs the frost propagation for a long time during freezing because of high water contents in peat. Once water in peat is frozen, higher thermal conductivity and lowered heat capacity of frozen peat-ice system helps in faster movement of the frost front. Climate change scenarios predict shorter periods of snow cover in northern latitudes (Serreze *et al.*, 2000; IPCC, 2007). This will increase the rate of freezing of peat pore water. If the peat contains

substantial water at the onset of winter, then this might lead into deeper frost depths. Mean annual air temperature and rainfall in the northern hemisphere are also predicted to increase (Serreze *et al.*, 2000; IPCC, 2007). A system with competing dynamics of frost penetration due to longer ground exposure to winter air temperatures and overall higher annual mean air temperature forcing deeper permafrost appears to be a possible scenario.

This study demonstrates that soil moisture profiles at the onset of winter play an important role in modulating the hydraulic and thermal properties of peat and therefore affecting the frost induced water redistribution and frost propagation during the freezing of active layer. The results of this study will help in understanding, and ultimately forecasting, the seasonal freeze-thaw hydrologic response of wetland-dominated terrain underlain by discontinuous permafrost. Further research through numerical modeling and laboratory work involving experimental design similar to that of this study is required to understand the exact impacts of the competing dynamics driving the water and heat movement in frozen peat.

#### **4.5. References**

ASTM Standard D2974, 2007a. Standard test methods for moisture, ash, and organic matter of peat and other organic materials. ASTM International, West Conshohocken, PA, 2003, DOI: 10.1520/D2974-07A, [www.astm.org](http://www.astm.org).

Carey, S. K., and M. K. Woo (2005). Freezing of subarctic hillslopes, Wolf Creek basin, Yukon, Canada, *Arctic Antarctic and Alpine Research* **37**, 1-10.

- Dall'Amico, M. (2010). Coupled water and heat transfer in permafrost modeling, Ph.D. Theses, University of Trento, Italy.
- de Vries, D. A. (1963). Thermal properties of soils, in *Physics of plant environment*, W. R. van Wijk (Editor), North-Holland Pub. Co., 210-235.
- Dirksen, C., and R. D. Miller (1966). Closed-system freezing of unsaturated soil, *Soil Science Society of America Proceedings* **30**, 168-173.
- Dirksen, C. (1964). Water movement and frost heaving in unsaturated soil without an external source of water, Ph.D. Thesis, Cornell University, United States.
- Grant, S. A., and J. Bachmann (2002). Effect of temperature on capillary pressure, *Geophysical Monograph, American Geophysical Union* **129**, 199-212.
- Gray, D. M., P. G. Landine, and R. J. Granger (1985). Simulating infiltration into frozen prairie soils in stream-flow models, *Canadian Journal of Earth Sciences* **22**, 464-472.
- Gray, D. M., B. Toth, L. T. Zhao, J. W. Pomeroy, and R. J. Granger (2001). Estimating areal snowmelt infiltration into frozen soils, *Hydrol.Process.* **15**, 3095-3111.
- Guymon, G. L., R. L. Berg, and T. V. Hromadka (1993). Mathematical model of frost heave and thaw settlement in pavements, *CRREL Special Report 93-2*, US Army Cold Regions Research and Engineering Laboratory, Hannover, 130 pp.
- Guymon, G. L., and J. N. Luthin (1974). Coupled heat and moisture transport model for Arctic soils, *Water Resour.Res.* **10**, 995-1001.
- Hansson, K., J. Simunek, M. Mizoguchi, L. C. Lundin, and M. T. van Genuchten (2004). Water flow and heat transport in frozen soil: Numerical solution and freeze-thaw applications, *Vadose Zone Journal* **3**, 693-704.

Harris, C., Arenson, L. U., Christiansen, H. H., Etzelmuller, B., Frauenfelder, R., Gruber, S., Haeberli, W., Hauck, C., Hoelzle, M., Humlum, O., Isaksen, K., Kaab, A., Kern-Luetschg, M. A., Lehning, M., Matsuoka, N., Murton, J. B., Noezli, J., Phillips, M., Ross, N., Seppala, M., Springman, S. M. and Muehll, D. V.: Permafrost and climate in Europe: Monitoring and modelling thermal, geomorphological and geotechnical responses, *Earth-Sci. Rev.*, 92, 117-171, 10.1016/j.earscirev.2008.12.002, 2009.

Hayashi, M., N. Goeller, W. L. Quinton, and N. Wright (2007). A simple heat-conduction method for simulating the frost-table depth in hydrological models, *Hydrol.Process.* **21**, 2610-2622.

Hoekstra, P. (1966). Moisture movement in soils under temperature gradients with cold-side temperature below freezing, *Water Resour.Res.* **2**, 241-250.

Jame, Y. W., and D. I. Norum (1980). Heat and mass-transfer in a freezing unsaturated porous-medium, *Water Resour.Res.* **16**, 811-819.

Jame, Y. (1977). Heat and mass transfer in freezing unsaturated soil, Ph.D. Thesis, The University of Saskatchewan, Canada.

Jorgensen. M. T., V. Romanovsky, J. Harden, Y. Shur, J. O'Donnell , E. A. G. Schuur, M. Kanevskiy, and S. Marchenko (2010). Resilience and vulnerability of permafrost to climate change, *Can. J. For. Res.*, **40**, 1219-1236.

Low, P. F., D. M. Anderson, and P. Hoekstra (1968). Some thermodynamic relationships for soils at or below freezing point .1. Freezing point depression and heat capacity, *Water Resour.Res.* **4**, 379-394.

Mizoguchi, M. (1990). Water, heat and salt transport in freezing soil, Ph.D. Theses, University of Tokyo, Tokyo.

- Nagare, R. M., R. A. Schincariol, W. L. Quinton, and M. Hayashi (2011). Laboratory calibration of time domain reflectometry to determine moisture content in undisturbed peat samples, *Eur. J. Soil. Sci.*, (in press).
- Painter, S. (2010). Three-phase numerical model of water migration in partially frozen geological media: model formulation, validation, and applications, *Computational Geosciences*, **15**(1), 69-85.
- Philip, J. R., and D. A. de Vries (1957). Moisture movement in porous materials under temperature gradient, *Transactions, American Geophysical Union* **38**, 222-232.
- Quinton, W. L., and M. Hayashi (2008). Recent Advances Toward Physically-based Runoff Modeling of the Wetland-dominated Central Mackenzie River Basin, in Cold Region Atmospheric and Hydrologic Studies. The Mackenzie GEWEX Experience: Volume 2: Hydrologic Processes, M. Woo (Editor), Vol. 2, Springer, Berlin. 257-279.
- Quinton, W. L., and M. Hayashi (2005). The flow and storage of water in the wetland-dominated central Mackenzie river basin: Recent advances and future directions, in Prediction in ungauged basins: Approaches for Canada's cold regions, C. Spence *et al.* (Editor), Canadian Water Resources Association, 45-66.
- Quinton, W. L., T. Elliot, J. S. Price, F. Rezanezhad, and R. Heck (2009). Measuring physical and hydraulic properties of peat from X-ray tomography, *Geoderma* **153**, 269-277.
- Quinton, W. L., T. Shirazi, S. K. Carey, and J. W. Pomeroy (2005). Soil water storage and active-layer development in a sub-alpine tundra hillslope, southern Yukon Territory, Canada, *Permafrost Periglacial Processes* **16**, 369-382.
- Quinton, W. L., M. Hayashi, and S. K. Carey (2008). Peat hydraulic conductivity in cold regions and its relation to pore size and geometry, *Hydrol.Process.* **22**, 2829-2837.

- Rezanezhad, F., W. L. Quinton, J. S. Price, D. Elrick, T. R. Elliot, and R. J. Heck (2009). Examining the effect of pore size distribution and shape on flow through unsaturated peat using computed tomography, *Hydrology and Earth System Sciences* **13**, 1993-2002.
- Schlotzhauer, S. M., and J. S. Price (1999). Soil water flow dynamics in a managed cutover peat field, Quebec: Field and laboratory investigations, *Water Resour.Res.* **35**, 3675-3683.
- Serreze, M. C., J. E. Walsh, F. S. Chapin, T. Osterkamp, M. Dyurgerov, V. Romanovsky, W. C. Oechel, J. Morison, T. Zhang, and R. G. Barry (2000). Observational evidence of recent change in the northern high-latitude environment, *Clim.Change* **46**, 159-207.
- Smerdon, B. D., and C. A. Mendoza (2010). Hysteretic freezing characteristics of riparian peatlands in the Western Boreal Forest of Canada, *Hydrol.Process.* **24**, 1027-1038.
- Stahli, M., and D. Stadler (1997). Measurement of water and solute dynamics in freezing soil columns with time domain reflectometry, *Journal of Hydrology* **195**, 352-369.
- Van Genuchten, M. T. (1980). A closed-form equation for predicting the hydraulic conductivity of unsaturated soils, *Soil Sci.Soc.Am.J.* **44**, 892-898.
- Van Loon, W.K.P., E. Perfect, P. H. Groenevelt, and B. D. Kay (1991). Application of dispersion theory to time domain reflectometry in soils. *Transp. Porous Media*, **6**: 391-406.
- Watanabe, K., T. Kito, T. Wake, and M. Sakai (2011). Freezing experiments on unsaturated sand, loam and silt loam, *Annals of Glaciology* **52**, 37-43.

Wohlfarth, C. (2010). Permittivity (Dielectric Constant) of liquids, in *CRC Handbook of Chemistry and Physics*, 91st Ed., W. M. (. Haynes (Editor), Taylor and Francis Group, LLC, 6-186-6-207.

Zhang, Y., S. K. Carey, W. L. Quinton, J. R. Janowicz, J. W. Pomeroy, and G. N. Flerchinger (2010). Comparison of algorithms and parameterisations for infiltration into organic-covered permafrost soils, *Hydrology and Earth System Sciences* **14**, 729-750.

# CHAPTER 5. A COUPLED CELLULAR AUTOMATA MODEL FOR HEAT AND WATER FLOW IN VARIABLY WETTED SOILS

## 5.1. Introduction

Incorporating soil freeze-thaw processes in land-surface schemes is important for detailed simulations of hydrological processes. Models with fully formulated frozen soil simulation modules do a better job of simulating soil temperatures and soil water storage (e.g., Luo *et al.*, 2003; Wang *et al.*, 2010). Zhang *et al.* (2008) categorized the frozen soil models into three broad classes: empirical and semi-empirical, analytical, and numerical physically-based. Empirical and semiempirical algorithms relate ground thawing-freezing depths (GTFD) to surface temperature by observation based coefficients (e.g., Quinton and Gray, 2001; Anisimov *et al.*, 2002). Analytical algorithms are specific solutions to heat conduction problems. These algorithms ignore volumetric heat removal and water redistribution towards the freezing front. Stefan's formula (Stefan, 1889 as cited by Aldrich and Paynter, 1966), modified Berggren equation (Aldrich and Paynter, 1966) and Hayashi's modified Stefan's algorithm (Hayashi *et al.*, 2007) are examples of analytical algorithms. Numerical physically-based algorithms simulate ground freezing by solving the Richard's equation and the complete energy equations using numerical methods. This class of models are the most accurate for both GTFD (Zhang *et al.*, 2008) and coupled heat and water movement as used in water balance studies (e.g., Wang *et al.*, 2010).

A variety of models solve the coupled Richard's and energy equations for unsaturated frozen/unfrozen soils using the finite difference (e.g., Harlan, 1973; SHAW model by Flerchinger and Saxton, 1989; SOIL model by Jansson, 1998; HYDRUS by Simunek *et al.* 1998 and Hansson *et al.*, 2004), finite element (e.g., Guymon and Luthin, 1974; Guymon *et al.*, 1993) and finite volume (e.g., Engelmark and Svensson, 1993; Painter, 2010) schemes. However, mathematical models for simulating freeze-thaw processes along with coupled heat and water transport in soils remain under development and refinement (e.g., Hansson, 2004; Dall'Amico, 2010). The problem of coupled heat and water transport along with phase change is traditionally solved by Harlan's method (Harlan, 1973). In Harlan's approach it is assumed that there is analogy between heat and water movement in unfrozen- and frozen unsaturated saturated soils. In other words, soil drying in unfrozen soils and soil freezing in frozen ground are assumed to be similar processes with exception of latent heat during phase change. The temperature induced potential gradient is assumed to be the major driving force behind mass movement and Clausius-Clapeyron equation is used to convert from temperature to soil matric potential assuming zero ice gauge pressure. Although the use of Clausius-Clapeyron equation has not been fully verified for its limitations, studies have experimentally verified its suitability in most cases (e.g. Williams, 1967). Traditional numerical methods solve Richard's equation as a diffusion equation, wherein the diffusivity term has no clear physical meaning. Further as argued by Mendicino *et al.* (2006) and Orlandini (1999) for the case of unsaturated soils, the solution of the diffusion equation using finite difference, element or volume methods requires fine discretization in time and space making the

models computationally expensive for large-scale systems. Consequently, it becomes increasingly necessary to find alternative numerical solutions that, under the aegis of the underlying physical phenomena, allow us to increase the spatial and temporal domain of simulations with acceptable computational performance (Mendicino *et al.*, 2006).

The objective of this paper is to present a more intuitive approach towards simulation of coupled heat and water transport in soils with phase change. In this study, heat and mass transfer equations for unsaturated soils are solved in conjunction with mass balance governed by freeze-thaw using coupled cellular automata. The corresponding phase change is handled based on a total energy balance inclusive of sensible and latent heat components. In a two step approach similar to that of Engelmark and Svensson (1993), the phase change is brought about by the residual energy after sensible heat removal has dropped the temperature of the system below freezing point. Knowing the amount of water that can freeze, the change in soil temperature is then modeled by integrating along the soil freezing curve. However, the system is modeled in terms of the empirically observed heat and mass balance equations (Fourier's heat law and Buckingham-Darcy equation). Coupled cellular automata have not yet been explored to simulate coupled heat and water transport in unsaturated porous media. The model was validated against the analytical solutions of (1) heat conduction problem given by Churchill (1972), (2) analytical solution for steady state convective and conductive heat transport in unfrozen soils given by Stallman (1965), (3) analytical solution of unilateral freezing of a semi-infinite region given by Lunardini (1985), (4) the experimental results for freezing induced water redistribution in soils of Mizoguchi (1990) as cited by

Hansson *et al.* (2004), and (5) the experimental results for freezing induced water redistribution and soil temperature of Jame and Norum (1980).

## **5.2. Cellular automata**

Cellular automata (CA), as first described by von Neumann in 1948 (von Neumann and Burks, 1966), describe the global evolution of a system in space and time based on predefined set of local rules (transition rules). Cellular automata are able to capture the essential features of complex self-organizing cooperative behaviour observed in real systems (Ilachinski, 2001). The basic premise involved in CA modeling of natural systems is the assumption that any heterogeneity in the material properties of a physical system is scale dependent and there exists a length scale for any system at which material properties become homogeneous (Hutt and Neff, 2001). This length scale characterizes the construction of the spatial grid cells (elementary cells) or units of the system. There is no restriction on the shape or size of the cell with the only requirement being internal homogeneity in material properties. Having mentioned that, CA models can be made scale-invariant (Schaller and Svozil, 2009). One can then recreate the spatial description of the entire system by simple repetitions of the elementary cells. The local transition rules are results of empirical observations and are not dependant on the scale of homogeneity in space and time. The traditional differential equation approaches do not work for very large discretizations in space and/or time because they try to simulate second order partial differential equations which can only be developed from these first order empirical laws under the assumption of continuity of the physical and material

properties. Moreover, the discretization needs to be over a grid spacing much smaller than the length scale of the system. The CA approach is not limited by this requirement and is better suited to simulate spatially large systems at any resolution, if the homogeneity criteria at elementary cell level are satisfied (Ilachinski, 2001; Parsons and Fonstad, 2007). Cellular automata represent a large class of exactly computable models since everything is discrete with no limitations imposed by system heterogeneities, anisotropy and non-linearity. In fact, in many highly non-linear physical systems such as those describing critical phase transitions in thermodynamics and statistical mechanical theory of ferromagnetism, discrete schemes such as cellular automata are the only simulation procedures as most analytical methods fail (Hoekstra *et al.*, 2010). In most complex problems, the efficiency of the cellular automata is much higher than any classical method, since the use of cellular automata decreases the level of dissipation of local information within the system (Hoekstra *et al.*, 2010). Solving differential equations requires computationally expensive and often unstable inversion schemes (Parsons and Fonstad, 2007) which are not required in the CA approach. The unnatural mathematical separation of the boundary and internal cells in the FEM/FDM approaches is also not required in the CA approach as already stated. Finite-difference or finite-element techniques require simplifying assumptions in order to solve complex systems (Parsons and Fonstad, 2007). The traditional numerical schemes are not well suited for complex systems wherein simplified assumptions are not possible, e.g., in case of perturbation analysis (Ilachinski, 2001). Because behaviour of such complex systems can generally be

obtained only through explicit simulations, CA approach is well suited to model such systems since it is a forward time stepping method.

Cellular automata approach also has its share of limitations as any other numerical scheme. It is common knowledge that explicit algorithms are not unconditionally convergent and hence given a fixed space discretization, the time discretization cannot be arbitrarily chosen. This makes the CA approach computationally expensive for very large simulation times. However, all numerical schemes become computationally expensive for complex systems and systems with large spatio-temporal scales. Another limitation of the CA approach was thought to be the need for synchronous updating of all cells for accurate simulations. This assumption is proven to be too strict and CA models can be made asynchronous (Hoekstra *et al.*, 2010). It is known that an asynchronous CA for a particular task is more robust and error resistant than a synchronous equivalent (Hoekstra *et al.*, 2010).

The following section describes a 1D CA in simplified, but precise mathematical terms. It is then explained with an example of heat flow (without phase change) in a hypothetical soil column subjected to a time varying temperature boundary condition.

### **5.2.1. Mathematical description**

Let  $S_t^i$  be a discrete state variable which describes the state of the  $i^{\text{th}}$  cell at time step  $t$ . If one assumes that an order of  $N$  elementary repetitions of the unit cell describe the system spatially, then the complete macroscopic state of the system is described by the ordered Cartesian product  $S_t^1 \otimes S_t^2 \otimes \dots \otimes S_t^i \otimes \dots \otimes S_t^N$  at time  $t$ . Let a local transition

rule  $\phi$  be defined on a neighbourhood of spatial indicial radius  $r$ ,  $\phi$ :

$S_t^{i-r} \otimes S_t^{i-r+1} \otimes \dots \otimes S_t^{i+r} \rightarrow S_{t+1}^i$  where  $i \in [1+r, N-r]$ . The global state of the system is

defined by some global mapping,  $\chi: S_t^1 \otimes S_t^2 \otimes \dots \otimes S_t^i \otimes \dots \otimes S_t^N \rightarrow \mathbf{G}_t$  where  $\mathbf{G}_t$  is the global state variable of the system defining the physical state of the system at time  $t$ .

Given this algebra of the system,  $\mathbf{G}_{t+1}$  is given by

$$\mathbf{G}_{t+1} = \chi(\phi(\omega_t^1) \otimes \phi(\omega_t^2) \otimes \dots \otimes \phi(\omega_t^i) \otimes \dots \otimes \phi(\omega_t^N)), \quad (5.1)$$

where  $\omega_t^i = S_t^{i-r} \otimes S_t^{i-r+1} \otimes \dots \otimes S_t^{i+r}$ . The quantity  $r$  is generally called the radius of interaction and defines the spatial extent on which interactions occur on the local scale. In the case of the 1D CA, the only choice of neighbourhood which is physically viable is the standard von Neumann neighbourhood (Figure 5.1).

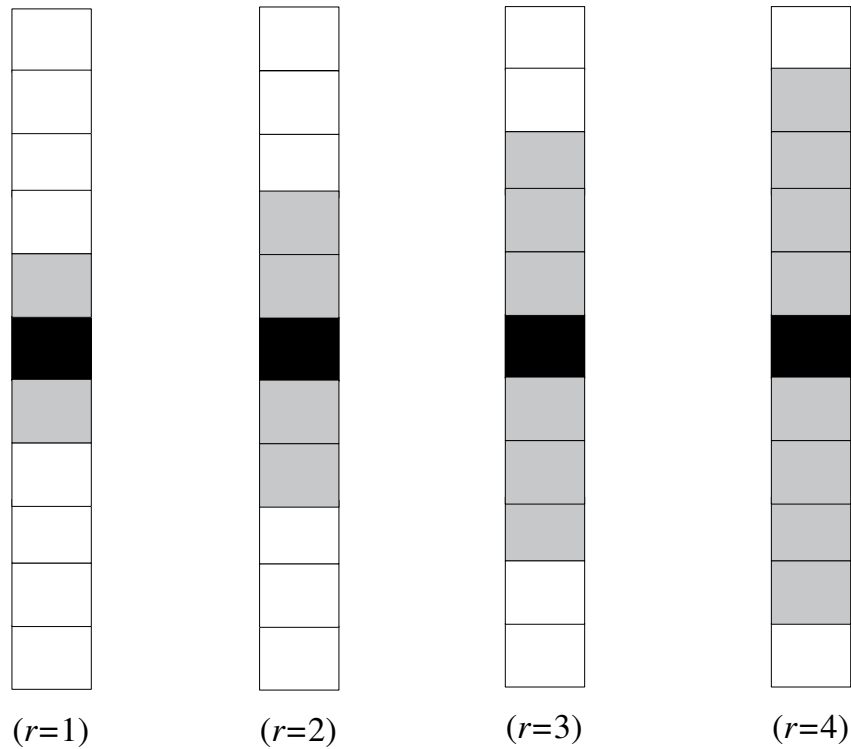


**Figure 5.1.** One dimensional cellular automata grids based on von Neumann neighbourhood concept. How many neighbours (grey cells) interact with an active cell (black) is controlled by indicial radius ( $r$ ).

### 5.2.2. Physical description based on heat flow problem in a hypothetical soil column

The mathematical description of the 1D CA can be understood in more physically intuitive terms using an example of CA simulation of heat flow in a soil column of length  $L_c$  and a constant cross sectional area. The temperature change in the column is driven by a time varying temperature condition applied at the top. It is assumed that no physical variation in the soil properties exist in the column at length intervals smaller than  $\Delta x$  (homogeneity resolution). Each cell in the 1D CA model can therefore be assumed to be

of length  $\Delta x$  with a constant cross sectional area equal to that of the column, and the column can be discretized using  $L_c/\Delta x$  number of elementary cells. To simulate the spatio-temporal evolution of soil temperature in the column, an initial temperature for each elementary cell has to be defined. To study the behaviour of the soil column under external driving (time varying temperature), a fictitious cell is introduced at the top and/or the bottom of the soil column and subjected to time varying temperatures. This is analogous to the imposition of a Dirichlet boundary condition in traditional FEM/FDM numerical simulations. The transition rules need to be defined now. Once the transition rules of heat exchange between neighbours are defined, the fictitious boundary cells interact with the top and/or bottom cells of the soil column as any other internal cell based on the prescribed rules and the predefined temperature time series. Although the same set of rules govern interaction among all cells of the column, heat exchange cannot affect the temperature of the fictitious cells as that would corrupt the boundary condition. This is handled by assigning infinite specific heats to the fictitious cells. This allows evolution of the internal cells and the boundary cells according to the same mathematical rules / empirical equations. This is unlike the unnatural separation of the differential equations and boundary conditions in FEM/FDM approach. This constitutes a very important but subtle difference between the CA approach and the FDM/FEM schemes. The preceding mathematical description of the CA algebra is based on the assumption that the state variable defining each cell is discrete in space and time. But soil temperatures are considered to be continuous in space and time. The continuous description of the soil temperature can be adapted to the CA scheme by considering small

time intervals over which the temperature variations are not of interest and hence for all practical purposes can be assumed constant. Conditions for convergence of the numerical temperature profile set an upper limit on the size of this time interval for a given value of  $\Delta x$ . Therefore, once the length scale of homogeneity  $\Delta x$  in the system and the local update rules have been ascertained, the CA is ready for simulation under the given initial and boundary conditions. Equation (5.2), which is analogous to Fourier's heat law without the convection term, and Equation (5.3) would be the local update rules for this simple case of heat flow in a soil column (without phase change) driven by time varying temperatures at the top. The meaning of the terms used in the mathematical description of CA can be now explained with respect to the heat flow simulation for the hypothetical soil column:  $S_r^i$  is the temperature of the  $i^{\text{th}}$  cell at time  $t$ ,  $r=1$ ,  $\phi$  is a sequential application of Equations (5.2) and (5.3) describing heat loss/gain by a cell due to temperature gradients with its two nearest neighbours and temperature change due to the heat loss/gain, respectively, and  $\chi$  is the identity mapping.

### **5.3. Coupled heat and water transport in unsaturated soils**

The algorithm developed for this study simultaneously solves the heat (sensible and/or latent due to phase change) and water mass conservation in the same time step. The one-dimensional heat transport in unsaturated soils can be given by the heat balance equation

$$q_h = \lambda_{nc} \cdot \frac{(T_n - T_c)}{l_c} + C_w \cdot T_n \cdot q_f, \quad (5.2)$$

where  $q_h$  is the heat flux ( $\text{J s}^{-1} \text{m}^{-2}$ ) for a given cell,  $T$  is cell temperature ( $^{\circ}\text{C}$ ),  $\lambda$  is the effective thermal conductivity of the cell ( $\text{J s}^{-1} \text{m}^{-1} \text{ }^{\circ}\text{C}^{-1}$ ),  $l$  is the length of cell (m),  $C_w$  is volumetric heat capacity ( $\text{J m}^{-3} \text{ }^{\circ}\text{C}^{-1}$ ) of water,  $q_f$  is fluid flux causing convective heat transfer (e.g., rate of infiltration), and subscripts  $c$  and  $n$  refer to the cell and its active neighbour. Effective thermal conductivity can be calculated using one of the popular mixing models (e.g., Johansen, 1975; Campbell, 1980). If the second term on the RHS is neglected, Equation (5.2) becomes Fourier's empirical heat law. The empirical relationship between heat flux from Equation (5.2) and resulting change in cell temperature ( $\Delta T_c$ ) is given as

$$q_h = C_c \cdot \Delta T_c, \quad (5.3)$$

where  $C_c$  ( $\text{Jm}^{-3}\text{ }^{\circ}\text{C}^{-1}$ ) is the effective volumetric heat capacity of a cell and is given by

$$C_c = C_w \theta_w + C_i \theta_i + C_s \theta_s + C_a \theta_a, \quad (5.4)$$

where  $\theta$  is volumetric fraction ( $\text{m}^3 \text{m}^{-3}$ ) and subscripts  $w$ ,  $i$ ,  $s$ , and  $a$  represent water, ice, soil solids and air fractions.

The mass conservation equation in 1D can be written as

$$\rho_w \cdot \frac{\Delta \Theta}{\Delta t} + \rho_w \cdot q_w + \rho_w \cdot S_s = 0, \quad (5.5)$$

$$\Theta = \theta_w + \frac{\rho_i}{\rho_w} \theta_i, \quad (5.6)$$

$\rho$  is density ( $\text{kg m}^{-3}$ ),  $\Theta$  is the total volumetric water content ( $\text{m}^3 \text{m}^{-3}$ ),  $q_w$  is the Buckingham-Darcy flux ( $\text{ms}^{-1}$ ), and  $S_s$  is sink/source term. In unfrozen soils,  $\theta_i = 0$  and  $\Theta = \theta_w$ .

Buckingham-Darcy's equation is used to describe the flow of water under hydraulic head gradients wherein it is recognized that the soil matric potential ( $\psi$ ) and hydraulic conductivity ( $k$ ) are functions of liquid water content ( $\theta_w$ ). The dependency of  $\psi$  and  $k$  on  $\theta_w$  can be expressed as a constitutive relationship. The constitutive relationships proposed by Mualem-van Genuchten (van Genuchten, 1980) defining  $\psi(\theta_w)$  and  $k(\theta_w)$  are used in this study

$$\psi(\theta_w) = \frac{\left[ (S_e)^{\frac{1}{m}} - 1 \right]^{\frac{1}{n}}}{\alpha}, \quad (5.7)$$

$$k(\theta_w) = K_s \cdot (S_e)^{0.5} \cdot \left[ 1 - \left( 1 - (S_e)^{\frac{1}{m}} \right)^m \right]^2, \quad (5.8)$$

$$S_e = \frac{\theta_w - \theta_r}{\eta - \theta_r}, \quad (5.9)$$

where  $\theta_r$  ( $\text{m}^3 \text{m}^{-3}$ ) is the residual liquid water content,  $\eta$  ( $\text{m}^3 \text{m}^{-3}$ ) is total porosity,  $K_s$  ( $\text{m s}^{-1}$ ) is the saturated hydraulic conductivity, and  $\alpha$  ( $\text{m}^{-1}$ ),  $n$  and  $m$  are equation constants such that  $m = 1 - 1/n$ . For an elementary cell in a 1D CA model, the Buckingham-Darcy flux in its simplest form can be written as

$$q_w = k_{nc}(\theta_w) \cdot \frac{(\psi_n - \psi_c + z_c - z_n)}{l_c}, \quad (5.10)$$

where  $z$  is the elevation and  $k_{nc}$  represents the geometric mean of hydraulic conductivities of the cell and its active neighbour. In this study, phase change and associated temperature change is brought about by integrating along a soil freezing curve (SFC). SFC's can be defined because the liquid water content in frozen soils must have a fixed

value for each temperature at which the liquid and ice phases are in equilibrium, regardless of the amount of ice present (Low *et al.*, 1968). Soil freezing curves for different types of soils developed from field and laboratory observations between liquid water content and soil temperature have been widely reported (e.g., Anderson and Morgenstern, 1973; Staehli *et al.*, 1996; Quinton and Hayashi, 2008). van Genuchten's model (van Genuchten, 1980) can be used to define a SFC (Equation 5.7), wherein  $\psi(\theta_w)$  is replaced with  $T(\theta_w)$ , and  $n$ ,  $m$  and  $\alpha$  ( $^{\circ}\text{C}^{-1}$ ) are equation constants.

#### **5.4. The coupled CA model**

Figure 5.2 shows a flow chart describing the algorithm driving the coupled CA code. Let the subscript  $j$  denote the present time step. The thermal conduction and hydraulic conduction modules represent two different algorithms that calculate the heat flux ( $q_{hj}$ ) and water flux ( $q_{wj}$ ) respectively. In essence, the thermal conduction and hydraulic conduction codes run simultaneously and are not affected by each other in the same time step. Hydraulic conduction is achieved by applying Equation (5.10) to each elementary cell using the hydraulic gradients between it and its immediate neighbours ( $r=1$ ). Similarly, Equation (5.2) is used to calculate the heat flux between each elementary cell and its immediate neighbours using the corresponding thermal gradients. The change in mass due to the flux  $q_{wj}$  is used to obtain change in pressure head ( $\Delta\psi_j$ ) from  $\psi_j(\theta_w)$  relationship. The updated value of total water content is then used to update the volumetric heat capacity ( $C$ ) of each cell (Equation 5.4). The updated value of  $C$  is used as input to the energy balance module along with computed heat flux  $q_{hj}$ . This

represents the first stage of coupling between hydraulic and thermal processes. The energy balance module computes the total change in ice and water content due to phase change, and the total temperature change ( $\Delta T_j$ ) due to a combination of thermal conduction and phase change.

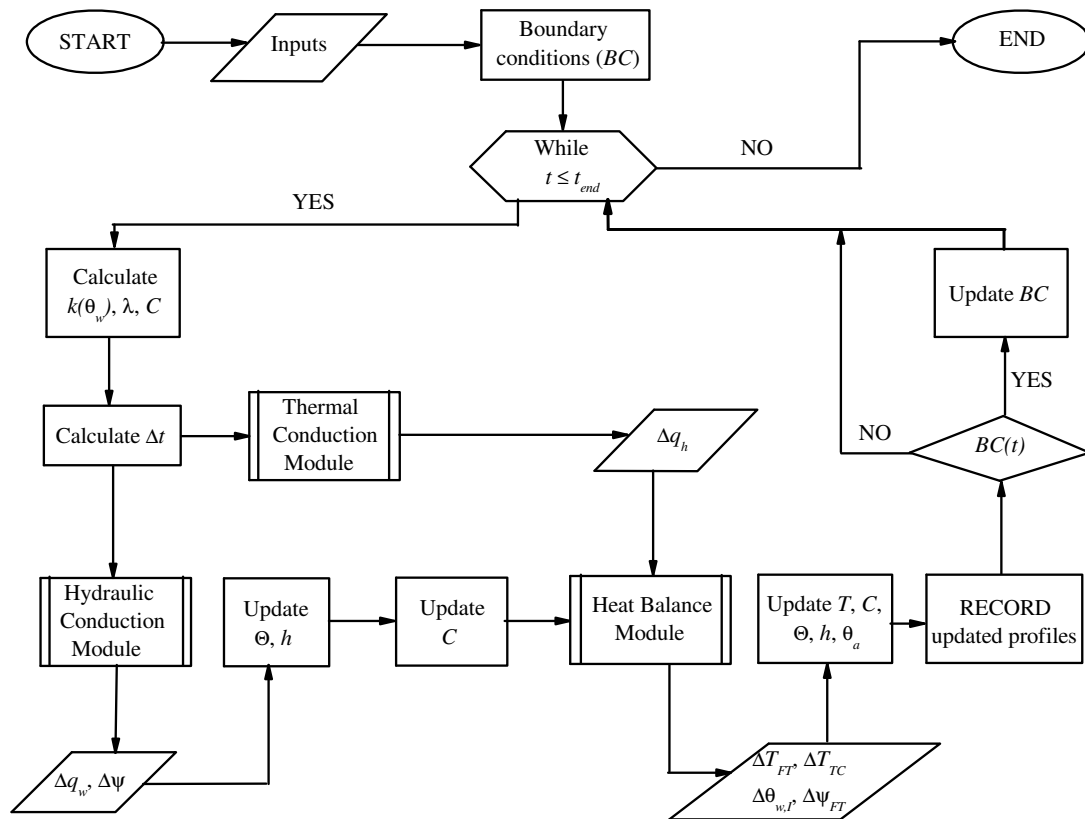


**Figure 5.2.** Flow chart describing the algorithm driving the coupled CA code. Subscripts *TC*, *HC* and *FT* refer to changes in physical quantities due to thermal conduction, hydraulic conduction and freeze-thaw processes respectively. Hydraulic conduction and thermal conduction are two different CA codes coupled though updating of volumetric heat capacity and the freeze-thaw module to simulate the simultaneous heat and water movement in soils.

The energy balance module is explained using an example of a system wherein the soil temperature is dropping and phase change may take place if cell temperature drops below freezing point of pure water ( $T_{fw} = 0^\circ\text{C}$ ). Inside the energy balance module, the change in temperature ( $\Delta T_j$ ) is calculated using Equation (5.3) and values of  $C$  and  $q_{hj}$  assuming that only thermal conduction takes place. If the computed  $\Delta T_j$  for a given cell is such that  $T_{j+1} \geq T_{fw}$ , then water cannot freeze; cell temperatures are updated without phase change and the code moves into the next time step. In the approach of this study, phase change and associated temperature change can occur if and only if the present cell temperature ( $T_j$ ) and water content ( $\theta_{wj}$ ) represent a point on the soil freezing curve (SFC). This point along the SFC (Figure 5.3) is defined here as the critical state point ( $T_{crit}, \theta_{wcrit}$ ). If  $\Delta T_j$  gives  $T_{j+1} < T_{fw}$  for any cell, then freezing point depression along the SFC accounts for change in temperature due to freeze-thaw. The freezing point depression or  $T_{crit}$  is defined for the cell by comparing the cell  $\theta_{wj}$  with the SFC. However, the coupled nature of heat and water transport in soils perturbs the critical state from time to time, e.g., when freezing induced water movement towards the freezing front or infiltration into frozen soil leads to accumulation or removal of extra water from any cell. In such a case,  $q_{hj}$  needs to be used to bring the cell to the critical state. This may require thermal conduction without phase change ( $T_{crit} > T_j$ ) or freezing of water without temperature change ( $T_{crit} < T_j$ ). This process gives us an additional change in temperature or water content which is purely due to the fact that the additional water accumulation disturbs the critical state. This is another and a more fine print form of coupling between heat and water flow. Because of the above consideration to perturbation of critical state

caused by additional water added/removed from a cell, infiltration into frozen soils during the over-winter melt events or during the spring melt events need no further modifications to the process of water and heat balance.

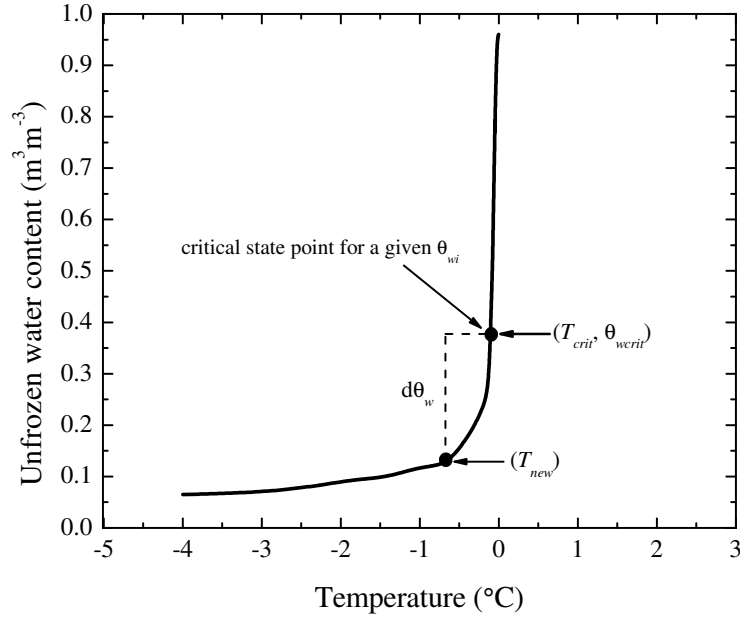


**Figure 5.3.** Graphical description of the phase change approach used in this study. The curve is a soil freezing curve for a hypothetical soil. The change in water content ( $d\theta_w$ ) due to  $q_{resj}$  is used to determine  $T_{new}$  by integrating along the SFC (Equation 5.11).

If  $q_{hj}$  is such that a cell can reach critical state and still additional heat needs to be removed, then the additional part ( $q_{resj}$ ) is used to freeze water. Freezing of water leads to change in the temperature of the cell such that

$$\min\left(\theta_w, \frac{\Delta q_{resj}}{L_f}\right) = \int_{T_{crit}}^{T_{new}} d\theta_w, \quad (5.11)$$

where  $T_{new}$  is the new temperature of the cell (Figure 5.3). If the change in water content due to freezing is such that  $\theta_{wj} = \theta_r$ , then no further freezing of water can take place and  $q_{resj}$  is used to decrease the temperature of the cell using Equation (5.3) and updated value of  $C$  (i.e., after accounting for change in  $C$  due to phase change). The soil thawing case is exactly similar as described above; the only dissimilarity is that a different SFC may be used if hysteric effects are observed in SFC paths as observed in studies by Quinton and Hayashi (2008), and Smerdon and Mendoza (2010). If the cell temperature is above freezing temperature, the matric potential is calculated using Equation (5.4). For cell temperatures below freezing point, the water pressure (matric potential) can be determined by the generalized Clausis-Clapeyron equation by assuming zero ice gauge pressure

$$L_f \cdot \frac{\Delta T}{T + 273.15} = g \cdot \Delta \Psi , \quad (5.12)$$

where  $L_f$  is the latent heat of fusion ( $334000 \text{ J kg}^{-1}$ ),  $T$  is the cell/soil temperature ( $^{\circ}\text{C}$ ), and  $g$  is acceleration due to gravity ( $9.81 \text{ m s}^{-2}$ ). At the end of the energy balance calculations temperatures of all cells are updated using the  $\Delta T_j$  computed in energy balance module. Water content for each cell is updated by considering the change due to freeze/thaw inside the energy balance module and  $q_{wj}$ . Hydraulic conductivity of each cell is updated (Equation 5.8) using the final updated values of water content. Pressure and total heads in each cell are updated considering water movement (Equation 5.7) and freezing/thawing (Equation 5.12). The volumetric heat capacity of each cell is updated one more time (Equation 5.4) to incorporate the changes due to freeze/thaw inside the

energy balance module. Thermal conductivity of each cell is updated using a mixing model (e.g., Johansen, 1985). This completes all the necessary updates and the model is ready for computations of the next time step.

## 5.5. Verification

The coupled CA model was tested for simultaneous heat and water transport in frozen and unfrozen soils using three analytical and two experimental examples.

### 5.5.1. Comparison with analytical solutions

#### 5.5.1.1. Heat transfer by pure conduction

The ability of the CA model to simulate pure conduction under hydrostatic conditions was tested by comparison to the analytical solution of one-dimensional heat conduction in a finite domain given by Churchill (1972). A soil column with total length ( $L_c$ ) of 4 m was assumed to have different initial temperatures in its upper ( $T_u = 10^\circ\text{C}$ ) and lower ( $T_l = 20^\circ\text{C}$ ) halves (Figure 5.4a). The system is hydrostatic at all times and there is no flow. At the interface, heat conduction due to the temperature gradient will occur until the entire domain reaches an average steady state temperature of  $15^\circ\text{C}$ . The analytical solution as given by Churchill (1972) can be expressed as

$$T(z,t) = T_u \cdot \left[ 0.5 + \frac{2}{\pi} \sum_{n=1}^{\infty} \frac{(-1)^{n-1}}{2n-1} \cdot \cos\left(\frac{(2n-1) \cdot \pi \cdot z}{L_c}\right) \cdot \exp\left(-\left[\frac{(2n-1) \cdot \pi}{L_c}\right]^2 \cdot \left(\frac{\lambda}{C}\right) \cdot t\right) \right] + T_l \cdot \left[ 0.5 - \frac{2}{\pi} \sum_{n=1}^{\infty} \frac{(-1)^{n-1}}{2n-1} \cdot \cos\left(\frac{(2n-1) \cdot \pi \cdot z}{L_c}\right) \cdot \exp\left(-\left[\frac{(2n-1) \cdot \pi}{L_c}\right]^2 \cdot \left(\frac{\lambda}{C}\right) \cdot t\right) \right] \quad (5.13)$$

The parameters used in analytical examples for Churchill (1972), and CA code are given in Table 5.1. There is excellent agreement between the analytical solution and the CA simulation (Figure 5.4b).

Symbol	Parameter	Value
$\eta$	porosity	0.35
$\lambda$	bulk thermal conductivity	$2.0 \text{ W m}^{-1} \text{ }^\circ\text{C}^{-1}$
$C_w$	volumetric heat capacity of water	$4174000 \text{ J m}^{-3} \text{ }^\circ\text{C}^{-1}$
$C_s$	volumetric heat capacity of soil solids	$2104000 \text{ J m}^{-3} \text{ }^\circ\text{C}^{-1}$
$\rho_w$	density of water	$1000 \text{ kg m}^{-3}$
$\rho_s$	density of soil solids	$2630 \text{ kg m}^{-3}$
$l$	length of cell	0.01 m
$t$	length of time step in CA solution	1 second

**Table 5.1.** Simulation parameters for heat conduction problem. Analytical solution for this example is given by Equation 5.13 as per Churchill (1972).

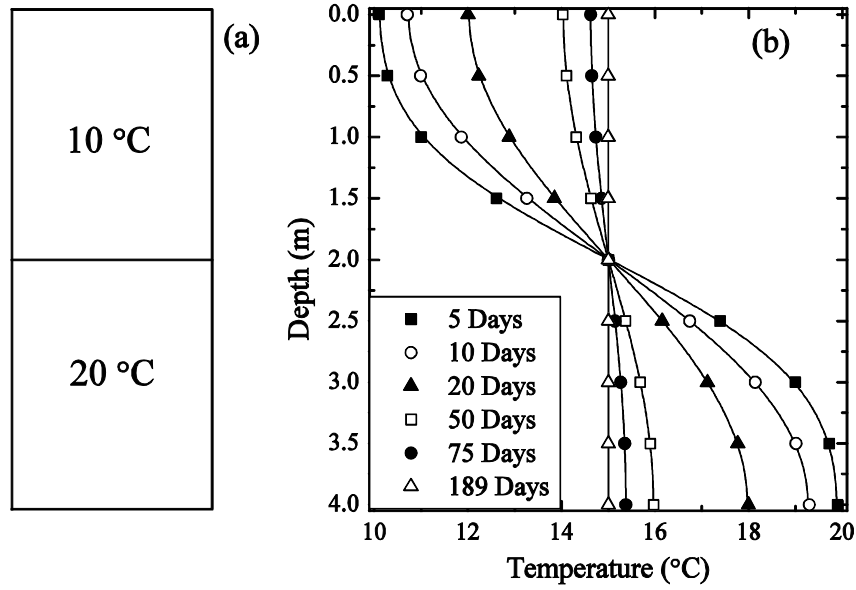


**Figure 5.4.** (a) Initial temperature distribution along a perfectly thermally insulated 4 m long soil column. (b) Comparison between the analytical solution given by Churchill (1972) and coupled cellular automata model simulation. Lines represent the analytical solution and symbols represent the CA solution for time points as shown in the legend.

### 5.5.1.2. Heat transfer by conduction and convection

Stallman's analytical solution (Stallman, 1965) to the subsurface temperature profile in a semi-infinite porous medium in response to a sinusoidal surface temperature provides a test of the CA model's ability to simulate one dimensional heat convection and conduction in response to a time varying Dirichlet boundary.

Given the temperature variation at the ground surface described by

$$T(z_0, t) = T_{surf} + A \cdot \sin\left(\frac{2 \cdot \pi \cdot t}{\tau}\right), \quad (5.14)$$

the temperature variation with depth is given by

$$T(z,t) = Ae^{-\alpha z} \cdot \sin\left(\frac{2 \cdot \pi \cdot t}{\tau} - \beta \cdot z\right) + T_{\infty}, \quad (5.15)$$

$$\alpha = \left\{ \left[ \left( \frac{\pi C \rho}{\lambda \tau} \right)^2 + \frac{1}{4} \left( \frac{q_f C_w \rho_w}{2\lambda} \right)^4 \right]^{0.5} + \frac{1}{2} \left( \frac{q_f C_w \rho_w}{2\lambda} \right)^2 \right\} - \left( \frac{q_f C_w \rho_w}{2\lambda} \right), \quad (5.16)$$

$$\beta = \left\{ \left[ \left( \frac{\pi C \rho}{\lambda \tau} \right)^2 + \frac{1}{4} \left( \frac{q_w C_w \rho_w}{2\lambda} \right)^4 \right]^{0.5} + \frac{1}{2} \left( \frac{q_w C_w \rho_w}{2\lambda} \right)^2 \right\}^{0.5}, \quad (5.17)$$

where  $A$  is the amplitude of temperature variation ( $^{\circ}\text{C}$ ),  $T_{surf}$  is the average surface temperature over a period of  $\tau$  (s),  $T_{\infty}$  is the initial temperature of soil column and temperature at infinite depth, and  $q_f$  is the specific flux through the column top.

The parameters used in analytical examples for Stallman (1965), and CA code are given in Table 5.2. The coupled CA code is able to simulate the temperature evolution due to conductive and convective heat transfer as seen from the excellent agreement with the analytical solution (Figure 5.5).

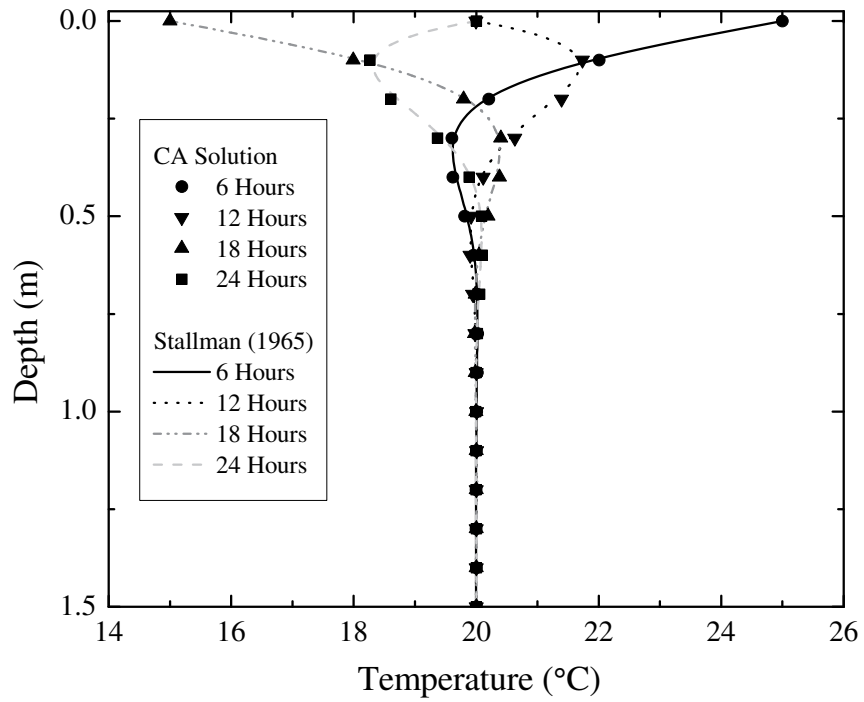


**Figure 5.5.** Comparison between analytical (Stallman, 1965) and coupled CA model steady state solutions for conductive and convective heat transfer. The soil column in this example is infinitely long, initially at 20 °C, and upper surface is subjected to a sinusoidal temperature with amplitude of 5 °C and period of 24 hours.

Symbol	Parameter	Value
$\eta$	porosity	0.40
$\lambda$	bulk thermal conductivity	$2.0 \text{ W m}^{-1} \text{ }^\circ\text{C}^{-1}$
$C_w$	volumetric heat capacity of water	$4174000 \text{ J m}^{-3} \text{ }^\circ\text{C}^{-1}$
$C_s$	volumetric heat capacity of soil solids	$2104000 \text{ J m}^{-3} \text{ }^\circ\text{C}^{-1}$
$\rho_w$	density of water	$1000 \text{ kg m}^{-3}$
$\rho_s$	density of soil solids	$2630 \text{ kg m}^{-3}$
$l$	length of cell	0.01 m
$t$	length of time step in CA solution	1 second
$q_f$	downward specific flux	$4 \times 10^{-7} \text{ ms}^{-1}$
$\tau$	period of oscillation of temperature at the ground surface	24 hours
$A$	amplitude of the temperature variation at the ground surface	$5^\circ\text{C}$
$T_{surf}$	average ambient temperature at the ground surface	$20^\circ\text{C}$
$T_\infty$	ambient temperature at depth	$20^\circ\text{C}$

**Table 5.2.** Simulation parameters for predicting subsurface temperature profile in a semi-infinite porous medium in response to a sinusoidal surface temperature. The analytical solution to this one dimensional heat convection and conduction problem in response to a time varying Dirichlet boundary is given by Equations 5.14-5.17 as per Stallman (1965).

### 5.5.1.3. Heat transfer with phase change

Lunardini (1985) presented an exact analytical solution for propagation of subfreezing temperatures in a semi-infinite, initially unfrozen soil column with time  $t$ . The soil column is divided into three zones (Figure 5.6a) where zone 1 is fully frozen with no unfrozen water; zone 2 is ‘mushy’ with both ice and water; and zone 3 is fully thawed. The Lunardini (1985) solution as described by McKenzie *et al.* (2007) and is given by following set of equations

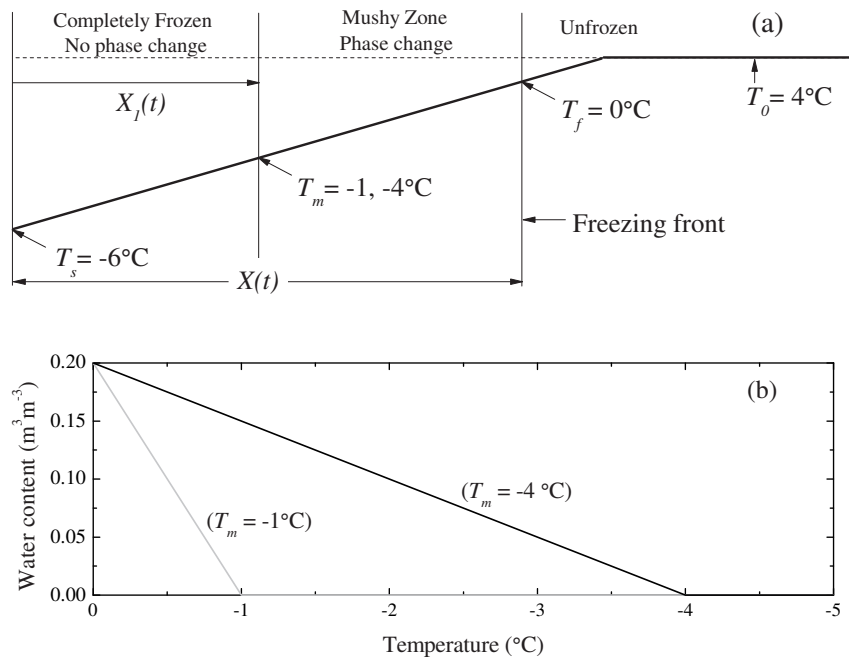


**Figure 5.6.** (a) Diagram showing the setting of Lunardini (1985) three zone problem. Equations 5.18, 5.19, and 5.20 are used to predict temperatures in completely frozen zone (no phase change and sensible heat only), mushy zone (phase change and latent heat + sensible heat), and unfrozen zone (sensible heat only) respectively. (b) Linear freezing function used to predict unfrozen water contents for two cases used in this study ( $T_m = -1^\circ\text{C}$  and  $T_m = -4^\circ\text{C}$ ).

$$T_1 = (T_m - T_s) \cdot \frac{\operatorname{erf}\left(\frac{x}{2\sqrt{D_1 t}}\right)}{\operatorname{erf}(\vartheta)} + T_s, \quad (5.18)$$

$$T_2 = (T_f - T_m) \cdot \frac{\operatorname{erf}\left(\frac{x}{2\sqrt{D_4 t}}\right) - \operatorname{erf}(\gamma)}{\operatorname{erf}(\gamma) - \operatorname{erf}\left(\vartheta\sqrt{D_1/D_4}\right)} + T_f, \quad (5.19)$$

$$T_3 = (T_0 - T_f) \cdot \frac{-\operatorname{erfc}\left(\frac{x}{2\sqrt{D_3 t}}\right)}{\operatorname{erf}\left(\gamma\sqrt{D_4/D_3}\right)} + T_0, \quad (5.20)$$

where  $T_1$ ,  $T_2$ , and  $T_3$  are the temperatures at distance  $x$  from the temperature boundary for zones 1, 2, and 3 respectively;  $T_0$ ,  $T_m$ ,  $T_f$ , and  $T_s$  are the temperatures of the initial conditions, the solidus, the liquidus, and the boundary respectively;  $D_1$  and  $D_3$  are the thermal diffusivities for zones 1 and 3, defined as  $\lambda_1/C_1$  and  $\lambda_3/C_3$  where  $C_1$  and  $C_3$ , and  $\lambda_1$  and  $\lambda_4$  are the volumetric bulk-heat capacities ( $\text{Jm}^{-3}\text{C}^{-1}$ ) and bulk thermal conductivities ( $\text{Wm}^{-1}\text{C}^{-1}$ ) respectively of the two zones. The thermal diffusivity of zone 2 is assumed to be constant across the transition region, and the thermal diffusivity with latent heat,  $D_4$ , is defined as:

$$D_4 = \frac{\lambda_2}{C_2 + \left(\frac{\gamma_d L_f \Delta \xi}{T_f - T_m}\right)}, \quad (5.21)$$

where  $\gamma_d$  is the dry unit density of soil solids, and  $\Delta\xi = \xi_1 - \xi_3$  where  $\xi_1$  and  $\xi_3$  are the ratio of unfrozen water to soil solids in zones 1 and 3 respectively. For a time  $t$  in the region from  $0 \leq x \leq X_1(t)$  the temperature is  $T_1$  and  $X_1(t)$  is given by:

$$X_1(t) = 2\vartheta\sqrt{D_1t}, \quad (5.22)$$

and from  $X_1(t) \leq x \leq X(t)$  the temperature is  $T_2$  where  $X(t)$  is given by:

$$X(t) = 2\gamma\sqrt{D_4t}, \quad (5.23)$$

and for  $x \geq X(t)$  the temperature is  $T_3$ . The unknowns,  $\vartheta$  and  $\gamma$ , are obtained from solution of the following two simultaneous equations

$$\frac{(T_m - T_s)}{(T_m - T_f)} \cdot e^{-\vartheta^2\left(1 - \frac{D_1}{D_4}\right)} = \frac{\frac{\lambda_2}{\lambda_1} \operatorname{erf}(\vartheta) \sqrt{\frac{D_1}{D_4}}}{\operatorname{erf}(\gamma) - \operatorname{erf}\left(\vartheta \sqrt{\frac{D_1}{D_4}}\right)}, \quad (5.24)$$

$$\frac{(T_m - T_f) \frac{\lambda_2}{\lambda_1}}{(T_0 - T_f)} \cdot \sqrt{\frac{D_3}{D_4}} \cdot e^{-\gamma^2\left(1 - \frac{D_4}{D_3}\right)} = \frac{\operatorname{erf}(\gamma) - \operatorname{erf}\left(\vartheta \sqrt{\frac{D_1}{D_4}}\right)}{\operatorname{erfc}\left(\gamma \sqrt{\frac{D_4}{D_3}}\right)}, \quad (5.25)$$

The verification example based on Lunardini (1985) analytical solution used in this study is the same as used by McKenzie *et al.* (2007). Lunardini (1985) assumed the bulk-volumetric heat capacities of the three zones, and thermal conductivities in each zone to be constant. It was also assumed for the sake of the analytical solution that the

unfrozen water varies linearly with temperature. As stated by Lunardini (1985), if unfrozen water varies linearly with temperature then an exact solution may be found for a three zone problem. Although this will be a poor representation of a real soil system, it will constitute a valuable check for approximate solution methods. The linear freezing function used in this study is shown in Figure 5.6b and the parameters used in Lunardini (1985) analytical solution are given in Table 5.3. The excellent agreement between the analytical solution and coupled CA model simulations (Figures 6a and 6b) for two different cases of  $T_m$  shows that the model is able to perfectly simulate the process of heat conduction with phase change.

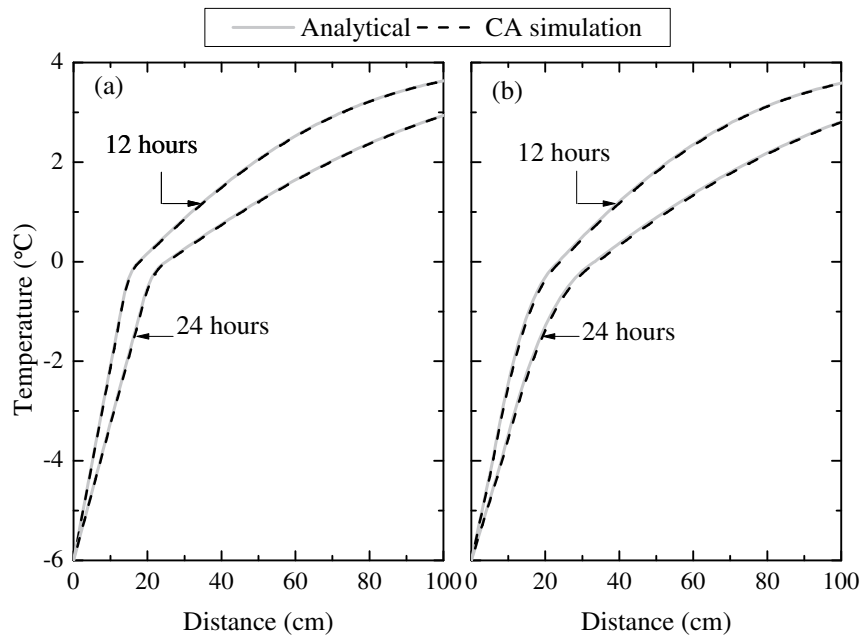


**Figure 5.7.** Comparison between analytical solution of heat flow with phase change (Lunardini, 1985) and coupled CA model solutions for heat transfer with phase change. Lunardini (1985) solution is shown and compared with CA simulation for two cases (a)  $T_m = -1^\circ\text{C}$  and (b)  $T_m = -4^\circ\text{C}$  (Table 5.3, Figure 5.6).

Symbol	Parameter	Value
$\eta$	porosity	0.20
$\lambda_1$	bulk thermal conductivity of frozen zone	3.464352 Wm <sup>-1</sup> °C <sup>-1</sup>
$\lambda_2$	bulk thermal conductivity of mushy zone	2.941352 Wm <sup>-1</sup> °C <sup>-1</sup>
$\lambda_3$	bulk thermal conductivity of unfrozen zone	2.418352 Wm <sup>-1</sup> °C <sup>-1</sup>
$C_1$	bulk-volumetric heat capacity of frozen zone	690360 J m <sup>-3</sup> °C <sup>-1</sup>
$C_2$	bulk-volumetric heat capacity of mushy zone	690360 J m <sup>-3</sup> °C <sup>-1</sup>
$C_3$	bulk-volumetric heat capacity of unfrozen zone	690360 J m <sup>-3</sup> °C <sup>-1</sup>
$\xi_1$	fraction of liquid water to soil solids in frozen zone	0.0782
$\xi_3$	fraction of liquid water to soil solids in unfrozen zone	0.2
$l$	length of cell	0.01 m
$t$	length of time step in CA solution	1 second
$L_f$	Latent heat of fusion	334720 Jkg <sup>-1</sup>
$\gamma_d$	dry unit density of soil solids	1680 kgm <sup>-3</sup>
$T_s$	surface temperature at the cold end	-6°C
$T_m$	temperature at the boundary of frozen and mushy zones	-1°C, -4°C

---

$\gamma^*$	equation parameter estimated using Equations 5.24, 5.25	1.395, 2.062
$\mathcal{J}^*$	equation parameter estimated using Equations 5.24, 5.25	0.0617, 0.1375
$T_0$	initial temperature of the soil column	4°C

---

\* values taken from McKenzie *et al.* (2007)

**Table 5.3.** Simulation parameters for predicting subsurface temperature profile with phase change in a three zone semi-infinite porous medium. The analytical solution to this one dimensional problem with sensible and latent heat zones is given by Equations 5.18-5.25 as per Lundardini (1985).

### 5.5.2. Comparison with experimental data

Two verification cases with laboratory data on water redistribution in frozen soils and soil temperature are described below. First one is the case used by Hansson *et al.* (2004) wherein only water redistribution results are compared with the CA solution. The second example is by Jame and Norum (1980) wherein both water redistribution as well as temperature results are compared with the CA solution. In both cases the soil physical properties were assumed to be unaffected by the freezing process (in reality porosity could change due to freezing, but this aspect is not dealt with in this thesis as there was no data for such measurements and also out of scope of the current validation exercise).

*Case I:* Hansson *et al.* (2004) describe laboratory experiments of Mizoguchi (1990) in which freezing induced water redistribution in 20 cm long Kanagawa sandy loam columns was observed. The coupled CA code was used to model the experiment as a

validation test for simulation of frost induced water redistribution in unsaturated soils. The experiments described in Hansson *et al.* (2004) are briefly discussed first. Four identical cylinders, 8 cm in diameter and 20 cm long, were packed to a bulk density of  $1300 \text{ kgm}^{-3}$  resulting into total porosity of  $0.535 \text{ m}^3\text{m}^{-3}$ . The columns were thermally insulated from all sides except the tops and brought to uniform temperature ( $6.7 \text{ }^\circ\text{C}$ ) and volumetric water content ( $0.33 \text{ m}^3\text{m}^{-3}$ ). The tops of three cylinders were exposed to a circulating fluid at  $-6^\circ\text{C}$ . One cylinder at a time was removed from the freezing apparatus and sliced into 1 cm thick slices after 12, 24, and 50 hours. Each slice was oven dried to obtain total water content (liquid water + ice). The fourth cylinder was used to precisely determine the initial condition. The freezing induced water redistribution observed in these experiments was simulated using the coupled CA code. Parameters used were: saturated hydraulic conductivity of  $3.2 \times 10^{-6} \text{ ms}^{-1}$  and van Genuchten parameters  $\alpha = 1.11 \text{ m}^{-1}$ ,  $n = 1.48$ . The hydraulic conductivity of the cells with ice was reduced using an impedance factor = 2. Thermal conductivity formulation of Campbell (1985) as modified and applied by Hansson *et al.* (2004) was used. In their simulations of the Mizoguchi (1990) experiments, Hansson *et al.* (2004) calibrated the model using a heat flux boundary at the top and bottom of the columns. The heat flux at the surface and bottom was controlled by heat conductance terms multiplied by the difference between the surface and ambient, and bottom and ambient temperatures, respectively. Similar boundary conditions were used in the CA simulations. The value of heat conductance at the surface was allowed to decrease nonlinearly as a function of the surface temperature squared using the values reported by Hansson *et al.* (2004). The heat conductance

coefficient of  $1.5 \text{ Wm}^{-2}\text{C}^{-1}$  was used to simulate heat loss through the bottom. Hansson and Lundin (2006) observed that the four soil cores used in the experiment performed by Mizoguchi (1990) were quite similar in terms of saturated hydraulic conductivity, but probably less so in terms of the water holding properties where more significant differences were to be expected. Such differences in water holding capacity would result in significant differences in unsaturated hydraulic conductivities of the columns at different times during the freezing experiments. The simulated values of total water content agree very well with the experimental values (Figure 5.8). The region with sharp drop in the water content indicates the position of the freezing front. There is clear freezing induced water redistribution, which is one of the principal phenomena for freezing porous media and is well represented in the coupled CA simulations. Mizoguchi's experiments have been used by number of researcher for validation of numerical codes (e.g., Hansson *et al.*, 2004; Daanen *et al.*, 2007; Painter *et al.*, 2010). In comparison, the CA simulation shows a much better agreement for total water content as well as for the sharp transition at the freezing front.

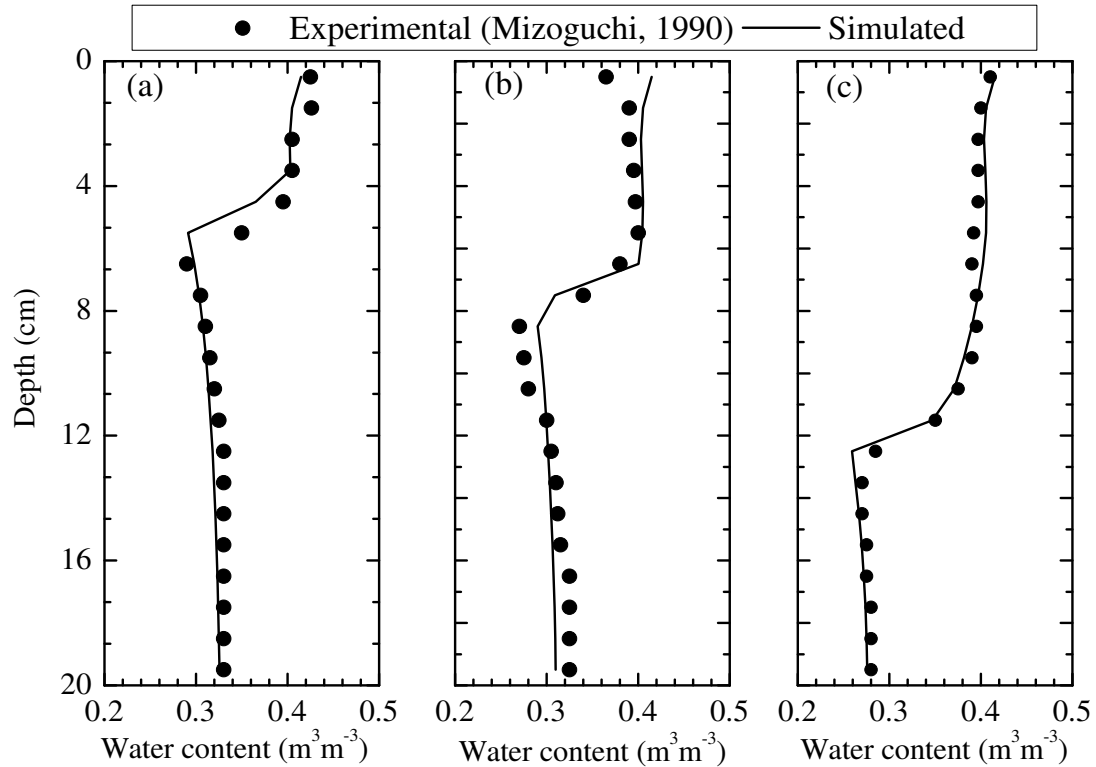


**Figure 5.8.** Comparison of total water content (ice + water) between experimental (Mizoguchi, 1990 as cited by Hansson, 2004) and coupled CA model results: (a) 12 hours, (b) 24 hours, and (c) 50 hours.

*Case II:* Jame and Norum (1980) report laboratory experiments involving freezing of partially saturated, 30-cm-long column oriented horizontally and packed with #40 silica flour. The column was thermally insulated on sides, sealed so that no water escapes, and initially unfrozen and partially saturated with liquid water. At the start of the experiment, the temperature at one end was lowered, while the other end was held at the initial temperature. Total water content (ice + liquid) and temperature was measured as a function of space and time using gamma ray attenuation and thermocouples respectively. One of the tests is used here for verification of the coupled CA code. In this test, the

temperature was initially 4.2°C and the initial volumetric water content was 0.15 m<sup>3</sup> m<sup>-3</sup>. The cold end temperature was -5.9°C. The CA simulations used experimental conditions and silica flour parameters as reported by Jame (1977) and Jame and Norum (1980). The thermal conductivity of solids of 8.54 Wm<sup>-1</sup>°C<sup>-1</sup> reported by Jame (1977) was used. Thermal conductivity formulation of Johansen (1975) was used after calibrating it with the thermal conductivity versus saturation data reported by Jame and Norum (1980). The soil freezing curve reported by Jame (1977) was used and was defined by van Genuchten's model using  $\alpha = 9.95 \text{ }^\circ\text{C}^{-1}$ ,  $n = 2.78$ , and porosity of 0.49. Saturated hydraulic conductivity of  $1.92 \times 10^{-5} \text{ ms}^{-1}$  (Painter, 2010) and impedance factor of 4.5 (Jame and Norum, 1980) was used. Figure 5.9a shows the comparison between the observed and simulated total (ice + liquid) water content for 6, 24, and 72 hours. Figure 5.9b shows the comparison between observed and simulated temperature profiles for the same times. There is fair agreement between the CA simulation and the experimental results (Figure 5.9). The freezing front location and temperatures are simulated with good agreement. Simulated total water content is fairly good as well, except for the 72 hours time point in the lower half of the column. It must be noted that Jame and Norum (1980) reported problems in the initial conditions as well as the evolution of surface temperature in first 6 hours. To account for these issues, they ran the simulations separately for first 6 hours and then again for the time period between 6 hours and 72 hours using the results of first simulation as the initial conditions for the remaining period. This was not done in the CA simulations. The value of saturated hydraulic conductivity is also not clearly known. In addition, as pointed out by Engelmark and Svensson (1993), the reported

boundary conditions for this experiment are probably not exact. These factors are the likely reasons for some of the deviation of modelled values from experimental results. Despite these limitations, this example shows that the CA code simulates the shape of the freezing front and the freezing induced water redistribution to a fair degree of accuracy and forms a second validation case using experimental data.

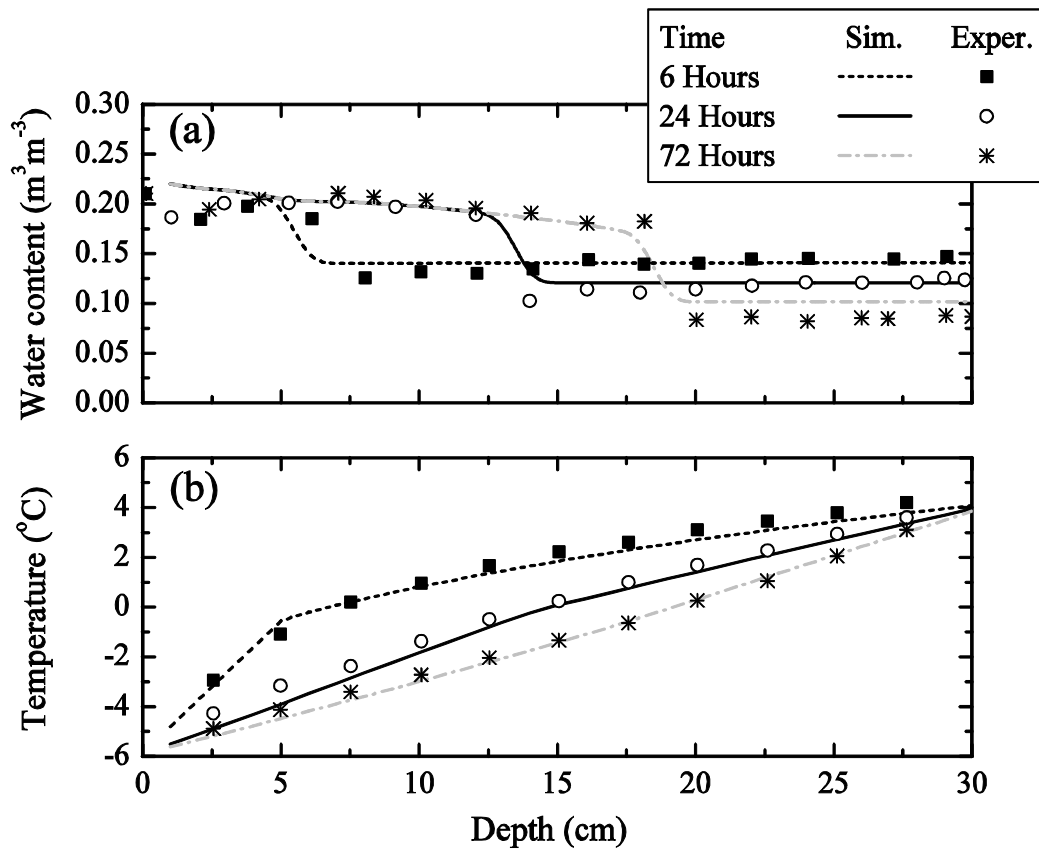


**Figure 5.9.** Comparison between experimental (Jame and Norum, 1980) and coupled CA model. (a) Total water content (ice + liquid water) and (b) temperature.

## 5.6. Conclusions

Coupled heat and water transport in partially saturated soils (frozen/unfrozen) has been developed by means of coupled cellular automata where local laws governing the automata interaction are based on physically based rules. The modeling uses a one dimensional CA structure wherein two cellular automata models simulate water and heat flow separately and are coupled through an energy balance module. In terms of performance, the model has been verified for heat flow due to pure conduction, conduction with convection, and conduction with phase change using analytical solutions. The simulations show excellent agreement with analytical solutions. The highly non-linear problem of coupled water and heat flow in unsaturated freezing soils was successfully verified with experimental data. For the phase change case, the model uses a simple heat balance approach with interactions between elementary cells based purely on empirical equations (e.g., Fourier's heat law) and observed constitutive relationships (e.g., soil freezing characteristics). Use of physically non-intuitive terms such as diffusivity is completely obviated and latent heat term is handled using a more intuitive energy balance approach instead of the apparent heat capacity as commonly used. The model is innovative because it uses coupled parallel running CA models to simulate two different processes, solves the coupled heat and water movement problem through a direct discrete approach, and verified against a wide range of analytical and experimental comparisons.

## 5.7. References

- Aldrich, H. P., and H. M. Paynter (1966). Depth of frost penetration in non-uniform soil, *CRREL Special Report 104*, US Army Cold Regions Research and Engineering Laboratory, Hannover, 148 pp.
- Anderson, D. M., and N. R. Morgenstern (1973). Physics, chemistry, and mechanics of frozen ground: A review, Yakutsk, USSR, National Academy of Science, Washington, D.C., 257-288.
- Anisimov, O. A., N. I. Shiklomanov, and F. E. Nelson (2002). Variability of seasonal thaw depth in permafrost regions: a stochastic modeling approach, *Ecol. Model.* **153**, 217-227.
- Churchill, R. V. (1972). Operational Mathematics, McGraw-Hill Companies, New York.
- Daanen, R. P., D. Misra, and H. Epstein (2007). Active-layer hydrology in nonsorted circle ecosystems of the arctic tundra, *Vadose Zone Journal* **6**, 694-704.
- Dall'Amico, M. (2010). Coupled water and heat transfer in permafrost modeling, Ph.D. Theses, University of Trento, Italy.
- Engelmark, H., and U. Svensson (1993). Numerical modeling of phase-change in freezing and thawing unsaturated soil, *Nordic Hydrol.* **24**, 95-110.
- Flerchinger, G. N., and K. E. Saxton (1989). Simultaneous heat and water model of a freezing snow-residue-soil System .1. Theory and Development, *Trans.ASAE* **32**, 565-571.
- Guymon, G. L., R. L. Berg, and T. V. Hromadka (1993). Mathematical model of frost heave and thaw settlement in pavements, *CRREL Special Report 93-2*, US Army Cold Regions Research and Engineering Laboratory, Hannover, 130 pp.

- Guymon, G. L., and J. N. Luthin (1974). Coupled heat and moisture transport model for Arctic soils, *Water Resour.Res.* **10**, 995-1001.
- Hansson, K., and L. C. Lundin (2006). Equifinality and sensitivity in freezing and thawing simulations of laboratory and in situ data, *Cold Reg.Sci.Technol.* **44**, 20-37.
- Hansson, K., J. Simunek, M. Mizoguchi, L. C. Lundin, and M. T. van Genuchten (2004). Water flow and heat transport in frozen soil: Numerical solution and freeze-thaw applications, *Vadose Zone Journal* **3**, 693-704.
- Harlan, R. L. (1973). Analysis of coupled heat-fluid transport in partially frozen soil, *Water Resour.Res.* **9**, 1314-1323.
- Hayashi, M., N. Goeller, W. L. Quinton, and N. Wright (2007). A simple heat-conduction method for simulating the frost-table depth in hydrological models, *Hydrol.Process.* **21**, 2610-2622.
- Hoekstra, A. G., J. Kroc, and P. M. A. Slood (2010). Introduction to modeling of complex systems using cellular automata, in *Simulating complex systems by cellular automata*, J. Kroc, P. M. A. Slood, and A. G. Hoekstra (Editors), Springer, Berlin. 1-16.
- Hutt, M. T., and R. Neff (2001). Quantification of spatiotemporal phenomena by means of cellular automata techniques, *Physica A-Statistical Mechanics and its Applications* **289**, 498-516.
- Ilachinski, A. (2001). *Cellular automata: a discrete universe*, World Scientific Publishing Company, Singapore.
- Jame, Y. W., and D. I. Norum (1980). Heat and mass-transfer in a freezing unsaturated porous-medium, *Water Resour.Res.* **16**, 811-819.

- Jame, Y. (1977). Heat and Mass Transfer in Freezing Unsaturated Soil, Ph.D. Thesis, The University of Saskatchewan (Canada), Canada.
- Jansson P-E. (1998). Simulating model for soil water and heat conditions: Description of SOIL model, Swedish University of Agricultural Sciences, Uppsala, 86pp.
- Johansen, O. (1975). Thermal conductivity of soils, Ph. D. Thesis, Trond-Heim, Norway. Cold Regions Research and Engineering Laboratory Draft Translation 637, 1977, ADA
- Low, P. F., D. M. Anderson, and P. Hoekstra (1968). Some thermodynamic relationships for soils at or below freezing point .1. Freezing point depression and heat capacity, *Water Resour.Res.* **4**, 379-394.
- Lunardini, V. J. (1985). Freezing of soil with phase change occurring over a finite temperature difference, in 4th international offshore mechanics and arctic engineering symposium, ASM.
- Luo, L. F., A. Robock, K. Y. Vinnikov, C. A. Schlosser, A. G. Slater, A. Boone, H. Braden, P. Cox, P. de Rosnay, R. E. Dickinson, Y. J. Dai, Q. Y. Duan, P. Etchevers, A. Henderson-Sellers, N. Gedney, Y. M. Gusev, F. Habets, J. W. Kim, E. Kowalczyk, K. Mitchell, O. N. Nasonova, J. Noilhan, A. J. Pitman, J. Schaake, A. B. Shmakin, T. G. Smirnova, P. Wetzel, Y. K. Xue, Z. L. Yang, and Q. C. Zeng (2003). Effects of frozen soil on soil temperature, spring infiltration, and runoff: Results from the PILPS 2(d) experiment at Valdai, Russia, *J.Hydrometeorol.* **4**, 334-351.
- McKenzie, J. M., C. I. Voss, and D. I. Siegel (2007). Groundwater flow with energy transport and water-ice phase change: Numerical simulations, benchmarks, and application to freezing in peat bogs, *Adv. Water Resour.* **30**, 966-983.

- Mendicino, G., A. Senatore, G. Spezzano, and S. Straface (2006). Three-dimensional unsaturated flow modeling using cellular automata, *Water Resour.Res.* **42**, W11419, 18 pp.
- Mizoguchi, M. (1990). Water, heat and salt transport in freezing soil, Ph.D. Thesis, University of Tokyo, Tokyo.
- Orlandini, S. (1999). Two-layer model of near-surface soil drying for time-continuous hydrologic simulations, *J.Hydrol.Eng.* **4**, 91-99.
- Painter, S. (2010). Three-phase numerical model of water migration in partially frozen geological media: model formulation, validation, and applications, *Computational Geosciences*, **15**(1), 69-85.
- Parsons, J. A., and M. A. Fonstad (2007). A cellular automata model of surface water flow, *Hydrol.Process.* **21**, 2189-2195.
- Quinton, W. L., and M. Hayashi (2008). Recent Advances Toward Physically-based Runoff Modeling of the Wetland-dominated Central Mackenzie River Basin, in *Cold Region Atmospheric and Hydrologic Studies. The Mackenzie GEWEX Experience: Volume 2: Hydrologic Processes*, M. Woo (Editor), Springer, Berlin. 257-279.
- Quinton, W. L., and D. M. Gray (2001). Estimating subsurface drainage from organic-covered hillslopes underlain by permafrost: toward a combined heat and mass flux model, *Soil-Vegetation-Atmosphere Transfer Schemes and Large-Scale Hydrological Models* 333-341.
- Schaller, M., and K. Svozil. (2009). Scale-invariant cellular automata and self-similar Petri nets, *Eur. Phys. J. B.* **69**: 297-311.

- Šimůnek, J., K. Huang, and M. Th. van Genuchten. (1998). The HYDRUS code for simulating the one-dimensional movement of water, heat, and multiple solutes in variably-saturated media. Version 6.0. 144, 1-164.
- Smerdon, B. D., and C. A. Mendoza (2010). Hysteretic freezing characteristics of riparian peatlands in the Western Boreal Forest of Canada, *Hydrol.Process.* **24**, 1027-1038.
- Stallman, R. W. (1965). Steady 1-Dimensional fluid flow in a semi-infinite porous medium with sinusoidal surface temperature, *Journal of Geophysical Research* **70**, 2821-&.
- Stefan, J. (1889). On the theory of ice formation, particularly ice formation in the Arctic ocean, S-B Wien Academy **98**, 173 pp.
- Van Genuchten, M. T. (1980). A closed-form equation for predicting the hydraulic conductivity of unsaturated soils, *Soil Sci.Soc.Am.J.* **44**, 892-898.
- Von Neumann, J., and A. W. Burks (1966). Theory of self-reproducing automata, Illinois University Press, Champaign.
- Wang, L., T. Koike, K. Yang, R. Jin, and H. Li (2010). Frozen soil parameterization in a distributed biosphere hydrological model, *Hydrology and Earth System Sciences* **14**, 557-571.
- Williams, P. J. (1967). Properties and behavior of freezing soils, Norwegian Geotechnical Institute, Research paper # 359, 128pp.
- Zhang, Y., S. K. Carey, and W. L. Quinton (2008). Evaluation of the algorithms and parameterizations for ground thawing and freezing simulation in permafrost regions, *Journal of Geophysical Research-Atmospheres* **113**, D17116.

# CHAPTER 6. CONCLUSIONS AND FUTURE RESEARCH RECOMMENDATIONS

## 6.1. General conclusions

Study of coupled heat and water transport in frozen soils is crucial to increase the understanding of active layer freezing and thawing processes. It is important to understand the effects of individual factors that affect the hydrological processes in permafrost areas in order to be able to better quantify and predict water resources of these regions. This is also important for prediction of the effects of climate change on the continuous and discontinuous permafrost regions. Study of such individual factors can be achieved by studying their effects in isolation in field or laboratory experiments. Hydrological studies in the Sub-Arctic are often discontinued, or relegated to field sensors, in winters due to logistical constraints. It is generally difficult to separate the influence of individual climatological and hydrological factors even when winter field observations are carried out. Correlating these factors is critical to improving hydrological model predictions. Carrying out fundamental process focused research in a controlled laboratory environment can help fill in critical knowledge gaps created by field accessibility limitations. Permafrost studies targeted at soil freeze-thaw, and associated biogeochemical and hydrological responses, require innovative laboratory setups to realistically replicate field conditions. It is further important to develop and test simpler numerical modeling methods based on field and laboratory experiments. Numerical models play an important role in situations where analytical descriptions of the observed

phenomena cannot be directly observed. For example, future effects of climate change cannot be observed, but can be predicted and studied using computer models. Therefore, there is a lot of benefit in developing and testing numerical models.

The research presented in this dissertation makes original contributions in heat and water transport studies of an organic active layer:

(1) Accurate vadose zone soil water content measurement is a critical requirement in coupled heat and moisture transport studies. Chapter 2 presents a detailed time domain reflectometry calibration for undisturbed peat samples. Past studies for peat report highly variable TDR calibrations, and suggest differences in origin of organic matter, degree of decomposition and bound water for such variability. This study shows that bound water appears to have minimal impact on calibration because of its negligible volumetric fraction owing to low bulk densities of peat. Increased volumetric air fraction at the same water content values attributed to high porosity of peat makes the empirical-TDR calibration models of mineral soils inapplicable in peat. Maxwell-De Loor's four-phase mixing model based on physical properties of the multi-phase soil system can efficiently simulate the effect of increased air volume and varying soil temperature on the TDR calibration in peat.

(2) In Chapter 3, an innovative experimental setup with a permafrost layer that underlies an active freeze-thaw zone is discussed and successfully evaluated for its ability to maintain one-dimensional change in soil moisture and temperature profiles. The setup allows physical simulation of effects on active layer heat and water transport processes one climatological factor at a time. The successful validation of the experimental setup is

a proof of concept for the unique two-level walk in environmental chamber specifically designed for permafrost studies.

(3) The freezing experiments on four Mesocosms held at different initial moisture content profiles are presented in Chapter 4. The effects of soil moisture dependant hydraulic conductivity and thermal properties of the active layer on soil water redistribution and freezing front propagation were studied. Soil water movement towards the freezing front (from warmer to colder regions) was inferred from soil freezing curves and from the total water content of frozen core samples collected at the end of freezing cycle. A significant amount of water redistribution, enough to raise the upper surface of frozen saturated soil within 15 cm of the soil surface at the end of freezing period, takes place towards the freezing front. Effects of temperature on soil matric potential appear to be primary cause for such movement as seen from analysis of soil freezing curves. Frost propagation is controlled by latent heat in the initial freezing periods, while thermal conductivity and heat capacity control the rate of frost migration once the majority of water is frozen. A simple, hypothetical conceptual model was developed based on the knowledge gained from the experiments discussed in Chapter 4 to discuss frost propagation and soil water redistribution in active layer on peat plateaus assuming variable moisture landscape at the start of winter.

(4) A one-dimensional model based on coupled cellular automata (CA) approach is developed and presented in Chapter 5. The model is based on heat and water balance to simulate heat and water flow in unsaturated soils. Buckingham-Darcy's law and Fourier's heat law are used to define the local interactions for water and heat movement

respectively. Phase change is handled by integrating along the experimentally determined soil freezing/moisture curve obviating the use of apparent heat capacity term. The 1D model is successfully tested by comparing with analytical and experimental solutions. A natural and simplified implementation of hydro-thermal coupling through synchronized heat and water balance makes this model a suitable candidate for more complicated 3D land surface schemes where complex coupling rules might be needed. The simulation of highly non-linear process of heat and water transport in soil (with and without phase change) using CA shows that the empirical laws can be directly used in computer models, thereby allowing a more natural evolution of the complex systems and obviating the need for expression of the system in non-observable terms (in this case diffusivity and apparent heat capacity were not used).

Overall understanding water movement towards freezing front is crucial to understanding the processes that control runoff from peat plateaus underlain by permafrost. Such understanding is crucial to water budget studies in the Arctic region. It appears from work done in this study that both inter-winter snowmelt and freezing induced water redistribution play a role in setting up of the impermeable frozen layer within upper 15 cm. With predicted warming and shortened, warmer winter scenarios for the future in the Canadian Arctic (IPCC, 2007), this could all change. In a warmer climate drainage through the subsurface could slow down as water may percolate deeper in absence of an impermeable frozen layer. It is not possible to make a generalized statement on the resilience of Canadian wetlands to climate change based solely on the experiments conducted in this thesis. However, it appears from this study that latent heat

effects would play a critical role in both freezing and thawing in modulating the response to climate change. A controlled freezing and thawing run simulating warmer climates would have been ideal for furthering our knowledge. More laboratory work using field representative boundary conditions in the upper chamber are required. In addition, numerical simulations using a wide range of scenarios are required to understand the local effects of climate change in Canadian sub-Arctic. Thus, it is critical to continuing the laboratory work as well as the development of the Cellular Automata model presented in this thesis.

## **6.2. Future research recommendations**

The research presented in this thesis answers some questions, while opening up demand for further research into quite a few aspects related to water and heat movement in organic soils:

It is important to further study the effects of temperature on soil matric potential in peat. This is important since the change in matric potential is because of several factors. Given ice content is one of the factors and ice content can vary over a very wide range in peat because of high total porosity, it is more crucial to study how the matric potential is affected in peat at temperatures below freezing. It is especially important to study the applicability of the generalized Clausius-Clapeyron equation (CCE) in peat soils in order to increase the faith in numerical models. This is crucial given the large pore size of peat and wide variety of pore size and geometry associated with pore structure. It is important to concentrate future efforts on studying the processes resulting

into such movement and quantifying the contributions from liquid water and vapour fluxes to total water movement.

It is observed that hydraulic conductivity plays an important role in water movement in partially frozen, unsaturated peat. Hydraulic conductivity in frozen soils must be measured in order to provide better parameterization for numerical studies. Using soil water retention data to predict unsaturated hydraulic conductivity in peat could result into serious errors (Price *et al.*, 2008). A calibration phase of numerical models based on manipulation of unsaturated hydraulic conductivity relationship is time consuming, and because calibrated models are not strictly physically based, they cannot be trusted for repeatability. Further research in developing methods to measure unsaturated hydraulic conductivity of frozen soils is therefore necessary. One method in frozen peat would be to conduct Mesocosm experiments with ability to measure total water content with time and use the Buckingham-Darcy's law to estimate hydraulic conductivity. However, again for this approach first it is necessary to thoroughly validate the CCE so that the total water content observed in Mesocosm experiments can be used along with CCE converted potential gradients to estimate hydraulic conductivity in frozen soil.

There is a need to continue the Mesocosm experiments as presented in Chapter 4 to study freezing and thawing of organic active layer. For example, snow melt infiltration into the highly porous peat surface layer during freezing needs to be studied in order to understand the dynamics between the freezing induced water redistribution and over-winter snowmelt processes. A first idea to study this aspect could be to use different thickness of snow packs on top of the mesocosms and subjecting the snow pack-peat

system to freezing. Total water content needs to be measured at the end of freezing (e.g., by taking soil cores). Following this phase, the snow pack-peat system can be subjected to thawing at similar air temperature and energy inputs from the light bank until the entire snow pack has melted. The total water content needs to be determined again in the same fashion in order to understand the differences in infiltration process. This is a primary suggestion and can be modified to extract the essence of the snowmelt infiltration process in frozen peat.

The cellular automata model presented in this thesis is a simple, but powerful model since it is based on basic concepts and does not rely on any other methods to simulate complex system of heat and water transport in soil. This model can be further developed into a complete land surface scheme. There are recent examples of CA being used in many hydrological studies to simulate processes, e.g., surface runoff (Parsons and Fonstad, 2007), groundwater flow (Ravazzani *et al.*, 2010), vadose zone water movement (Mendicino, 2006). These experiences can be used to develop a complete 3D land surface scheme capable of simulating surface and subsurface flows in a coupled model.

### **6.3. References**

IPCC (2007). Climate Change 2007: The Physical Science Basis. Contribution of Working Group I to the Fourth Assessment Report of the Intergovernmental Panel on Climate Change [Solomon, S., D. Qin, M. Manning, Z. Chen, M. Marquis, K.B. Averyt, M.Tignor and H.L. Miller (eds.)]. Cambridge University Press, Cambridge, United Kingdom and New York, NY, USA.

- Mendicino, G., A. Senatore, G. Spezzano, and S. Straface (2006). Three-dimensional unsaturated flow modeling using cellular automata, *Water Resour.Res.* **42**, .
- Parsons, J. A., and M. A. Fonstad (2007). A cellular automata model of surface water flow, *Hydrol.Process.* **21**, 2189-2195.
- Price, J. S., P. N. Whittington, D. E. Elrick, M. Strack, N. Brunet, and E. Faux (2008). A method to determine unsaturated hydraulic conductivity in living and undecomposed Sphagnum moss, *Soil Sci.Soc.Am.J.* **72**, 487-491.
- Ravazzani, G., D. Rametta, and M. Mancini (2011). Macroscopic cellular automata for groundwater modelling: A first approach, *Environmental Modelling & Software* **26**, 634-643.

## APPENDIX

### A1. Description of peat corer

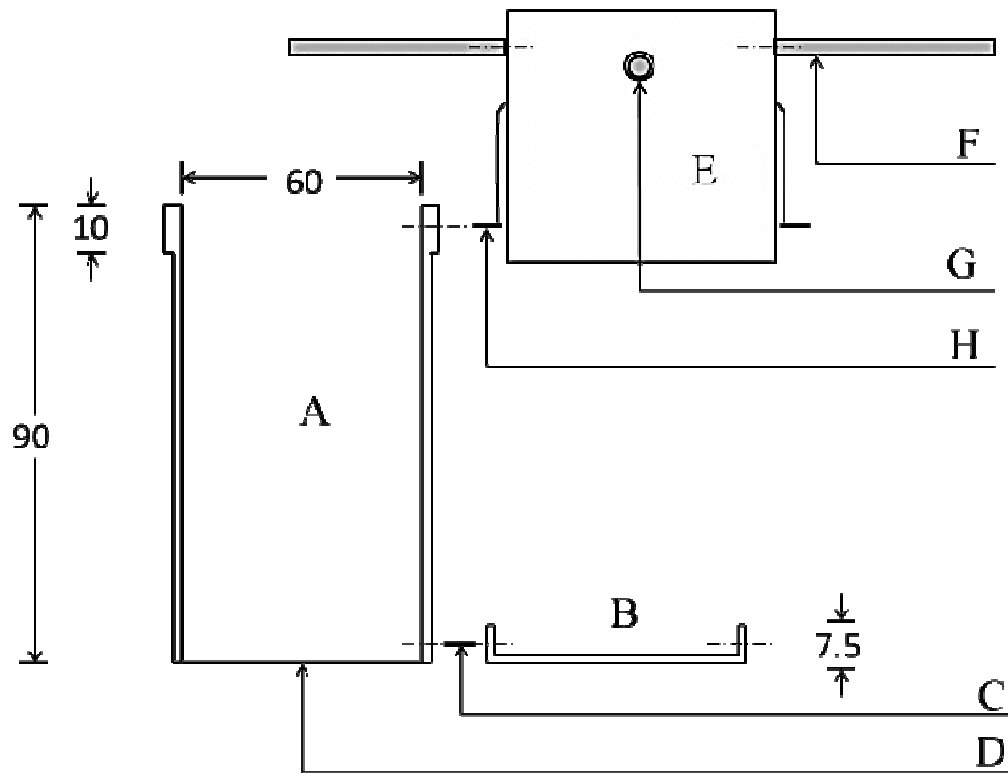


**Figure A1.** The corer assembly (all dimensions in cm, not to scale). A: sample holder made out of fiber reinforced glass pipe material; B: bottom cap made out of same material as A; C: push-in plastic fasteners to secure bottom cap to the sample holder; D: alloyed carbon steel band saw blade; E: rotational head made of aluminum to facilitate rotation of the corer assembly; F & G: steel rods used as levers for rotating the corer assembly; H: quick release pins for quick mounting of rotational head on to the sample holder.

Figure A1 shows the line diagram and gives a short description of all the components of the peat corer. Figure A2 shows a picture of the corer being used in the field to sample peat cores.



**Figure A2.** Peat core sampling.

Peat cores were extracted at a field site located in the Scotty creek watershed, Northwest Territories, Canada ( $61^{\circ}18'N$ ;  $121^{\circ}18'W$ ). The site consists of closely spaced matured varieties of Black Spruce, Tamarack Larch, Lodgepole Pine and White/Paper Birch. The sampling areas were chosen such that the location is under the canopy yet sufficiently away from the trees so that any major interference with strong tree roots is avoided. The sampling procedure consisted of rotating the corer in the direction of cutting edge of the band saw blade using the steel rods as levers. Four people are needed to rotate the sampler and at the same time are required to apply downward pressure to advance the

corer after cutting action is performed. Sampling in peat is relatively easy, more so when the soil is wet, with less force required than in mineral soils. At the same time it is tricky because if too much force is applied, the sample may compress beyond acceptable limits.

The corer was assembled by mounting the rotational head onto the sample holder. The depth from the upper lever to the ground surface was recorded at the start and after every rotation. If there was interference from stronger roots, the corer would experience rotation without change in the depth of cutting. A long wood saw was used to cut around the corer to free the blades stuck in such roots. We stopped rotating the corer any further when the corer reached desired depth or if the blades hit frost table. At this stage an access trench was dug on one side and a 5 mm thick bottom plate (60 cm diameter) was forced below the blades to hold the sample inside the sample holder. The sampler was then lifted by two people using the levers while the others held the plate in place. Once out of the pit, the rotational head was removed and the sample holder, with the sample in it, was laid horizontally on the ground. The bottom cap was carefully put on to the sample holder keeping the blade in place. The cap was secured using push in fasteners and the sample holder was made to stand upright and moved to a location from where it can be airlifted.

Figures A3 and A4 show the sample surface with live vegetation when the sampling was in progress, and the core bottom being detached from the permafrost at the time of sample uplifting once the core was fully sampled. Four cores varying from 45 cm to 70 cm in depth were sampled in one day. Observed compression was less than 10% for all the cores. All four samples were packed in separate wooden boxes made to tightly fit

the sample holder and airlifted from the field site to Fort Simpson, NWT from where they were transported on a cargo plane to London, ON.



**Figure A3.** Sample surface with live vegetation at the time of sampling.



**Figure A4.** The core bottom being detached from the permafrost at the time of sample uplifting once the core was fully sampled.

## **A2. Description of experimental setup**

The base layer was packed using unprocessed catotelmic peat extracted near Thunder Bay, ON Canada. In order to match the hydraulic conductivities of the deeper peat layers, which were not directly sampled due to permafrost conditions, saturated hydraulic conductivity tests were conducted. Constant head permeameter tests were run on circular peat columns 12 cm long and 8 cm in diameter. These columns were prepared by dividing the depth into eight layers of equal thickness and then packing them to same density using wetted peat. The base layers in the experimental Mesocosms were then prepared in the similar way as done for the columns used in saturated hydraulic conductivity tests. Each layer was compacted by applying equal number of blows from a 6.60 kg, 25.4 cm x 25.4 cm tamper until the depth to attain required density was reached.

Figure A5 shows all the stages of setting up of the experiments with brief explanations given in the caption. Time domain reflectometry probes were inserted into the sample through rectangular holes made in the container walls and the neoprene liner. This way there is no correction needed in the TDR calibration equation to include the effects of the wall and neoprene combination. The line diagram (Figure A6) shows the final setup with all components explained in the caption.

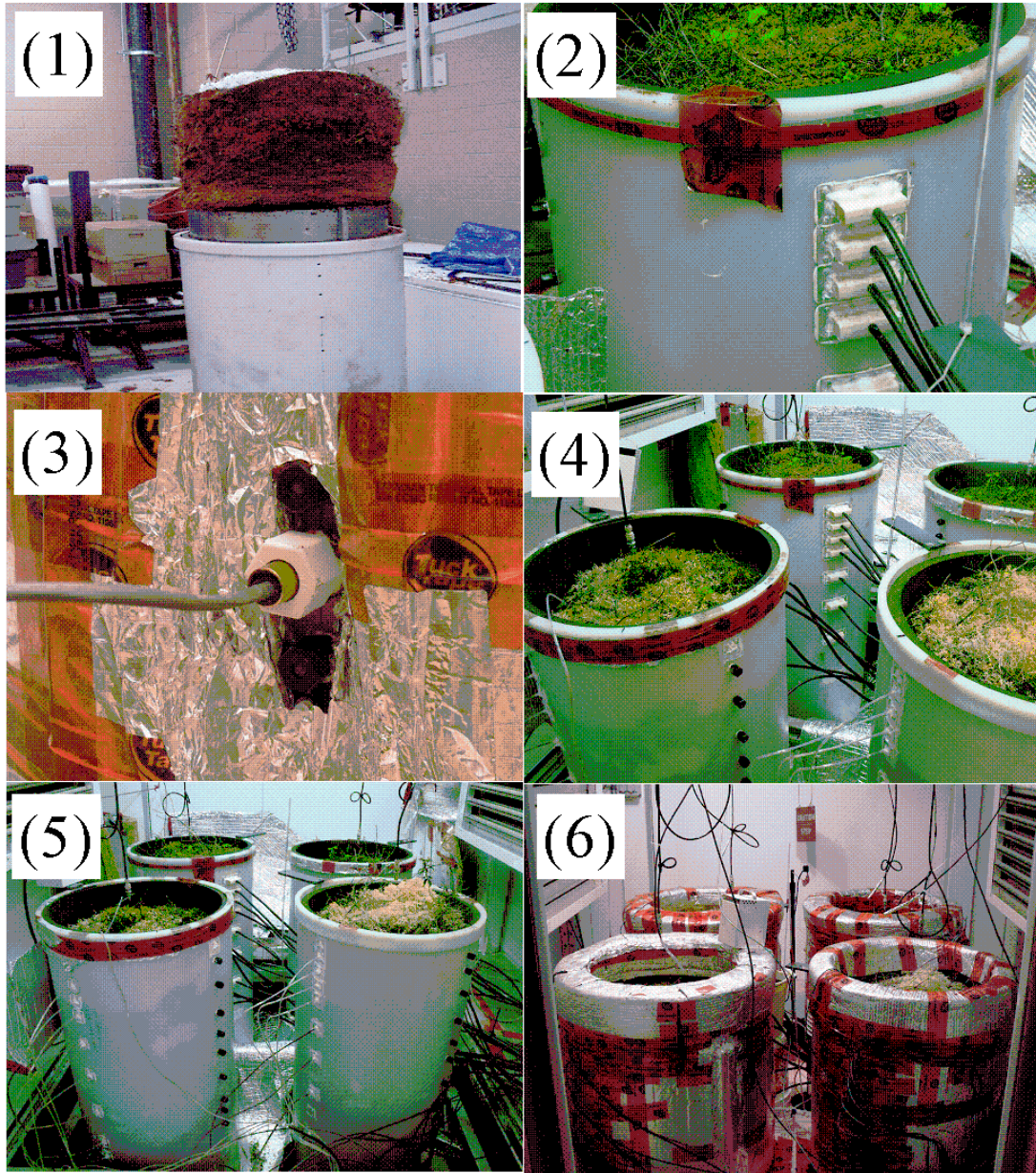


**Figure A5.** Experimental setup. 1: Symmetrically loaded undisturbed frozen sample being readied for insertion into EH; 2: Close-up of TDR probes inserted into the soil through rectangular holes with aluminum plates around probe heads; 3: Temperature probe inserted through male pipe adapter; 4: TDR probes, temperature probes and sampling ports shown on three different drums; 5: All the four LDPE containers placed in the upper chamber ready to be insulated from outside; 6: Completed and ready for experiments.

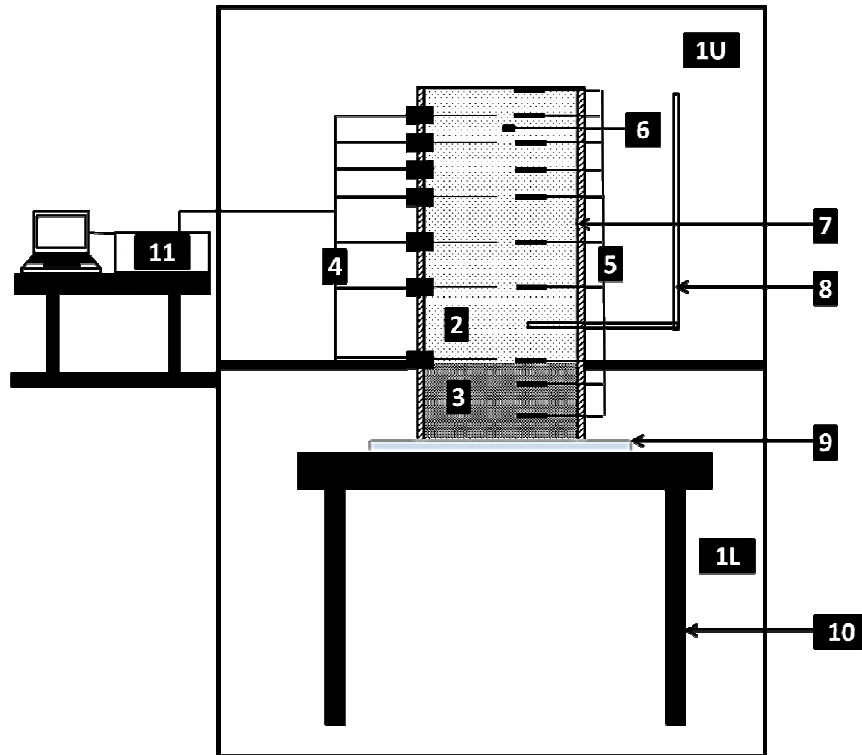


**Figure A6.** Line diagram showing the experimental setup. 1U: Upper level chamber of the BESM; 1L: Lower level chamber of the BESM; 2: 65-70 cm deep unfrozen layer; 3: 35-40 cm bottom frozen layer (fully saturated before freezing); 4: TDR probes connected to 11 through low-loss coaxial cables; 5: temperature probes connected to 11; 6: heat flux plate; 7: LDPE container lined with neoprene from inside and insulated from outside; 8: stand pipe for water level measurements; 9: weighing scale; 10: custom made stand to support the entire experimental setup; 11: multiplexers and datalogger connected to a personal computer.

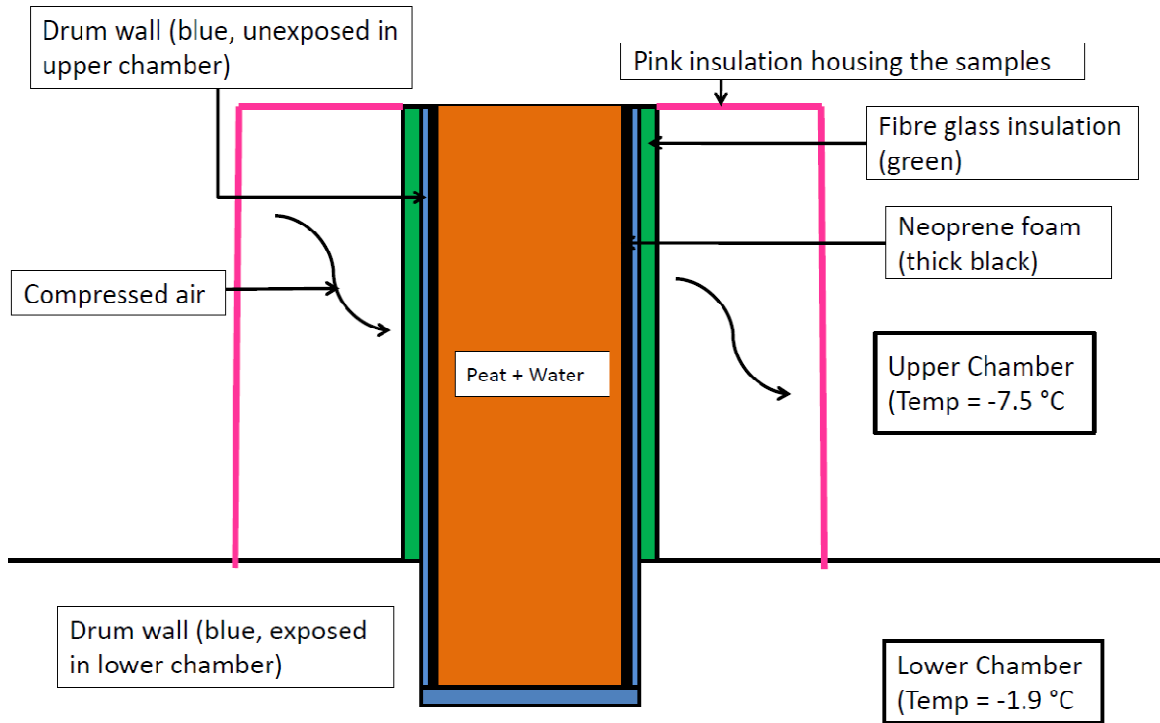


**Figure A7.** The external insulation housing and compressed air circulation around the peat samples.

# Curriculum Vitae

**Name:** Ranjeet Nagare

**Post-secondary Education and Degrees:** Pune University, India  
1997 – 2001 B.Eng. (Civil)

Brandenburg Technical University  
Cottbus, Germany  
2002 – 2005 M.Sc. (Environment and Resource Management)

The University of Western Ontario  
London, ON, Canada  
2006 – 2011 Ph.D. (Geology)

**Honours and Awards:** Pune University Freeship  
1997 – 2001

Western Graduate Research Scholarship  
2006 – 2010

Special Science Scholarship  
2006 – 2010

Canadian Geophysical Union Student Travel Grant  
CGU-CMOS Joint Assembly, Ottawa  
2010

**Related Work**

Research Assistant

**Experience:**

The University of Western Ontario  
2006 – 2010

Teaching Assistant

The University of Western Ontario  
2006 – 2010

Sessional Lecturer

The University of Western Ontario  
2008

**Publications:**Peer Reviewed Journals

- **Nagare, R.M.**, Schincariol, R.A., Quinton, W.L., and Hayashi, M. (2011). Laboratory calibration of time domain reflectometry to determine moisture content in undisturbed peat samples. *Euro. J. Soil. Sci.* (published online, 4<sup>th</sup> April 2011).
- **Nagare, R.M.**, Schincariol, R.A., Quinton, W.L., and Hayashi, M. Moving the field into the lab: Physical simulation of heat and water movement in sub-Arctic peat. *Permafrost and Periglacial Processes* (in review).
- **Nagare, R.M.**, Schincariol, R.A., Quinton, W.L., and Hayashi, M. Effects of freezing on soil temperature, frost propagation and moisture redistribution in peat: Laboratory investigations, *Hydrol. Earth. Sys. Sci.* (in review).
- **Nagare, R.M.**, Bhattacharya, P., Khanna, J., and Schincariol, R.A. A coupled cellular automata model to simulate freeze-thaw processes in soils (in preparation).

- **Nagare, R.M.**, Schincariol, R.A., Quinton, W.L., and Hayashi, M. A simple modification of cube method for laboratory determination of saturated hydraulic conductivity of peat (in preparation).

#### Book Chapters

- Ulrich Beims, **Ranjeet Nagare**, Claus Nitsche, Michael Porzig & H-J Voigt (2008). In Environmental Geology: Handbook of Field Methods and Case Studies, Springer, 643-648.
- Florian Jenn, **Ranjeet Nagare**, Michael Porzig & H-J Voigt (2008). In Environmental Geology: Handbook of Field Methods and Case Studies, Springer, 649-680.

#### Conference Presentations

- **Nagare, R. M.**, Schincariol, R.A., Quinton, W.L., and Hayashi, M. (2010). Effects of initial water content on freeze-thaw processes in peat mesocosms. Canadian Geophysical Union, Banff, May 2011.
- **Nagare, R. M.**, Schincariol, R.A., Quinton, W.L., and Hayashi, M. (2010). Laboratory simulation of water and heat transport in sub-Arctic peat: experimental setup. CGU-CMOS Joint Assembly, Canadian Geophysical Union, Ottawa, June 2010.
- **Nagare, R. M.**, Schincariol, R.A., Quinton, W.L., and Hayashi, M. (2009). Calibration of time domain reflectometry using undisturbed peat samples, AGU-CGU Joint Assembly, American Geophysical Union, Toronto, May 2009.
- **Nagare, R.M.**, Schincariol, R.A., Quinton, W.L., and Hayashi, M. (2009). Use of time domain reflectometry in peat mesocosm laboratory experiments, Kenn Hewitt Symposium, Waterloo, March 2009.
- R. Schincariol, **R. Nagare**, W. Quinton, and M. Hayashi. (2008). The supporting role of mesocosm-scale laboratory experiments in solving critical issues at hydrogeological research sites. Annual Meeting Fall of the American Geophysical Union, San Francisco, 15-19 December.

- R. Schincariol, **R. Nagare**, W. Quinton and M. Hayashi. (2008). The supporting role of laboratory mesocosm studies in the Scotty Creek watershed field studies. 3rd Annual IP3 Meeting and Workshop, Whitehorse, Yukon, 12-15 Nov.
- Quinton, W.L., M. Hayashi, N. Wright, E.D. Soulis, R. Heck, T. Elliot, L. Chasmer, R. Bemrose, **R. Nagare**, R. Schincariol, Y. Zhang, S. Carey, T. Myers, F. Rezanezhad, P. Whittington, 2007. Advances in processes and parameterisation studies at Scotty Creek. 2nd Annual IP3 Meeting and Workshop, Cold Regions Research Centre, WLU, 8-10 Nov.
- **R. Nagare**, M. Liese, H-J. Voigt (2006). Hydrogeochemistry at the 100 years old sewage farms Berlin Karolinenhoehe, Geophysical Research Abstracts, Vol. 8, 03042, 2006, European Geosciences Union 2006.